7-3-2012

Laboratory investigation of fatigue endurance limits in asphalt concrete

Damien Bateman

Damien Bateman
Candidate

Civil Engineering
Department

This dissertation is approved, and it is acceptable in quality and form for publication:

Approved by the Dissertation Committee:

Dr. Rafiqul Tarefder , Chairperson

Dr. John Stormont

Dr. Arup Maji

Dr. Percy Ng

Dr. Yu-Lin Shen

LABORATORY INVESTIGATION OF FATIGUE ENDURANCE LIMITS IN ASPHALT CONCRETE

by

DAMIEN BATEMAN

B.S., Civil Engineering
&
M.S., Civil (Geotechnical) Engineering

McNeese State University, Lake Charles, Louisiana

DISSERTATION

Submitted in Partial Fulfillment of the

Requirements for the Degree of

Doctor of Philosophy
Engineering

The University of New Mexico

Albuquerque, New Mexico

May 2012

DEDICATION

This work is dedicated to my parents and to my friend Yi Huang.

ACKNOWLEDGMENTS

First and foremost, I want to thank my parents for their unconditional support and encouragement throughout my time in the US. I would like to thank my supervisor Dr. Rafiqul Tarefder for his guidance, opinion, and support throughout this study. I would like to express my sincere thanks to my committee members: Professors Arup Maji, John Stormont, Percy Ng, and Yu-Lin Shen for their valuable time and advice. I would like to thank New Mexico State Department of Transportation for their support in this study; Jeff Mann (Head of Pavement Design, NMDOT), Bob Meyers (Geotechnical Section Manager, NMDOT), Robert McCoy (Head of Pavement Exploration, NMDOT), Parveez Anwar (State Asphalt Engineer, NMDOT), Scott McClure (Research Bureau Chief), and Virgil Valdez (Research Bureau, NMDOT) for their valuable suggestions and continuous support during the entire duration of the project. Special thanks to Mr. John Galvin of LaFarge Construction Materials for providing me with asphalt concrete mixtures. I wish to thank Dr. Aravind Swamy for allowing use of his viscoelastic model and Mesbah Ahmed for his help in developing a viscoelastic model using Matlab. I also wish to thank Mekdim Weldegiorgis, Rashadul Islam, and Ghazanfar Barlas for their laboratory assistance on many tasks. Finally, I am thankful to my colleagues and friends at the Civil Engineering Department who have helped me through good times and bad, to eventually get to this point; I will be forever grateful.

Laboratory Investigation of Fatigue Endurance Limits in Asphalt Concrete

BY

DAMIEN BATEMAN

B.S., Civil Engineering, McNeese State University.
Louisiana, 2005

M.S., Civil (Geotechnical) Engineering, McNeese State University,
Louisiana, 2007

PhD., Engineering, University of New Mexico, Albuquerque,
New Mexico, 2012

ABSTRACT

It is believed that Hot Mix Asphalt (HMA) mixtures used in long-lasting pavements contain a threshold of strain value below which no fatigue damage occurs. This concept is known as the fatigue endurance limit (FEL). Although previous studies have shown that an endurance limit does exist for HMA mixtures, an established value is yet to be determined, with values varying from 70-400 microstrain (με) based on mixture variability. Traditional FEL

identification is based on the phenomenological approach, which relates the number of loading cycles to fatigue failure with applied tensile strain and initial stiffness of material. This study determined the FEL of two HMA mixtures, SP-II (coarse mix) and SP-III (fine mix), using the phenomenological approach as well as a fundamental energy based approach, the dissipated energy concept. Results show that the dissipated energy approach estimates higher FEL values for both mix types than those estimated using the phenomenological approach. The FEL values for the SP-II and SP-III mixtures are estimated to be approximately 200 and 300 με respectively.

Furthermore, laboratory fatigue failure criterion is defined as the number of loading cycles at which the stiffness of a material reduces by 50%. This study evaluated stiffness-based failure criteria for laboratory fatigue testing using the viscoelastic continuum damage mechanics (VCDM) approach. Results show that fatigue failure criterion of the VCDM approach correlates well with the stiffness-based fatigue failure criterion. In addition, the effect of polymer-modified binder on the FEL of HMA materials is investigated. The addition of modified binder to the SP-II mixture reduced the estimated FEL by 27%. On the other hand, the addition of modified binder to the SP-III mixture improved its estimated FEL value by 30%.

TABLE OF CONTENTS

LIST OF TABLES

LIST OF FIGURES

CHAPTER I

INTRODUCTION

1.1 Problem Statement

The predominant use of Hot Mix Asphalt (HMA) in pavement structures within the United States and worldwide has brought about a significant change in the way pavements are built today. Pavement design standards are continuously changing as researchers develop new ways to analyze and predict the behavior of HMA, which significantly improves design reliability for pavement design projects. Not for the first time, researchers can look to the past as a way to improve flexible pavement design. Records have shown that some asphalt concrete pavements have been performing for 40 years or more without exhibiting any fatigue damage (Romanoschi et al. 2008, Tarefder and Bateman 2010). It is believed that the HMA mixtures used in these long-lasting pavements contain an endurance limit below which no fatigue damage occurs. This concept is known as the Fatigue Endurance Limit (FEL). Determining the FEL of HMA mixtures is directly related to the design and construction of long-life or perpetual pavements. The inclusion of FELs in current pavement design guides is only now being considered and is still a long way from being implemented on a project-to-project basis. However, the existence of a FEL in HMA is still relatively new and the purported value has yet to be established.

HMA mixtures are designed primarily to resist rutting and fatigue cracking. In saying this, HMA mixtures are still vulnerable to fatigue cracking, if not designed to meet specific traffic loads. Bottom-up fatigue cracking initiates at the base HMA layer of a pavement due to tensile strains induced from repeated traffic loading. If the applied tensile strain is greater than the endurance strain of the HMA material, cracking initiates and propagates toward the surface. Once the cracks are visible from the surface of the pavement, the only solution is complete reconstruction. This problem can be avoided by implementing two different design approaches; (*1*) build a pavement thick enough so that the tensile strains experienced at the base of the pavement are negligible, and (*2*) use a rich-bottom base layer (RBL) that is flexible enough to withstand the tensile strains caused by repeated traffic loading. The first option is a conservative approach and is expensive. The other alternative is much more appealing because a thinner pavement containing a flexible base layer will provide the same performance as the thicker pavement, for less cost. However, the binder rich layer creates a 'bath-tub' effect due to its lower permeability, and moisture becomes trapped within the asphalt layers above which can lead to extensive moisture damage to the mixture. At any rate, the endurance strain of the HMA mixture used in this flexible layer must be known in order to prevent fatigue cracking. In summary, identifying the FEL, if it exists, will improve current design guides for both conventional and perpetual pavements.

Up until now, the fatigue endurance limit of HMA mixtures is determined by conducting laboratory fatigue testing whereby the number of loading cycles to failure is related to applied tensile strain and initial stiffness of material. This is called the phenomenological approach because the relationship is purely empirical and does not explain the fundamentals of fatigue failure. Laboratory fatigue testing of HMA mixtures is generally done either by repeated load flexure or by direct tension tests. From the literature search, the FEL of HMA mixtures may vary from 70-200 microstrain, depending on mixture properties (Monismith et al. 1970, Tayebali et al. 1992). In the state of New Mexico, the FEL of local HMA mixtures is unknown. Determining the FEL of HMA mixtures can provide valuable data for current pavement design methods and provide significant economic contribution to the state of New Mexico.

Due to significant design and economic benefits, research in this area is gaining popularity. A nationwide study is currently being done by the National Cooperative Highway Research Project (NCHRP 9-44), with the specific goal of validating the existence of FELs in HMA. In addition to this, the NCHRP intends to incorporate the use of a FEL in current pavement design guidelines. However, there is still a need to establish the same design criteria for state highway agencies. By determining the FEL for local HMA mixtures, improved designs for longer-lasting pavements can be implemented on a site-specific basis.

1.2 Hypotheses

1.2.1 Hypotheses One

Although fatigue endurance limit is well defined in several materials such as steel, polymer, it is only in recent years that this concept has become an important factor in asphalt pavement design. Previous studies have shown that some asphalt concrete does have a FEL, though its exact value varies due to the varying factors within asphalt mix design. This is to be hypothesized that the FEL of two HMA mixtures can be determined through laboratory fatigue testing using four-point bending method and application of analytical models.

Studies have shown that the fatigue life HMA mixtures is affected by mixture variables such as aggregate gradation, binder content, percent air voids, etc. However, there are few studies which have described the relationship between the Performance Grade (PG) binder and the FEL. Therefore, it is hypothesized that the effects of polymer-modified binder on the FEL of HMA mixtures can be determined through the use of dissipated energy method as well as using the empirical strain-fatigue life relationship.

1.2.2 Hypotheses Two

Traditional stiffness-based fatigue failure criteria for HMA materials are not well defined and often ignore viscoelastic effects. It is also hypothesized that the application of a viscoelastic damage mechanics approach can identify fatigue

failure in HMA materials, as well as evaluate traditional stiffness-based failure criteria.

1.3 Objectives and Scope

The primary objectives of this study are;

- To determine the FEL of four New Mexico HMA mixtures using two analytical approaches and two stiffness-based fatigue failure criteria. Four-point beam fatigue testing using controlled strain is performed on laboratory aged HMA samples. The Plateau Value approach and the strain-fatigue life relationship are applied to test data to determine the FEL.
- To identify fatigue failure in HMA materials through the use of the Plateau Value, Energy Ratio, and Pseudostrain approaches and to determine the effects of crack propagation paths on the fatigue life of HMA materials. Dynamic modulus testing is done to determine the linear viscoelastic range where dynamic modulus master curves are used in Pseudostrain approach.
- To evaluate and recommend the use of FEL in designing both conventional and perpetual pavements using the MEPDG and life-cycle cost analysis (LCCA).

CHAPTER II

LITERATURE REVIEW

2.1 Introduction

A comprehensive literature review is conducted to gather information on current fatigue design and analysis approaches, related laboratory tests, corresponding standards, and methodologies used to obtain fatigue endurance limits of HMA mixtures. Factors that affect HMA mixture fatigue performance are also reviewed and the literature found is summarized and documented.

2.2 Current Fatigue Design and Analysis Approaches

The FEL is commonly found in metallic materials. However, not all metals have a well defined FEL, aluminum being a prime example (Hibbeler 2005). Figure 2.1 presents such a case where Figure 2.1(a) describes the increasing fatigue life of a material as the stress is decreased. Figure 2.1(b) shows the fatigue life of another material increasing until a limit is reached where the fatigue life becomes indefinite.

There are limited studies on the FEL of HMA mixes. Early work by Carl Monismith at the University of California, Berkley, suggested that an endurance limit does exist for HMA (Monismith et al. 1970). Monismith performed laboratory fatigue testing of local California HMA mixtures using both controlled stress and controlled strain modes of loading. No indication is given from the

literature if rest periods are included in the testing or if it is continuous loading. The results suggested that a FEL of 70 με exists for the HMA mixtures. Further research done by the University of Illinois presented HMA endurance limits ranging from 70-100 με taken from 120 different HMA mixes (Carpenter et al. 2003, Shen and Carpenter 2005). However, due to limited research, an established FEL value has not been confirmed.

Identifying the FEL of HMA mixtures can greatly improve the current design of perpetual pavements. Conventional pavements are typically designed for 20-30 years. A perpetual pavement is designed to last more than 50 years with minimal rehabilitation. More on perpetual pavement design is presented in Appendix A. Considering FEL in perpetual pavement design can greatly reduce total HMA layer thickness, which would provide significant economic benefits.

In summary, there is sufficient evidence to suggest that a FEL does exist for HMA. The following sections present different test methods and analytical models which are currently being used to prove the existence of a FEL in HMA materials.

2.2.1 Laboratory Fatigue Test Methods

Traditional mechanistic-empirical approaches for predicting fatigue of HMA mixtures require controlled stress (strain) laboratory testing, usually dictated by a single temperature over a range of applied stress (strain) levels. The number of

cycles to failure is then recorded along with the critical stress (strain) level and this determines the fatigue life of a HMA mixture. Measured fatigue life in the field can also be incorporated to validate this approach.

Four Point Bending Test

Four-point bending is the most commonly used HMA fatigue test. The standards for this bending beam fatigue test (BBFT) are AASHTO T321 and ASTM D7460. Cyclic loading is applied to an asphalt beam until fracture or failure occurs. Prowell et al. applied this test method as part of the NCHRP 9-38 project to validate the existence of a FEL in HMA mixtures (Prowell et al. 2008). HMA beam samples are tested (380 mm long by 50 mm thick by 63 mm wide) under constant strain mode using sinusoidal loading at 10 Hz. Testing is conducted using six different strain levels; 800, 400, 200, 100, 70, 50 $\mu\varepsilon$, and the test is terminated once a 50 percent reduction in initial flexural stiffness (E_0*) is reached. The study concluded that a FEL for HMA does exist and can be reasonably extrapolated from 10-12 million cycles using the Weibull function. However, the major drawback of this study is the time required to run 12 million cycles, which may take as long as 14 days. Another major shortcoming is the absence of rest periods during testing where the beneficial effects of healing are not accounted for. The concept of healing in asphalt concrete is discussed in greater detail in the Section 2.5.1.

Uniaxial Tension Test

Direct tension testing has been used by some researchers to determine the FEL of HMA mixtures. Fatigue testing on sample cores (3 in. diameter, 6 in. tall) consisted of haversine load pulses. Fatigue damage required increasing blocks of constant strain (each block = 10,000 cycles), where each block had greater amplitude than the previous one. Steel plates are glued to the ends of the samples with plastic epoxy glue and the specimens are aligned vertically. Testing is conducted until failure. The crosshead displacement is computer-controlled and test results are recorded using a data acquisition system. Linear Variable Differential Transducers (LVDT) are attached to the specimen and a data acquisition system is set up to record the deformation (strain) of the specimen. This test method is favorable among many researchers as it more simplified than traditional fatigue test methods. This is because direct tension testing does not require the production of HMA beam samples and uses HMA core samples instead. In addition to uniaxial testing, the development of a viscoelastic continuum damage mechanics (VCDM) model enabled FEL identification. The application of VCDM models in determining the FEL is discussed in greater details in the next section.

2.2.2 Fatigue Failure Criteria

Flexural Stiffness Reduction

Figure 2.2 describes the different stages in a typical fatigue test of HMA. The stiffness reduction process is characterized by three phases of degradation. The

first phase results from internal heating caused by dissipated energy generation due to the materials viscous properties (Di Benedetto et al. 1997). This occurs at the beginning of the test when the beam sample is repeatedly flexed and the sample reaches a new thermal equilibrium ($T + \Delta T_{heat}$). According to Di Benedetto et al (1997), this increase in temperature has a significant effect on the stiffness reduction and can be identified as the initial portion of the fatigue curve where the slope is steep. Samples tested at higher strains generate more heat and therefore experience a higher rate of stiffness reduction. As the cyclic loading continues, two major stages are illustrated; formation of micro-cracks which reduce the stiffness by 25%, and crack formation which further reduces the stiffness by 35-40%. Failure of the specimen is expected once these two stages are identified. However, it must be noted that traditional controlled stress (strain) fatigue tests (failure pronounced at 50% stiffness reduction) do not account for internal heating of a HMA specimen. A correction factor can be applied here to account for the internal heating, but testing within a temperature controlled chamber can reduce the effect of internal heating.

Four point beam fatigue testing of HMA materials is usually performed according to AASHTO T 321 Standards (2007). Asphalt concrete beams undergo damage inducing cyclic loading (displacement control). Using the deflection history, load response history, and geometry of test specimen, the maximum strain and stress in specimen can be calculated using Eq. 2.1 and Eq. 2.2, respectively.

$$\varepsilon = \frac{12\, h\, \delta}{3L^2 - 4a^2} \tag{2.1}$$

$$\sigma = \frac{P\,L}{b\,h^2} \tag{2.2}$$

where ε = maximum strain, σ = maximum stress, *P* = load applied by actuator at time *t*, *b* = average specimen width and *h* = average specimen height, *δ* = deflection at center of beam at time *t*, *a* = distance between inside clamps and *L* = distance between outside clamps. Figure 2.3 illustrates a schematic of test set-up.

Sample flexural stiffness is then calculated using σ and ε data recorded from each cycle.

$$E = \frac{\sigma_t}{\varepsilon_t} \tag{2.3}$$

where *E* = flexural stiffness.

Then, number of cycles at 50% reduction in stiffness is recorded as failure of beam. Similar process is repeated at other strain levels to obtain relation between applied strain and number of cycles to failure. The same relation is given in Eq. 2.4. Sometimes, initial stiffness of material is also incorporated into fatigue model as shown in Eq. 2.5.

$$N_f = k_1 \left(\frac{1}{\varepsilon}\right)^{k_2} \tag{2.4}$$

$$N_f = k_1 \left(\frac{1}{\varepsilon}\right)^{k_2} \left(\frac{1}{E}\right)^{k_3} \tag{2.5}$$

Four-point flexural bending of a beam implies that the middle third of the beam is subjected to pure bending. The flexural stiffness in the mid-section is reduced at a higher rate than the outer sections due the presence of higher stresses and strains,

where eventually micro-cracking will initiate and propagate. Although the stiffness varies along the length of the beam during fatigue testing, for interpreting measured deflections, it is assumed that there is a constant stiffness throughout the beam. A study by Pronk (2009) on the stiffness variation of an asphalt beam during four-point fatigue testing showed that errors are induced in the data measurement if the beam stiffness does not reduce at the same rate as that of the mid-section. Pronk (2009) recommends using strain gauges when performing fatigue tests so as to determine the rate of stiffness reduction in the outer sections and thereby establishing correction factors.

Energy Ratio

Rowe and Bouldin (2000) introduced the Energy Ratio for modeling fatigue behavior. The Energy Ratio approach is based on a stress-controlled study by Hopman et al. (1989) which claims to identify the point at which micro-cracking becomes a macro-crack (defined as fatigue failure). The Energy Ratio is obtained by multiplying stiffness by corresponding number of cycle. Laboratory fatigue testing is conducted until flexural stiffness is reduced to at least 20 percent.

The Energy Ratio is cross plotted against number of cycles to find failure location. Such a plot has two distinct regions. In first region, the stiffness parameter is monotonically increasing where as in second region stiffness parameter is monotonically decreasing. The reduction in stiffness is linear (dE^*/dn = slope = constant) in the micro-crack formation phase. As cracks form

and begin to propagate, the relative damage (*dE*/dn*) accelerates and resulting product, the energy ratio (*ER*), decreases. The junction of these two regions indicates peak value of stiffness parameter. The peak in the curve indicates the transition point between micro-crack formation and propagation of a macroscopic crack, as shown in Figure 2.4. The point at which the maximum value of *ER* occurs is defined as the fatigue failure. The peak value can be identified by systematic search or by curve fitting. A systematic search can be made to locate maximum value and then back-calculating number of cycles. The Energy Ratio is defined in Eq. 2.6:

$$Energy\ Ratio\ (ER) = (E_i/E_0)\ x\ N_i \tag{2.6}$$

where E_0 is the initial flexural stiffness (MPa) E_i is the flexural stiffness at cycle *i* (MPa), and N_i is cycle number.

Rowe and Bouldin (200) point out that beam samples showing 50 percent $|E_0^*|$ reduction may not yet experience crack initiation. The authors recommend that testing be conducted until the modulus has dropped to 20 percent $|E_0^*|$. Another disadvantage with traditional controlled stress (strain) tests is that they do not show the point where micro-crack formations become macro-crack formations (defined as fatigue failure), as highlighted in Figure 2.4.

Traditional FEL Criteria

Finally, when a beam sample is subjected to 50 million cycles or more, it is considered to have a FEL close to that applied strain level. To better define the

exact FEL, further fatigue testing may be required at a slightly higher strain to identify the approximate FEL of the mixture. Target failure by loading cycles is determined by the Highway Capacity manual (2000) which states that 500 million load cycles is estimated as the maximum possible number of load repetitions expected in a 40 year period. When considering a shift factor of 10, laboratory testing to 50 million cycles would equate to approximately 500 million loading cycles in the field. Based on these analyses, a mix which provided 50 million cycles or more is considered to be below the FEL.

2.2.3 Fatigue Analysis Approaches

The trend of fatigue analysis approaches has changed significantly over the past decade due to the rapid growth in computer technology. Initially, empirical approaches are used to determine fatigue behavior in HMA. However, the introduction of damage mechanics, discrete element analysis, dissipated energy and fracture mechanics along with flexure, direct, and/or indirect tension testing has brought about a shift from empirical-based approaches to mechanistic-based approaches. This has allowed for a more fundamental understanding of crack initiation, propagation and fracture.

Traditionally, FEL testing is conducted to a maximum of 50 million cycles which may take as long as two months to complete. This amount of time is not practical for routine determination of a FEL. Reducing fatigue testing and introducing a function (Weibull, Power, logarithmic etc.) to extrapolate the strain level required

to reach 50 million cycles is one way to reduce testing time. Furthermore, the use of fatigue analysis approaches reduces extensive testing time required to confirm the existence of FEL. Previous studies show the time-saving benefits of applying fatigue analysis approaches to determining the FEL of HMA mixes (Prowell et al. 2008, Carpenter and Shen 2005, 2006, and 2007, Carpenter et al. 2003). Fatigue analysis approaches include energy-based techniques as well as viscoelastic damage mechanics models and extrapolation techniques. Each of these approaches are described in the following sections.

RDEC Approach

The Ratio of Dissipated Energy Change (RDEC) approach is perhaps the most refined energy method, which can be used not only to extrapolate fatigue life, but also determine the FEL. The RDEC is defined as the difference in dissipated energy between two loading cycles which contributes to damage. In other words, the area found inside a hysteresis loop (created during cyclic loading and unloading of HMA) is the dissipated energy. The difference in area of each loop indicates the damage produced by dissipated energy.

$$RDEC = \left(\frac{DE_n - DE_{n+x}}{DE_n}\right) \div x \tag{2.7}$$

where DE_n = total dissipated energy at cycle n, DE_{n+x} = total dissipated energy at cycle $n+x$, and x = the number of cycles between the two data points.

Previous studies by Ghuzlan (2001) and Carpenter et al. (2003) described the damage curve using the RDEC versus loading cycles shown in Figure 2.5. It can be seen that the damage curve is separated into three stages: the initial period (Stage I), the plateau period (Stage II), and the failure period (Stage III). Stage I shows rapidly decreasing dissipated energy ratio which indicates 'settling' of the beam sample. The average dissipated energy ratio in Stage II is known as plateau value. The plateau stage is when a constant percentage of dissipated energy produces damage. This behavior continues until an increase in dissipated energy ratio occurs which signifies fatigue failure and unstable crack propagation (Stage III).

From the plateau stage (Stage II), a value can be determined which indicates fatigue failure in a sample. This is called the Plateau Value and is defined as the RDEC value at the number of cycles equal to the failure point (N_{f50}). Failure is defined as a 50 percent reduction in initial stiffness, with the initial stiffness being determined at the 50^{th} loading cycle. Lower PVs correspond to longer fatigue lives (Ghuzlan and Carpenter 2000). According to Carpenter and Shen (2005, 2006, and 2009), the PV-N_f relationship is not mixture specific and is supposedly independent of temperature, mode of loading, frequency, and healing capacity (rest periods). However, the relationship between the strain amplitude and the PV must be determined for each HMA mixture.

The PV approach can also be used to determine the effects of mixture variables on the fatigue life. A study by Shen and Carpenter (2007) produced a PV prediction model based on applied strain and material properties. By varying material properties such as binder content, flexural stiffness, nominal maximum size of aggregate gradation, the predicted PV changes, and in turn the predicted fatigue life is changes. Therefore, this unique *PV*-N_f relationship suggests that the PV can be used to predict fatigue life (damage) as well as the effect of mixture variables and load on the fatigue life.

Furthermore, the PV approach can also be used to determine the FEL. A study by Carpenter and Shen (2005), included fatigue testing of 98 different mixtures, using both modes of loading (stress and strain), and varying rest periods (0-0.4 sec) and frequency (0.5-10 Hz). From the *PV*-N_f relationship, a PV threshold is identified where the fatigue behavior changes considerably between low and normal strain fatigue tests. Below PV of 6.74e-09, HMA mixtures showed extraordinary long fatigue life regardless of applied strain amplitude. Therefore, a strain level which provides a PV of 6.74e-09 or less, indicates FEL behavior.

In this study, a relationship between the PV and the strain amplitude, which is not independent of mixture or temperature, is developed. The PV-strain amplitude relationship is used to predict the strain amplitude that yields a PV of $6.74e^{-09}$ which is the FEL.

$$PV = \alpha(\varepsilon)^{\beta} \tag{2.8}$$

where ε = strain amplitude, and α and β are regression coefficients (Carpenter and Shen 2005, Underwood and Kim 2009).

Pseudo Strain Approach

Some fatigue analysis approaches such as the RDEC approach consider asphalt concrete as an elastic material. However asphalt concrete is a viscoelastic material and exhibits rate dependent and temperature dependent behavior. Kim (1988) successfully applied the elastic-viscoelastic correspondence principle for modeling sand-asphalt mixture behavior under multi level cyclic loading. With the elastic-viscoelastic correspondence principle, the physical strain ε in the elastic theory is replaced with a pseudostrain, ε^R. A pseudo strain is similar to a physical strain, except that it is independent of time or loading history. The pseudostrain accounts for the linear viscoelastic hereditary effects of the material through the convolution integral (Eqn. 2.9) so that damage may be evaluated separately from viscoelastic effects. Without this substitution, identifying damage during cyclic loading is very difficult as there may only be a slight difference in hysteresis loops. The hysteresis loop itself is a direct result of the viscoelastic response of asphalt concrete. However, when applying very low strains, i.e. no damage occurring, the hysteresis loops should lie on top of one another. By applying a pseudo strain, the hysteresis loop collapses and the stress-strain curve should forms a straight line (line of equality). However, if damage occurs, then the line of equality changes whereby (*i*) a reduction in the slope of the pseudo

strain line (secant pseudo stiffness) occurs, and/or (*ii*) the pseudo strain line forms a loop.

$$\varepsilon^{R} = \frac{1}{E_R}\int_0^t E(t-t')\frac{\partial' \varepsilon}{\partial t'}dt' \tag{2.9}$$

where E(t, t′) = relaxation modulus; and E_R = constant reference modulus (usually taken as unity).

The relaxation modulus describes the linear visoelastic properties and is determined from dynamic modulus (E*) testing. Data obtained from the E* testing is used to develop a mastercurve and from this, the relaxation modulus is determined.

Kim (1988) found that the secant pseudostiffness (stress corresponding to maximum pseudostrain divided by maximum pseudostrain in each cycle) value decreases with increasing damage. Daniel (Daniel 2001, Daniel and Kim 2002) found that the relationship between the normalized pseudostiffness (*C1*) and the damage parameter (*S1*) is unique for a given asphalt concrete mix (hereafter referred to as damage characteristic curve) under uniaxial mode of loading. The normalized pseudostiffness (*C1*) is obtained by dividing secant pseudostiffness by initial pseudostiffness, while damage parameter (S1) is a function of normalized pseudostiffness, time and material properties and is shown in Eq. 2.10.

$$S1_i \cong \sum_{i=1}^{N}\left[\frac{I}{2}\left(\varepsilon_{max,i}^{R}\right)^2 (C1_{i-1} - C1_i)\right]^{\frac{\alpha}{1+\alpha}} (t_i - t_{i-1})^{\frac{1}{1+\alpha}} \tag{2.10}$$

where $\varepsilon^{R}_{max,i}$ = maximum pseudostrain in cycle *i*, $C1_i$ = normalized pseudostiffness in cycle *i*, $S1_i$ = damage parameter in cycle *i*, α = material constant and *t* = time to maximum pseudostrain in cycle *i*.

Due to continuous growth of damage, numerical value of damage parameter continuously increases (with initial value of 0). Further, the normalized pseudostiffness is plotted against the damage parameter to obtain damage characteristic curve. Swamy (2011) extended viscoelastic continuum damage mode to flexure mode of loading and found that damage characteristic curve is unique at given temperature under flexure mode of loading. Swamy and Daniel (2011) found a point of inflection in the damage characteristic curve beyond which the material loses its structural integrity at faster rate. Also, it is observed that normalized pseudostiffness at this inflection point depends on mixture properties. The failure criterion used by Swamy and Daniel (2011) is included in Chapter V where different HMA fatigue failure criteria are analyzed.

The pseudostrain approach can also be used to determine the FEL of HMA. Pseudo strain calculation requires time history of the applied strain. This is achieved using increasing strain amplitude testing where direct tension or uniaxial tension testing is usually performed. Finally, using a cross-plot of stress vs. pseudo strain, damage is identified when there is a reduction in the slope or the appearance of a hysteresis loop. At this point, the FEL can be determined (Kim and Underwood 2009).

2.2.4 Extrapolation Techniques

One of the two main requirements for this analytical approach is to choose the appropriate model for the fatigue analysis. The other main requirement is to determine the minimum number of cycles to use in the model in order to produce an accurate fatigue life estimate. A study done by Prowell et al. discusses five different models used with beam fatigue testing of HMA mixtures; exponential model, logarithmic model, single-stage Weibull function, three-stage Weibull function, and the ratio of dissipated energy change (RDEC). HMA mixtures that did not fail within 50 million cycles are extrapolated to the number of cycles corresponding to 50 percent reduction of the stiffness. In addition, each model is evaluated in terms of predicting fatigue failure, using HMA samples that had fatigue lives of 20-50 million cycles. The authors concluded that the best extrapolation method for low-strain fatigue tests is the single-stage Weibull function, which appeared to be the most conservative and also had the least variability (Prowell et al. 2008).

However, there are some drawbacks to using these models. The AASHTO T321 standard does not state whether all of the data (especially the initial data) should be used when solving the constants of the exponential model. The power, logarithmic and RDEC models all overestimate the fatigue life when applied to tests of low cyclic loads (less than 10 million). These models are recommended for estimating fatigue life at strain levels less than or equal to the FEL. A number of initial cycles also need to be eliminated in order to obtain a good fit to the slope

at high numbers of cycles. Failure to eliminate some of the initial cycles may result in an overestimation of the fatigue life (Prowell et al. 2008).

For this study, the single-stage Weibull function and the RDEC approach are used to extrapolate the fatigue life of HMA samples tested at low and normal strains.

Weibull Single-Stage Function

The single-stage Weibull function has been used before with some success in predicting FEL in HMA, as discussed earlier in Chapter II. The NCHRP Project 646 in particular compared several extrapolation techniques in determining the FEL. The NCHRP Project 646 concluded that the single-stage Weibull function provided the most reliable results, when compared with actual FEL test data. Based on this recommendation, the single-stage Weibull approach is included in this study to predict the fatigue life of low strain tests, and if possible, provide confirmation of the FEL for SP-II and SP-III mixtures. A step-by-step procedure for applying this approach to predicting fatigue life is shown in the NCHRP 646 Project report (Prowell et al. 2010). The general form of the Weibull function is shown in Eq. 2.11:

$$R(t) = exp\left[-\left(\frac{t-\delta}{\theta-\delta}\right)^{\gamma}\right] \quad (2.11)$$

where *R(t)* = the reliability at time *t* where *t* might be time or another life parameter such as loading cycles, γ = the slope, δ = the minimum life, and θ = the characteristic life.

Tsai et al. (2003) adapted this Eq. 2.11 where the minimum life, δ, is assumed to be 0. The general form is then simplified into Eq. 2.12, where the hazard function is equal $1/\gamma$. Since the beam fatigue loading cycles are applied at a constant frequency of 10 Hz, the loading cycles, *n*, can be substituted for time, *t*.

$$S(t) = exp\ (-\lambda \times n^{\gamma}) \tag{2.12}$$

where *S(t)* = probability of survival until time *t*, *n* = number of loading cycles, λ = scale parameter (intercept, b), γ = shape parameter (slope, m).

To characterize fatigue damage, the stiffness ratio (*SR*) is used, which is the stiffness measured at any cycle, divided by the initial stiffness. According to Tsai et al (2002), *SR(n)* can be substituted for *S(t)* given the fact that at any one cycle, the sample has a probability of survival past that cycle equal to the stiffness ratio times 100 percent. Eq. 2.13 allows the scale and shape parameters for laboratory beam fatigue data to be determined by linear regression.

$$ln(-ln(SR)) = ln\ (\lambda) + \gamma \times ln(n) \tag{2.13}$$

This equation is applied to fatigue test data taken from low strain testing. A plot of the data shows the left-hand side of the equation versus the natural logarithm of the number of cycles, and from this, a straight line regression is produced. Using the slope and intercept parameters as well as a SR of 0.5, Equation 2.13 is solved for *n* by Excel solver function. This value of *n* is the extrapolated fatigue life for 50 percent initial stiffness.

Figure 2.6 presents typical fatigue curves of two HMA samples fitted to the single-stage Weibull function. Both samples are tested at the same strain, and the point where both curves intersect is where both tests initiated. However, from this point on, both curves diverge and follow different paths. The paths are indicative of the rate of fatigue damage occurring in both samples. From this, one can see that sample K_2 has a much steeper slope, which corresponds to a higher rate of fatigue damage, and hence a shorter fatigue life. A linear regression of the curves is shown which can be used to estimate fatigue life using Eq. 2.13.

Fatigue Life Extrapolation Using RDEC Approach

For fatigue testing at normal strain amplitudes, the number of cycles to failure, N_{f50}, is plotted versus the dissipated energy (kPa). Figure 2.7 shows an example of the DE-LC relationship for an SP-II mixture. A best fit equation for the DE-LC data is obtained, using a power law relationship. From the best fit equation, the slope, *f*, of the curve, is noted. As stated earlier, the RDEC is defined as the ratio of dissipated energy change between two loading cycles by the number between the cycles, that is, the average ratio of dissipated energy change per loading cycles, as seen in Eq. 2.7. However, because of the presence of noise in the raw data, the average RDEC for an arbitrary 100 cycles at cycle '*n*' is calculated using Eq. 2.14.

$$RDEC_n = \frac{1-\left(1+\frac{100}{n}\right)^f}{100} \tag{2.14}$$

where *f* = the slope from the regressed DE-LC curve.

PV calculation from low strain fatigue test data is similar to what is shown above for normal strain testing. The RDEC (Eq. 2.7) versus loading cycles is plotted using a log-log scale. Carpenter and Shen's unique PV-N_f curve, Eq. 2.15, is then used with fatigue test data (N_{f50}) from previous fatigue tests performed at normal strain amplitudes. The intersection of these two curves is the estimated fatigue life of the sample tested at low strain. Figure 2.6 provides an example of a RDEC vs. loading cycle curve for a fatigue test (SP-II-L2) conducted at low strain. Shown on the same plot is a curve displaying the fatigue life of tests conducted at normal strain, which are fitted Eq. 2.15.

$$PV = 0.4428{N_{f50}}^{-1.1102} \tag{2.15}$$

The RDEC-LC curve is extended until it crosses the unique PV-N_f curve. The intersection point of these two curves produces the PV (y) and N_{f50} (x). The PV and N_{f50} are then calculated using Eq. 2.16 and 2.17, respectively.

$$PV = \frac{1-\left(1+\frac{100}{N_{f50}}\right)^{f}}{100} \approx -\frac{f}{N_{f50}} \tag{2.16}$$

$$N_{f50} = \left(\frac{-f}{0.4428}\right)^{-9.0744} \tag{2.17}$$

2.3 Factors Affecting the FEL of Asphalt Concrete

2.3.1 Effects of Rest Periods

An important concept that has been highlighted recently in pavement design, which directly affects the FEL of HMA, is damage recovery or healing that occurs during rest periods. Current research undertaken by the National Cooperative Highway Research Program considers this concept as their primary objective in

designing a perpetual pavement. The aim of the research is to design/build a pavement that ensures that the damage induced by the loading is low enough so that healing occurs. Therefore, there is no accumulation of damage over the life of the pavement (Advanced Asphalt Technologies 2008). This design approach differs from traditional perpetual pavement design approaches which do not consider healing.

Healing is a well known phenomenon in materials such as polymers, glass and portland cement (Jud and Kausch 1979, Stavrinidis et al. 1983, Sukhotskaya et al. 1983, Clear 1985, and Edvardsen 1999). The healing phenomenon is generally considered as the capability of a material's self-recovery which occurs between loads when damage is reversed as the asphalt–aggregate interface reattaches, thereby closing microcracks. However, according to some researchers, it is a continuous physical-chemical reaction that may occur as applied load damage develops, not just between load applications (Carpenter and Shen 2006). According to another study by Freund and Suresh (2003), when considering a viscoelastic material such as HMA, the actual fatigue behavior can be explained as energy equilibrium between surface energy and the dissipated damage energy. Healing potential is the difference between surface energy and the dissipated damage energy. Little et al. (1999) showed that surface energy is responsible for microcrack damage rates using Schapery's viscoelastic fracture theory. According to Little et al., if surface energy is smaller than the dissipated damage energy, the healing potential is negative; hence the material will increase surface energy

through microcracking. This is the process of crack initiation and propagation (damage). However, if the dissipated damage energy is low, the positive healing potential controls the energy equilibrium whereby a reduction in surface energy will close crack openings through a healing process. The dissipated energy level is determined by external load and internal material properties (Carpenter and Shen 2005).

Another study which helps explain the mechanism of healing in asphalt materials is that of Petersen (1984), which stated that the association force (secondary bond) is considered the main factor in controlling the physical properties of asphalt. Petersen's concludes that the higher the polarity, the stronger the association forces. Lytton (2000) conducted a similar study which concluded that the fracture or healing of an asphalt mixture is related to two mechanisms: the surface energy storage and the surface energy release. Therefore, microfracture and healing of HMA are governed by the energy balance per unit of crack area between the dissipated energy released and the energy that is stored on the surface of the crack.

However, the effects of healing and its contribution to fatigue life of HMA are very much unknown. As yet, there is no current pavement design method that considers the effects of rest periods under real traffic conditions, except for the use of shift factors, which are arbitrary at best. A study done by Carpenter and Shen (2006) described the effects of healing or rest periods on the fatigue life of

HMA and in particular, explains the existence of a FEL in HMA. Data recorded from strain-controlled flexural-fatigue tests on two different mixes (neat and polymer-modified) is analyzed using the RDEC approach (Carpenter and Shen 2005). Figure 2.8 described the effect of rest periods on two HMA mixes. As the rest period increased, the fatigue life also increased for both HMA mixes (Carpenter and Shen 2006). However, the major disadvantage of this method is the additional time required to incorporate healing. A short rest period of 0.9 second can increase testing time from 3 to 30 hours. A more reasonable rest period of 90 seconds would require 10 to 100 days of continuous testing (Underwood and Kim 2009).

2.3.2 Effect of Applied Strains

There are times during the service life of a perpetual pavement that it will experience strains greater than the design FEL (usually 70 με) which will certainly reduce the fatigue life of the pavement and may even eliminate possible FEL behavior. Some studies have shown that higher applied strains reduce the fatigue life of HMA. In particular, a study by Carpenter and Shen (2006) applied continuous loading on two different HMA mixes and then compared the fatigue test results of both mixes. The study concluded that higher applied strains yielded higher plateau values, which correspond to a lower fatigue life. This result is expected as higher applied strains are more likely to cause more damage. In addition, healing of the HMA requires more time and if full recovery is not achieved, damage accumulates and the fatigue life shortens.

The theory of reduced fatigue life due to higher applied strain levels is discussed in greater detail by Thompson and Carpenter (2004) where they investigated the effects of overloading HMA mixtures beyond the FEL. Cyclic loading is carried out to about 50 million cycles at 70 με on a HMA mixture with a fatigue life of 6 x 10^{11} cycles. At this point the strain level is increased to 500 με and loading is continued for another 6000 cycles. It is also noted that the fatigue life of the undamaged mixture at 500 με is about 20,000 cycles. Following the 6000 cycles, the strain level is reduced to 70 με with the remaining fatigue life expected to be around 2.3 x 10^{11} cycles, which suggests FEL behavior. Thompson and Carpenter's paper (2004) concluded that the effects of overloading do not alter the existence of a FEL. This study also confirms that at higher applied strains, fatigue life is shortened but does not necessarily eliminate the FEL behavior of a perpetual pavement.

2.3.3 Effect of Multiple Temperatures

Environmental effects, especially temperature variations, are considered one of the main contributors to long-life flexible pavement deterioration according to pavement experts in the United Kingdom (Brown et al. 2004). To be of practical use, strain amplitudes on HMA mixes must be applied using a wide range of temperatures. As mentioned previously, applied strains are usually tested in a controlled environment with a temperature of 20°C. Healing can also be considered but the effect of temperature on healing is very much unknown. Some studies indicate that the healing effect of rest periods increases with increasing

temperature (Bonnaure et al. 1982). Research spearheaded by the NCHRP Project 9-19 investigated the effects of using multiple temperatures (along with rest periods) on allowable strains of HMA mixes by applying a time-temperature superposition (Chehab et al. 2003). Results showing allowable to applied strain ratios of a specific HMA mix at different temperatures revealed that critical fatigue cracking conditions are more apparent at low-moderate pavement temperatures (10-15°C). This is expected as fatigue damage is usually reduced at higher temperatures where the HMA mixture softens and the healing rate of damage increases.

2.3.4 Effects of Aging

The effects of aging are very important when characterizing the fatigue life of HMA and the establishing the subsequent FEL. It is well known that as the pavement life ages, the stiffness of the asphalt binder increases and in turn, the dynamic modulus of the HMA increases. Hence, the applied strains must be loared in order to prevent fatigue cracking. In addition, healing of HMA is also affected and one can assume that as the asphalt binder hardens, the healing effect decreases. Only one study has been found from the literature review that comprehensively describes the effects of long-term aging of HMA. Laboratory aging exposure conditions are varied (0, 3, and 6 months) at 60°C which simulated approximately up to 12 years of aging. Results of strain-controlled laboratory testing showed that binder oxidative aging reduced HMA mixture resistance to cracking and its ability to heal. In addition, all mixtures tested

showed an exponentially declining N_f trend due to aging (Walubita 2006). The recent pavement design guide developed by AASHTO, the mechanistic-empirical pavement design guide (MEPDG), uses a global aging model to determine aged modulus values of HMA mixes. Further research is needed in this area to determine the effect of aging on HMA healing and consequently the effect of aging on the FEL.

2.3.5 Effects of Binder Content and Mixture Variables

Research on the effect of mix variables on the FEL of HMA have shown a wide range of FEL values depending on binder selection and HMA mix composition. The FEL of HMA mixtures is said to be affected by mixture variables such as percent air voids, aggregate gradation, asphalt binder content etc. However, from the literature search, there are very few studies about the effect of polymer-modified binders on the FEL. Some studies have shown that using certain polymer binders (PG 76-22) in particular HMA mixtures enhances the ability to withstand fatigue cracking. Therefore, the presence of modified binder in HMA materials should improve the FEL of HMA mixtures (Von Quintas et al. 2004, Prowell et al. 2010). Another study showed mixed results with mixtures containing two different modified binders showing greater fatigue life than mixtures containing one of the unmodified binders. However, mixtures containing unmodified binder with lower temperature susceptibility, achieved two to three times the fatigue life of the polymer modified mixtures (Goodrich 1988).

One particular study utilized the RDEC approach and a fatigue life equation developed by the University of Illinois, to determine the effects of stiffness (flexural), air void content, binder content, and aggregate gradation on the tensile strain experienced in a HMA mixture (Carpenter and Shen 2009). Plateau values are determined for HMA mixtures using the RDEC approach. As stated earlier, the PVs are directly related to the fatigue life of a mixture, with lower PVs indicating longer HMA fatigue lives. The relationship between the PV and mixture variables is developed by Carpenter and Shen (2005) using over 120 mixtures. The equation is shown below;

$$PV = 44.422\varepsilon^{5.140}E^{2.993}VP^{1.850}GP^{-0.4063} \quad (2.18)$$

Where ε = tensile strain, E = flexural stiffness of HMA from laboratory fatigue test, VP = volumetric parameter,

$$VP = \frac{AV}{AV+V_b} \quad (2.19)$$

AV = percent air voids, V_b = asphalt content by volume (Roberts et al. 1996),

$$V_b = 100 \times \frac{G_{mb} \times P_{ac}}{G_b} \quad (2.20)$$

G_{mb} = bulk density of HMA, P_{ac} = percent asphalt content by weight, G_b = bulk specific gravity of binder, GP = aggregate gradation parameter,

$$GP = \frac{P_{NMS} - P_{PCS}}{P_{200}} \quad (2.21)$$

P_{NMS} = percent aggregate passing nominal max. size sieve, P_{PCS} = percent aggregate passing primary control sieve (PCS = NMS*0.22), and P_{200} = percent aggregate passing #200 sieve. Table 2.1 presents PCS data for different nominal size mixtures.

Once the PV is known, the allowable strain, ε, where no damage accumulates, can be determined using Equation 2.2, and this is considered to be the FEL strain of a mixture. Applying a PV of $6.74e^{-09}$, which represents FEL behavior in a HMA mixture (Carpenter and Shen 2005), to Equation 2.22, enables a prediction of the FEL using material properties.

$$FEL = 0.0123E^{-0.5832}VP^{-0.3599}GP^{0.0790} \quad (2.22)$$

The paper concluded that the flexural stiffness, volumetric parameter, percent air voids, and percent asphalt content had the most significant impact on the fatigue life of HMA. Early research conducted by Monismith indicated that an increase in HMA stiffness due to a decrease in air voids, and an optimum asphalt content produced longer HMA fatigue life (Monismith et al. 1970). The mix variable that affected the FEL of HMA the least is the aggregate gradation. Variables included within the aggregate gradation included the gradation parameter, GP, percent passing the nominal maximum size sieve, P_{NMS}, percent passing the primary control sieve, P_{PCS}, and percent passing the #200 sieve, P_{200}. Little or no change is observed due to changes made to these mix variables. Research conducted by Monismith also concludes that aggregate grading also has little effect on fatigue life of HMA (Monismith et al. 1970). However, this conclusion does not seem practical as gradation plays a significant role in the stiffness of HMA mixtures and this in turn may be highly influential on the FEL of HMA (Prowell et al. 2010).

Finally, recent studies (Lee et al. 2002, Von Quintus 2004) have shown that HMA mixtures containing modified binders have a greater laboratory fatigue life than those that contain unmodified binders. However, there are very few studies which have explored this area, and more research is needed in order to know more about the effect of modified binders on the fatigue life of HMA mixtures.

2.4 Correlating Laboratory Testing to Field Performances

Many studies have been conducted to determine the relationship between laboratory fatigue test results and subsequent field performances (Leahy et al. 1995, Pierce and Mahoney 1996, Harvey et al. 1997, Romero et al. 2000, Zhou et al. 2007). The conclusions of some of these studies indicate that the laboratory fatigue life of HMA specimens do not match the field fatigue life of tested pavements (Romero et al. 2000, Zhou et al. 2007). One study in particular tried to identify the relationship between laboratory FEL, measured strains of pavement test sections (National Center for Asphalt Technology, NCAT), and the overall performance of these test sections (Willis and Timm 2009). Results indicated that no relationship could be found between laboratory testing, measured field strains, and overall pavement performance. Although this paper is not successful in its objective, it does illustrate the difficulty in producing laboratory test results that can be related to field performances.

The other alternative to relating laboratory testing to field performances is the application of shift factors. The application of shift factors to laboratory test

results is well documented and from the literature, shift factors vary from 4 to 100 depending on mix design and state agency (Harvey et al. 1997, Priest 2006). It appears that from the literature reviewed, the fatigue life of HMA pavements in the field is much greater than the HMA mixes tested in the laboratory. Reasons for this vary from wheel wander in field pavements and fatigue test methods (loading/temperature variations) to the effect of healing/rest periods on the fatigue life of field pavements (Tangella et al. 1990). However, the use of shift factors clearly underlines the difficulty of applying field fatigue conditions to laboratory fatigue test set ups.

2.5 FEL in Current Flexible Pavement Design

Traditionally the inclusion of fatigue in flexible pavement design requires the use empirical relationships which relate the tensile strain to the number of load cycles to failure. An example of this relationship is shown earlier in Eq. (2.4). This empirical relationship has since been modified based on observed behavior in the field. An example of this can be seen in the Mechanistic Empirical Pavement Design Guide (MEPDG);

$$N_f = K_1(\frac{1}{\varepsilon})^{k_2}[(\frac{1}{E})^{k_3}] \quad (2.23)$$

where N_f = number of cycles to failure, $|E^*|$ is the dynamic modulus of the HMA, and K, n, and b are the regression constants determined from laboratory testing.

2.5.1 MEPDG

The basic inputs for the MEPDG include environmental conditions, materials, and traffic data. The material characterization provides two major inputs; pavement response properties which predict the states of stress, strain and displacement within the pavement due to traffic loading, and distress/transfer functions which relate traffic loading to fatigue cracking, rutting, and other pavement distresses (Walubita 2006). The latest version of the MEPDG considers two fatigue factors; (*i*) a HMA fatigue algorithm shown in Eq. 2.23, and (*ii*) a FEL. The first option determines the tensile strain, ε_t, at the base of the HMA layer due to traffic-induced loading. MEPDG plugs this value into Equation 2.23 to determine N_f which is then used to calculate percent fatigue cracking. The second option compares the calculated ε_t to the predetermined FEL (input value). If the resulting ε_t is below the FEL, fatigue cracking will be negligible (zero). Thompson and Carpenter did a study where they applied a FEL input value and then compared the results with the predicted fatigue cracking (no FEL input) using the HMA fatigue algorithm. Results indicated that the FEL input has very little effect on the estimated HMA fatigue cracking (Thompson and Carpenter 2009).

2.5.2 Illi-Pave

Illi-Pave is a stress-dependent elastic layer program (ELP) developed at the University of Illinois (Thompson and Carpenter 2006). Tensile strains at the base of HMA pavements can be calculated using the following fatigue algorithm developed at the University of Illinois;

$$Log\ \varepsilon_{HMA} = 5.746 - 1.549\ LogT_{HMA} - 0.774\ Log\ E_{HMA} - 0.097\ LogE_{Ri} \quad (2.24)$$

where ε_{HMA} = HMA flexural strain (micro-strain) for a 9-kip wheel load, T_{HMA} = HMA thickness (inches), E_{HMA} = HMA modulus (ksi), and E_{Ri} = subgrade modulus (ksi).

No traffic input is required. Through iterations, the pavement thickness required to achieve a specific FEL can be determined. Illi-Pave is a program that can determine a pavement thickness that ensures HMA strains are less than or equal to the FEL.

2.5.3 PerRoad

Another ELP model widely used is the PerRoad program which is developed at Auburn University, Alabama (Timm and Young 2004). The HMA fatigue algorithm is identical to Eq. 2.4 shown earlier. Fatigue results are presented as the percent of HMA strain less than the FEL, which should be close to 100 percent if a perpetual pavement is required. Basic inputs to PerRoad are similar to those used in the MEPDG and both programs can accommodate FEL as design input. However, the major drawback of these two programs is that predicted HMA strains are not provided as outputs. Thompson and Carpenter emphasized this point in their study on the suitability of these three programs in designing perpetual pavements using the FEL. They also stated that the simplicity of the Illi-Pave procedure is an attractive feature compared to the comprehensive nature of the other two programs. However, the take-home message of this paper is that all

three programs are more than capable of providing perpetual pavement designs (Thompson and Carpenter 2009).

Table 2.1 Control Sieves for Various Asphalt Mixes

	Sieve Size					
NMS mm (in.)	37.5 (1.5)	25 (1)	19 (0.75)	12.5 (0.5)	9.5 (0.375)	4.75 (#4)
PCS mm (in.)	9.5 (0.375)	4.75 (#4)	4.75 (#4)	2.36 (#8)	2.36 (#8)	1.18 (#16)

Note: NMS=Nominal Max Sieve Size, PCS=Primary Control Sieve

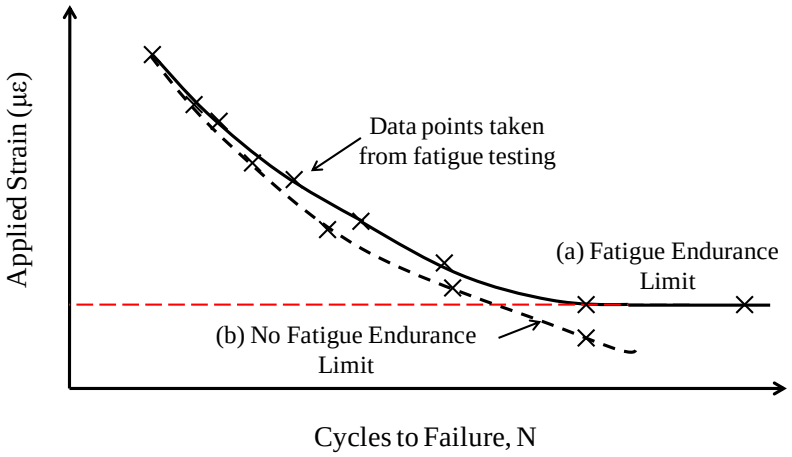

Figure 2.1. Typical S-N Diagram for Laboratory Fatigue Tests:
(a) Endurance Limit; (b) No Endurance Limit (Advanced Asphalt Technologies 2008)

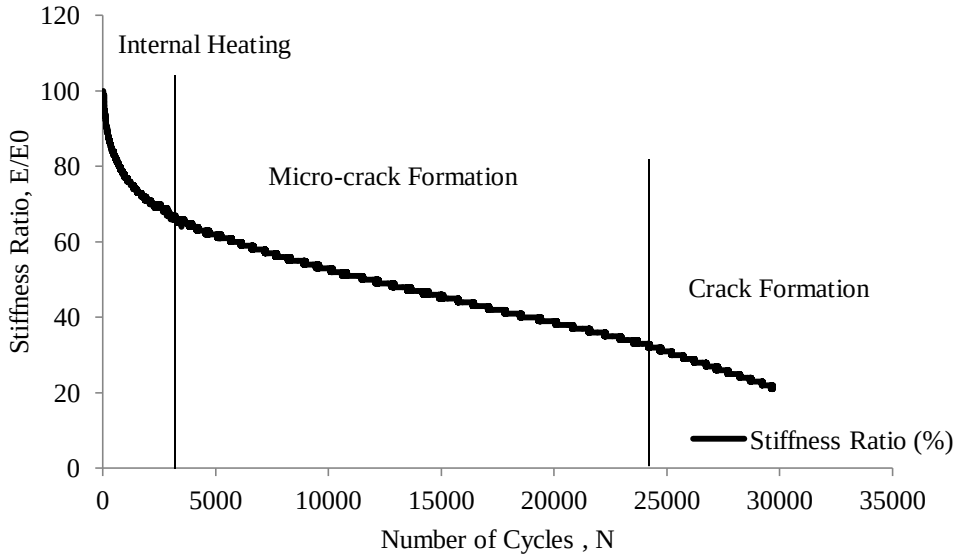

Figure 2.2. Typical Flexural Stiffness Reduction Curve Fatigue Test

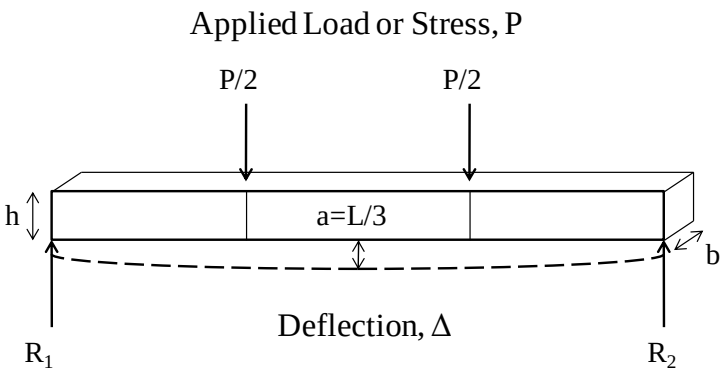

$$\text{Applied Strain, } \varepsilon = \frac{12*h*\Delta}{3L^2 - 4a^2}$$

$$\text{Measured Stress, } \sigma = \frac{P*L}{b*h^2}$$

Figure 2.3 Schematic of Four-Point Beam Fatigue Test

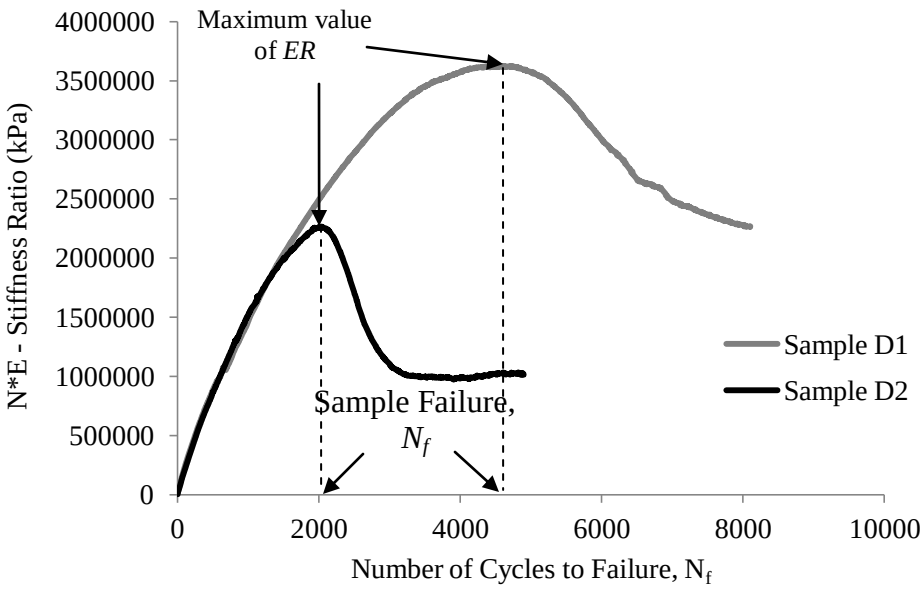

Figure 2.4. Energy Ratio (Rowe) vs. number of cycles to failure

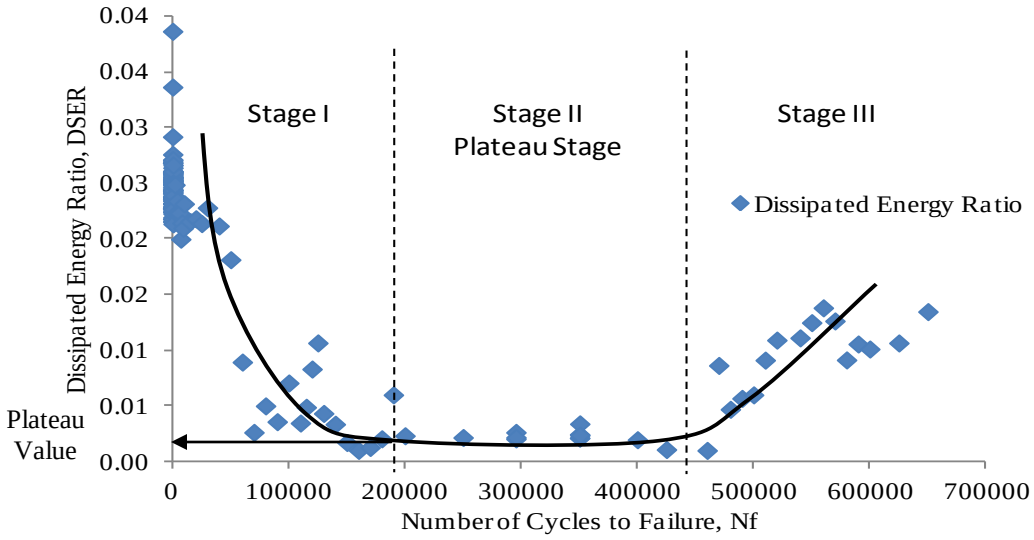

Figure 2.5. Typical Dissipated Energy Ratio Plot Showing Three Stages of Fatigue

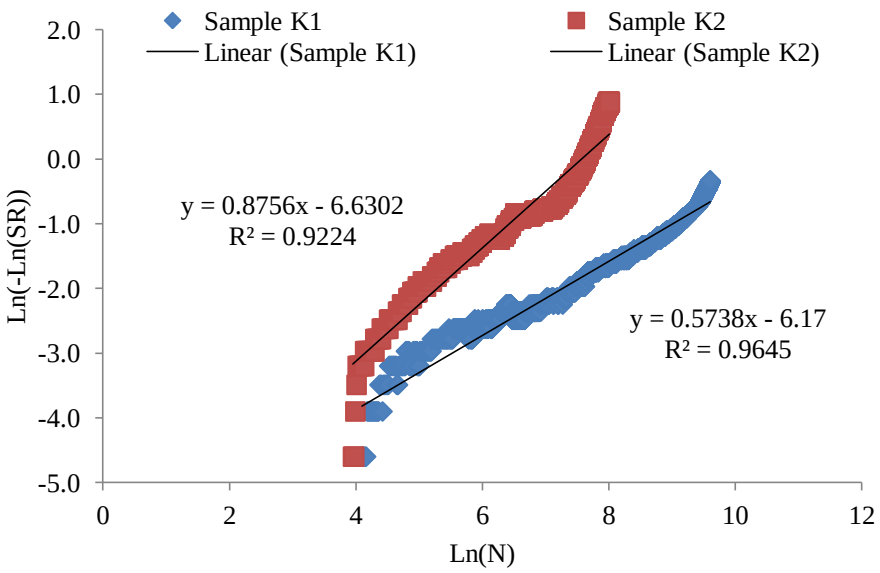

Figure 2.6 Typical Fatigue Curves for SP-II Mixture using Single-Stage Weibull Fuction

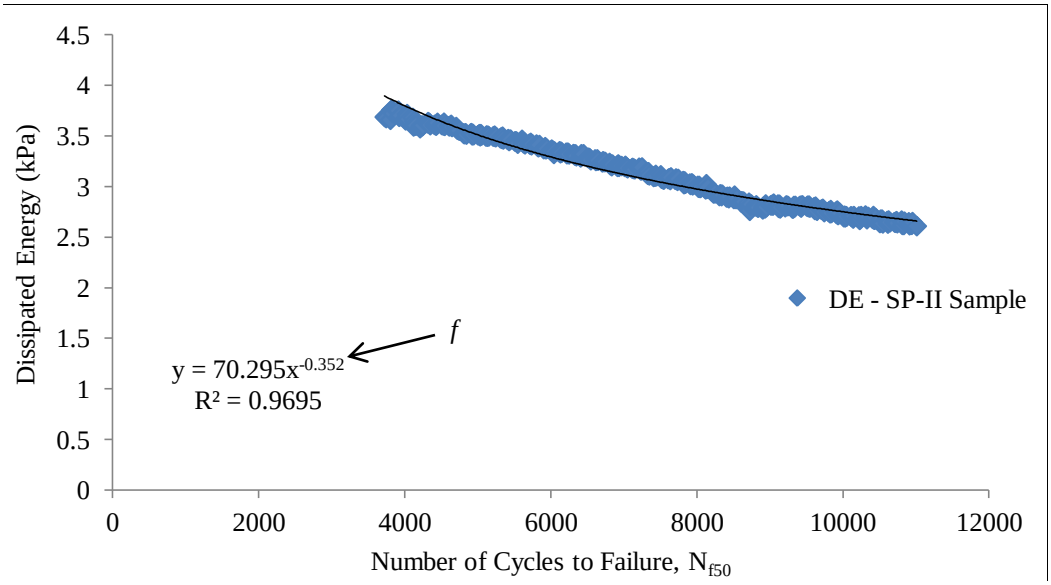

Figure 2.7 Dissipated Energy vs. Number of Cycles to Failure for SP-II Sample

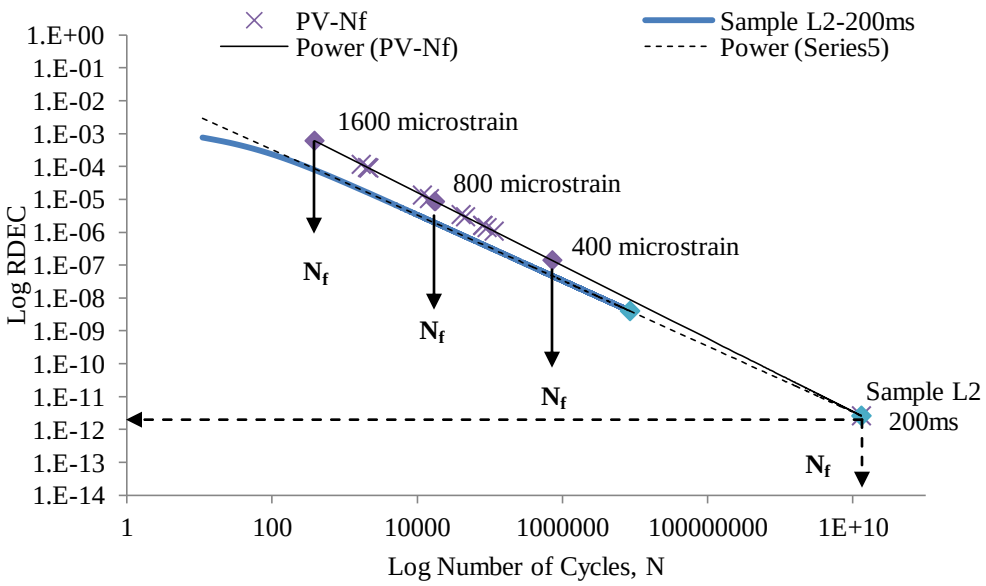

Figure 2.8 Fatigue Life Prediction of SP-II Sample using RDEC Approach

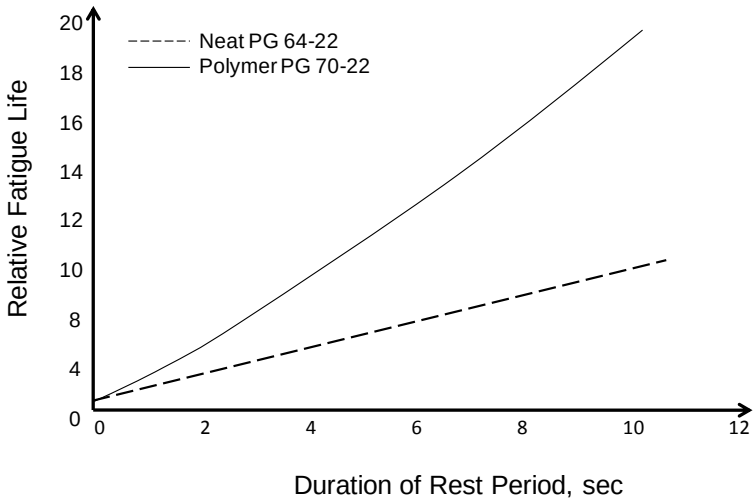

Figure 2.9. Effect of Rest Period on Fatigue Life
(Advanced Asphalt Technologies 2008)

CHAPTER III

EXPERIMENTAL WORK

3.1 General

This chapter describes the experimental plan which includes materials selection and sample preparation. Laboratory fatigue testing is described in this chapter.

3.2 Experimental Plan

Two HMA mixtures: SP-II and SP-III mixtures, which are typically used in major highways and primary routes in the State of New Mexico are used in this study. The SP-II mixture is considered a rut-resistant HMA mixture, predominantly used in intermediate AC layers of a pavement structure. This type of HMA mixture is selected for fatigue analysis on the assumption that although considered a rut-resistant mixture, it may perform poorly in fatigue or other forms of cracking. The SP-III mixture is considered a finer Superpave HMA mixture than SP-II mixture, and is designed with a PG 70-22 binder. SP-III mixture is considered a fatigue resistant HMA mixture usually used in the intermediate and base AC layers of a pavement structure.

HMA mixtures and aggregate materials are obtained from on-site construction projects and from source batch plants. Sampling methods in accordance with AASHTO T-168 (bituminous mixtures) standards and T-2 (aggregates) procedures are followed. In total, about 40-50 bags containing 18-20 kg of HMA

mixtures are collected from the project site and about 25-30 bags of similar weight containing HMA granular materials are also collected from the source batch plant. HMA mixtures are sampled using paper bags (double-bagged) where a smaller sample size is more efficient for the heating/compaction process. Samples of PG 64-22 binder and PG 70-22 binder grades are also collected from the source batch plant.

Laboratory testing is performed to determine the physical properties of the HMA mixtures subsequently used for this project. Laboratory testing includes the bulk specific gravity test (G_{mb}), the theoretical maximum specific gravity test (G_{mm}), as well as binder content and aggregate gradation testing.

3.2.1 HMA Mixture Gradation

Aggregate gradation chart of SP-II and SP-III mixtures is shown in Figure 3.1. Maximum density lines for maximum aggregate sizes of 1 in. and 1.5 in. are plotted in Figure 3.1, corresponding to maximum aggregate sizes of respective SP-III and SP-II mixtures. Mixes that plot above the maximum density line are generally fine mixes while mixes that plot below the maximum density line are generally coarse mixes. Both SP-II and SP-III mixtures plot below their respective maximum density lines. Therefore, SP-II and SP-III are coarse mixes with SP-II somewhat coarser than SP-III due to larger size aggregates. Table 3.1 shows aggregate gradations of three SP-II mixture samples that are tested using AASHTO T30-08 standards. Also shown in Table 3.1 are the upper and lower

limits of the SP-II aggregate gradation. Results show that all three sample gradations fall within these limits. Table 3.2 shows similar results for aggregate gradations of the SP-III mixture, with sample gradations falling within the specified limits.

3.2.2 Selected Binder Grades and Binder Contents

Among the performance grade (PG) binders typically used in New Mexico, the selected binders for this study are PG 64-22 and PG 70-22. Unlike PG 64-22, PG 70-22 is a modified binder with a polymer that improves its high-temperature properties in terms of the shear and viscosity properties. The design asphalt content for SP-II and SP-III mixtures is 4.4% and 4.6% respectively (NMDOT Specifications 2007). Laboratory testing to determine the binder content of SP-II and SP-III mixtures is performed according to AASHTO T 308 standards with the results presented in Table 3.3. Once again, three samples of each HMA mixture are tested and an average percentage of binder content is presented. Results show that the SP-II and SP-III mixtures contain 4.3% and 4.5% respectively.

3.3 Sample Preparation

In the early stages of sample preparation, there are some major concerns in achieving target density of HMA beam specimens which are highlighted and discussed below. The dimensions of the HMA beam samples used in FEL laboratory testing are approximately 380 mm x 65 mm x 50 mm (15″ x 2.5″ x 2″). Samples are compacted to dimensions slightly greater than those shown above

using an asphalt beam compactor (due to mold size). In terms of heating and transferring the HMA mixtures, AASHTO T312 standards are followed. HMA mixtures are heated to 150°C for no more than one hour and are then compacted using a GCTS beam compactor, shown in Figure 3.3. HMA beam samples are compacted using a sinusoidal loading of 80 kN at a frequency of 1 Hz until they reached the specified density (2 in. height). Sample density is determined following AASHTO T 269 standards. There are currently no AASHTO standards for HMA beam compaction so a lot of time is spent adjusting compaction methods in order to achieve the target density. However, the target density of 94.5±0.5% is not achieved with the percentage air voids varying from 9 to 12 %.

The problem of high air voids in specimens lay with the compaction method which is inadequate. Reasons for this may be due to absence of kneading action during the compaction process which provides a better compaction without fracturing the aggregate. However, these issues are resolved with the acquisition of a new linear kneading compactor. Once installed, the target density of 94.5±0.5% for both SP-II and SP-III mixtures is achievable. The compaction method is very similar to what is used in the field. Figure 3.4 shows the linear compactor used by the UNM research team. The compactor is very impressive in terms of size and is made primarily of stainless steel and 1045 steel for rugged functionality. The compactor is driven by a hydraulic unit located next to the compactor which is also shown in Figure 3.4.

The compactor is capable of fabricating two test specimens (18″ x 6″ x 3″) in less than five minutes. Figure 3.5 shows freshly compacted HMA mixtures within the heated molds and those which have been previously compacted.

3.4 HMA Sample Cutting

Once cooled, the compacted HMA specimens are then cut into two beams (15″ x 2.5″ x 2.0″) using a GCTS stone-cutting saw, as shown in Figure 3.6. The stone-cutting saw originally did not come with a clamp which is suitable for cutting beam specimens. So the UNM research team enlisted the help of David Woods who is a prototype machinist from the Department of Mechanical Engineering, UNM. With his help, a new clamp assembly is designed to enable safe and precise cutting of the compacted beams.

3.5 Specimen Volumetric Proportions

The theoretical maximum specific gravity (G_{mm}) of the loose HMA mixtures is determined by using the AASHTO T 209 standards and the results are shown in Table 3.4. The G_{mm} at design AC for SP-II and SP-III mixtures is typically 2.439 and 2.430 respectively (NMDOT Specifications 2007). Three samples of each HMA mixture are tested. Table 3.4 shows that the average G_{mm} for SP-II and SP-III mixtures is 2.401 and 2.420 respectively.

Bulk specific gravity (G_{mb}) testing is performed on HMA beam samples according to AASHTO T 269 standards. NMDOT specifications for HMA percent air voids (AV) call for the G_{mb} to be between 5 to 6%.

3.6 Sample Conditioning

Prior to laboratory fatigue testing, the HMA beam samples are conditioned to simulate short-term aging in the field. Short-term aging of the HMA mixtures is considered during the compaction process whereby loose HMA mixtures are exposed to 163°C for one hour prior to compaction. Once cooled, the beam samples are cut to the dimensions specified earlier. Each sample is then conditioned to test temperature, 20°C, using an environmental test chamber for 2 hours. Figure 3.7 presents the environmental chamber where sample conditioning is conducted.

3.7 Four Point Bending Beam Fatigue Test

This study applies the traditional approach to fatigue analysis of asphalt concrete in accordance with the AASHTO T 321-07 Standards. This approach consists of relating stress (strain) to the number of load repetitions to failure and is described using Wohler Curves. In addition to this, the energy approach is utilized, which defines fatigue life as a function of dissipated energy change with each loading cycle. This is called the Plateau Value approach, as described earlier in Section 2.5.

Cyclic loading using continuous controlled strain is applied to an asphalt concrete beam sample until it fails, where both the critical strain and the number of cycles to failure data is recorded. Figure 3.8 presents the beam fatigue apparatus. Loading is done using a sinusoidal waveform at a frequency of 10 Hz at a fixed temperature of 20°C. Two replicate samples are tested at each strain level. Cyclic loading of the beam sample induces tension in the bottom section where microcracking and subsequent macrocracking will propagate to the top of the beam. This behavior in essence simulates field fatigue cracking due to traffic loading. Fatigue testing is conducted at stain levels varying from 400–1200 με, from which a ε-N relationship is developed, in the form of Eq. 2.4.

Although much has been said about the benefits of including rest periods in fatigue testing, this study did not consider this option due to the additional time required. Rather testing is performed at 10 Hz which simulates traffic speed of 60 mph, similar to what is expected on New Mexico's highways. The time recorded to run each test varied from two hours (high strain) to one month (low strain).

3.8 Selected Mode of Cyclic Loading

Controlled strain mode of loading is selected for this study because it best represents the type of loading experienced by thin pavement layers (2-3 inches). Thin asphalt pavement layers are not the main load-carrying components and the strain in the asphalt layer is governed by the underlying layers, and is not affected by the reduction in asphalt stiffness. Therefore, this creates a constant strain mode

of loading. The SHRP A003-A project, evaluated various laboratory fatigue test methods of asphalt concrete, and stated that unless thick pavements sections are being considered (4-8 inches), controlled strain mode should be used for all fatigue testing (Tangella et al. 1990, Tayebali et al. 1992). For thicker pavements, the asphalt layer is the main load-carrying component and as the asphalt material stiffness reduces, the changes in stress are not significant, which leads to a constant stress mode of loading.

In addition, field fatigue cracking is usually determined by calculating expected strains at the base of the pavement, which means the performance of thick pavements can be determined by constant strains test (Tayebali et al. 1992, Prowell et al. 2010). Finally, perpetual pavements usually contain a thin HMA layer which is placed at the bottom of the section designed especially to resist fatigue cracking. More about perpetual pavements can be found in Appendix A.

3.9 Data Acquisition and Analysis

Laboratory fatigue testing is controlled using GCTS software and fatigue test data is recorded using a GCTS data acquisition system. From this system, test results featuring the stiffness reduction, dissipated energy, Energy Ratio, and applied strain plots are generated.

Table 3.1 Aggregate Gradation for SP-II Mixture

SIEVE SIZE		NMDOT Specification SP-II		PERCENT Passing		
	(mm)	Lower Limit (%)	Upper Limit (%)	Sample A	Sample B	Sample C
2.0″	50.8	100	100	100.00	100.00	100.00
1.5″	38.1	100	100	100.00	100.00	100.00
1.0″	25.4	90	100	97.32	92.18	100.00
3/4″	19	-	90	83.67	87.75	87.98
1/2″	12.7	-	-	58.46	66.70	64.64
3/8″	9.51	-	-	50.27	56.92	54.50
#4	4.76	-	-	33.40	35.82	34.02
#8	2.38	19	45	20.43	21.94	20.81
#16	1.19	-	-	13.75	14.49	13.75
#30	0.595	-	-	9.26	9.59	9.16
#50	0.297	-	-	5.95	5.87	5.66
#100	0.149	-	-	3.36	3.03	2.91
#200	0.075	1	7	1.90	1.40	1.35

Table 3.2 Aggregate Gradation for SP-III Mixture

SIEVE SIZE		NMDOT Specification SP-III		PERCENT Passing		
	(mm)	Lower Limit (%)	Upper Limit (%)	Sample A	Sample B	Sample C
2.0″	50.8	100	100	100.00	100.00	100.00
1.5″	38.1	100	100	100.00	100.00	100.00
1.0″	25.4	100	100	100.00	100.00	100.00
3/4″	19	90	100	95.83	93.58	93.65
1/2″	12.7	-	90	72.11	81.56	70.42
3/8″	9.51	-	-	61.95	62.25	60.78
#4	4.76	-	-	34.78	34.08	34.70
#8	2.38	23	49	25.15	25.52	25.59
#16	1.19	-	-	18.21	18.28	19.05
#30	0.595	-	-	7.90	9.55	8.73
#50	0.297	-	-	5.82	6.01	5.53
#100	0.149	-	-	4.44	4.34	4.15
#200	0.075	2	8	3.03	3.75	3.75

Table 3.3 Asphalt Binder Content for NMDOT SP-II and SP-III Mixtures

Asphalt Binder Content	Sample A	Sample B	Sample C	Average
SP-II	4.13	4.76	4.26	4.38
SP-III	4.29	4.63	4.52	4.48

Table 3.4 Theoretical Maximum Specific Gravity of SP-II and SP-III Mixtures

Max. Theoretical Sp. Gravity (G_{mm})	Sample A	Sample B	Sample C	Average
SP-II	2.416	2.386	2.401	2.401
SP-III	2.414	2.415	2.432	2.420

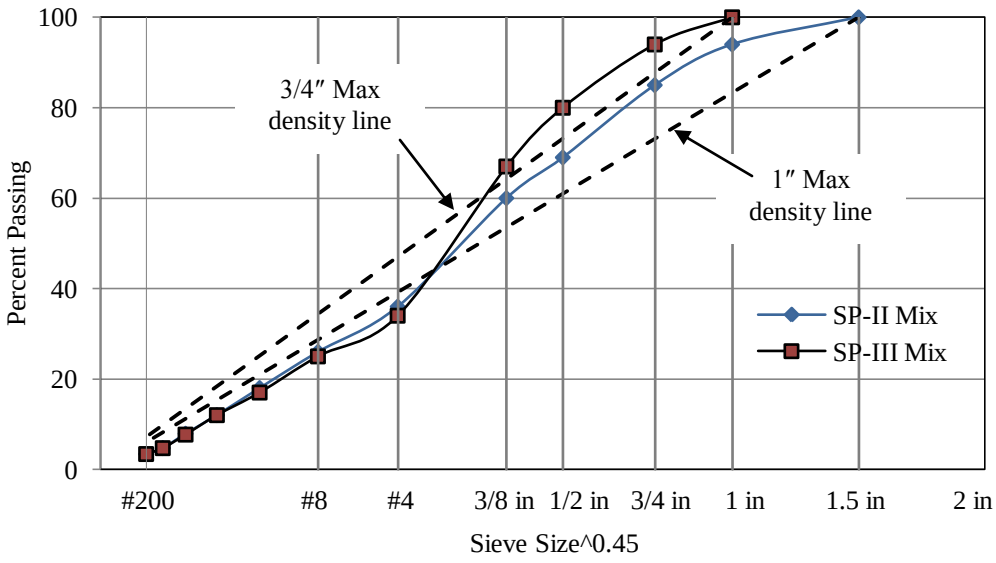

Figure 3.1 Aggregate Gradations for Superpave SP-II and SP-III Mixtures

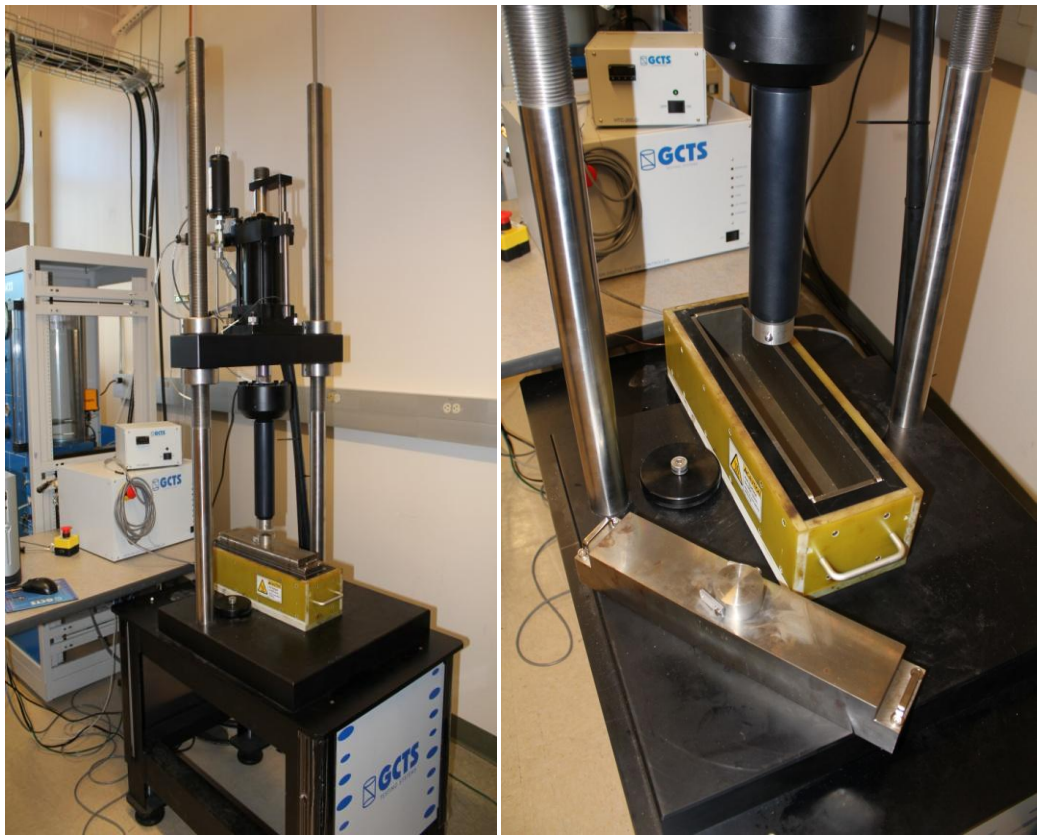

Figure 3.3 Loading Frame and Sample Mold for Beam Compaction

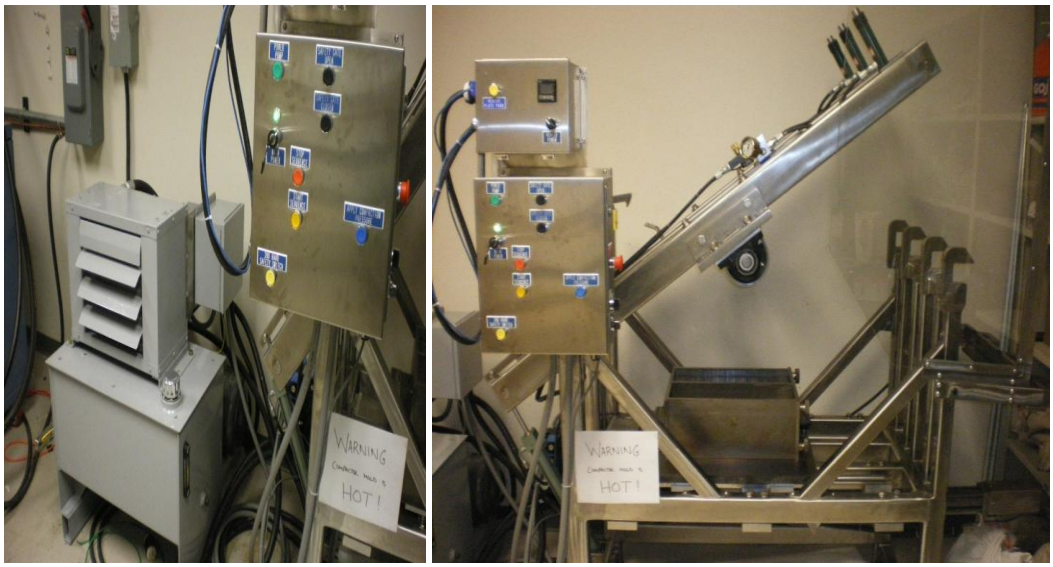

Figure 3.4 PMW Linear Kneading Asphalt Compactor

Figure 3.5 HMA Beam Samples Compacted by Linear Kneading Compactor

Figure 3.6 Stone Cutting Saw with Modified Clamp

Figure 3.7 Environmental Chamber and Beam Fatigue Apparatus

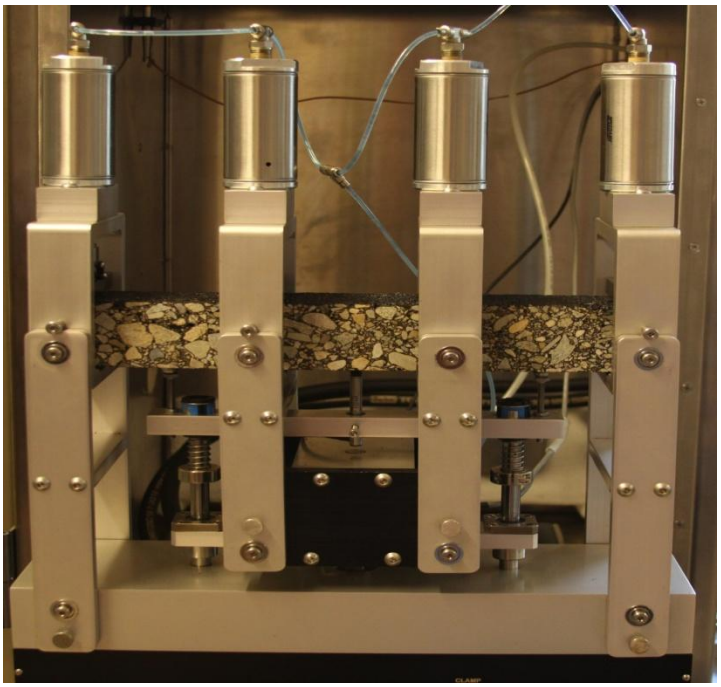

Figure 3.8 Beam Fatigue Apparatus

CHAPTER IV

FATIGUE TEST RESULTS AND ANALYSIS

4.1 Introduction

In this section, laboratory fatigue test results of four HMA mixtures are presented and analyzed. These test results are presented in terms of applied strain amplitude, initial flexural stiffness (psi), percent air voids, and the number of cycles to failure. As stated earlier, fatigue failure is presented using two stiffness-based approaches; number of cycles to attain 50% reduction in stiffness (N_{f50}), and number of cycles at peak Energy Ratio ($N_{f(ER)}$). The Energy Ratio curve is obtained by multiplying stiffness ratio by corresponding cycle number. Laboratory fatigue testing is performed at normal strain amplitudes (600-1200 με) and at low strain amplitudes (200-400 με). Although this study discusses 'normal and low strain' in terms of applied amplitude, these terms are actually referring to the levels of fatigue damage. Low strain usually refers to low damage accumulation whereas normal strain refers to high damage accumulation. In this case, low strain usually ranges from 200-400 με. However, there are some fatigue test results in this study that show high fatigue damage at 400 με.

If the stiffness reduces by 50% as the number of cycles increases, sample is considered failed. Samples which did not fail during testing are analyzed using extrapolation techniques, to determine their fatigue life. The extrapolation

techniques used for this analysis are the single-stage Weibull function, and the RDEC approach. Previous studies have recommended these techniques in providing good results for extrapolating fatigue life data from low strain fatigue testing (Prowell et al. 2008).

4.2 Objective

The objective of this study is to determine the FEL of New Mexico's HMA mixtures by laboratory testing. In addition, two analytical models are used to estimate the FEL: the Plateau Value approach and the phenomenological approach. The estimated FEL values produced from these two models are compared to those estimated by stiffness-based fatigue failure criteria: traditional N_{f50} and Energy Ratio (ER) criteria. In addition, the effect of binder's performance grade (PG) on the estimated FEL of the four HMA mixtures is also investigated.

4.3 Test Matrix

Table 4.1 presents a test matrix describing laboratory fatigue test parameters for this study. Two different mixture types are tested; SP-II and SP-III mixtures, and these mix types are prepared in the laboratory as well as collected from the field. Field SP-II mixture is designed with PG 64-22 binder, while laboratory SP-II mixture is designed with PG 70-22. For the SP-III mixture, the field design contains PG 70-22. However, laboratory SP-III mixture contains PG 64-22

binder. The applied strain amplitude varies from 400 to 1200 με while the percent air voids varies from 5 to 6%.

4.4 Laboratory Fatigue Test Results

Table 4.2 presents laboratory fatigue test results for field-collected HMA mixtures. An alternative Beam ID is shown which represents the mix-type (SP-II or SP-III), the source of the material (F=field, or L=laboratory), replicate sample notation (S_1, S_2, S_3 etc.), and the percent air voids. To prevent confusion with sample referencing, the original Beam ID is also provided. Samples that did not meet the percent air voids target criteria are not considered for further FEL analysis. The PG binder grade used for each mix type is also shown, along with the initial stiffness. The fatigue failure criteria listed in Table 4.2 includes traditional N_{f50} and ER criteria. Figure 4.1 presents stiffness-based failure curves of an SP-II sample, SP-II-N1. The left and right axis describes the stiffness ratio and Energy Ratio behavior with increasing cycles, respectively. SP-II-N1 is tested at 1000 με where failure is recorded at 1,085 cycles and at 1,249 cycles, according to N_{f50} and $N_{f(ER)}$ failure criteria, which is highlighted in Figure 4.1.

Table 4.3 presents laboratory fatigue test results for two HMA mixtures which are prepared in the laboratory. As stated earlier, the only difference between the field and laboratory mixes (SP-II or SP-III) is the binder grade. The respective aggregate gradation and binder content remain the same for both SP-II and SP-III

mixes. Similar to the field mixture fatigue results, the fatigue life of the laboratory HMA mixtures is presented using N_{f50} and $N_{f(ER)}$ failure criteria.

4.5 Analysis of Laboratory Data

Individual fatigue life results (N_{f50} and $N_{f(ER)}$) show considerable variation. For example, SP-II sample N2 has a much lower fatigue life than its replicate, sample A1, and the same can be said again for SP-II samples A1 and M2, even though all three are tested under the same conditions and load. One would attribute to testing three samples can take care of this issue. Figure 4.2 illustrates the varying stiffness reduction rates for these SP-II samples. This may be attributed to the effect of percent air voids, as it can be seen that the fatigue life of these three samples increases as the percent air voids increases. However, this theory does not hold true when looking at the fatigue life data of SP-III samples J1, M2, and F2 (three replicates). These replicate SP-III samples are each tested at 800 με yet their associated fatigue life did not follow the same trend as shown earlier for the SP-II samples. SP-III-M2 had the highest percent air voids of the replicate samples, yet showed a similar fatigue life to SP-III-J1, and much lower fatigue life than SP-III-F2. Due to complex nature of fatigue crack initiation and propagation, replicate samples of similar air voids did not show similar behavior due to density gradient that exists in samples. A more in-depth analysis of the fatigue life of these HMA samples is required and this is shown in Chapter 6. The average fatigue life of replicate samples decreases as the strain amplitude increases, with the exception of SP-II samples, K1 and K2, which did not meet

the target air voids criteria. Finally, there is no apparent trend from Table 4.2 that indicates high initial stiffness has an effect on the associated fatigue life. SP-II sample stiffness varied from 470 to 900 ksi and SP-III sample stiffness varied from 300 to 600 ksi.

In terms of laboratory fatigue life data, Table 4.3 shows a similar trend to what is observed in field HMA mixtures. The majority of the results show replicate samples with lower percent air voids have lower fatigue life. That being said, SP-III samples SP-III-4B and SP-III-10A show the opposite behavior, albeit with percent air voids that are slightly higher the target criteria. SP-II sample stiffness varied from 480 to 830 ksi and for the SP-III samples, initial stiffness varied from 520 to 1000 ksi. Once again, no apparent trend could be seen which suggests that variation in stiffness affects the fatigue life of replicate samples.

Figure 4.3 compares the average fatigue life of field-collected mixtures with laboratory prepared mixtures tested at varying strain amplitudes (N_{f50} results only). It can be seen here that the SP-II samples show similar results, as shown in Figure 4.3(a). For the SP-III mixture, Figure 4.3(b) shows that the fatigue life of the laboratory prepared samples is slightly lower than that shown for the field samples. Mixture variables for laboratory prepared SP-III specimens are identical to those shown in field collected SP-III materials except for the PG binder grade. Laboratory prepared mixtures contained neat PG 64-22 binder, whereas field mixtures used modified PG 70-22. Therefore, the difference in observed fatigue

lives may be attributed to change in PG binder. More discussion on the effect of PG binder on fatigue life of HMA mixtures is shown in Section 4.8.

4.6 Extrapolation of Fatigue Life

Low strain fatigue testing (70 – 500 με) may often lead to an unreasonable number of loading cycles without ever achieving failure. In order to confirm the existence of the endurance limit, fatigue test data from low strain testing needs to be extrapolated to predict a failure point. Table 4.4 shows extrapolated fatigue failure for failed samples as well as those which have not failed. SP-II and SP-III mixtures both contained samples which did not fail; SP-II-L2 and SP-III-B1. For the SP-II sample (SP-II-L2), approximately 8.5 million cycles are run yet the initial stiffness only reduced by 30%. Therefore, the fatigue life is extrapolated using the single-stage Weibull function and the RDEC approach, and the estimated fatigue life is 81.5 million cycles and 102.5 million respectively. Figure 4.4 presents the fatigue curve of SP-II-L2 fitted to the single-stage Weibull function.

SP-III sample, SP-III-B1, yielded a 20% reduction in stiffness after 3.5 million cycles. The fatigue life is extrapolated using the single-stage Weibull function and the RDCE approach, showing an estimated fatigue life of 1.46e09 cycles and 4.81e19 cycles respectively. Although there is no failed fatigue test data to confirm these fatigue lives, the estimated values are extremely high. In order to determine whether these two extrapolation techniques provide reasonable

predictions, fatigue life of failed samples is also predicted. Figure 4.5 compares predicted fatigue life of SP-II samples with the fatigue life recorded from laboratory testing using both extrapolation techniques. It can be seen here that there is good consistency between the predicted and laboratory tested fatigue life, especially for the tradition N_{f50} criterion. For the SP-III samples, Figure 4.6 also shows good consistency, more so for the single-stage Weibull function, whereas the RDEC approach seems to overestimate the fatigue life.

4.6.1 The Effect of Applied Strain on Fatigue Life

The applied strain amplitude plays a vital role in the fatigue life of asphalt concrete. Figure 4.7 shows flexural stiffness vs. initial number of loading cycles for both SP-II and SP-III mixtures tested under increasing strain levels. Figure 4.7(a) shows that even though SP-II samples SP-II-M2 and SP-II-L1 have the same initial stiffness, the fatigue damage rate is much different due to the difference in strain amplitude with sample SP-II-L1 showing a greater reduction in stiffness. The same can be said for SP-III mixtures as shown in Figure 4.7(b). SP-III-E2 has a much higher rate of fatigue damage in the initial cycles, than SP-III-F2. However, as the loading cycles continue the rate of fatigue damage rate reduces where the fatigue curves of both SP-III-E2 and SP-III-F2 show similar stiffness reduction rates. However, sample SP-III-E2 is close to failure as it approaching 50% of its initial stiffness, whereas sample SP-III-F2 will not fail for another 100,000 cycles.

Figure 4.8 also shows strain amplitude vs. the fatigue life curves (ε-N_f) of SP-II mixture. As the tensile strain is reduced, the number of cycles to failure increased, exhibiting an asymptotic curve. This behavior is indicative of FEL, which suggests that below a specific strain level, a material can experience infinite loading cycles without accumulating damage. Figure 4.8(a) features log-log plots of ε-N_f curves fitted to both failure criteria using the power series, where both curves exhibit similar fatigue behavior of SP-II mixtures. The traditional approach (N_{f50}) showing a slightly better fit than that of Rowe's stiffness ratio approach. The same can be said of Figure 4.9(a), where the fatigue curves of the SP-III mixture are almost identical. It must be noted that even though the two different failure criteria provided similar results, the Energy Ratio approach showed samples failing long after they had exceeded the 50% stiffness reduction. Figure 9(b) illustrates the asymptotic behavior of the SP-III mix fatigue curve as the applied strain reduces.

4.7 Fatigue Endurance Limit Prediction

The fatigue endurance limit of SP-II and SP-III mixtures is determined using two different approaches: (*i*) the strain amplitude-fatigue life (ε-N) approach, and (*ii*) the RDEC approach. The ε-N approach is considered the traditional approach to determining the FEL which is equivalent to 50 million cycles. The RDEC approach applies the unique PV-N_f relationship where the strain amplitude which yields a PV equivalent to a fatigue life of 50 million cycles is deemed the FEL.

4.7.1 FEL Prediction Using the ε-N_f Method

Plots (log-log) of applied strain levels versus the number cycles to failure (ε-N_f) of field SP-II and SP-III mixtures are shown in Figure 4.8 and Figure 4.9. Research has shown that the log-log transformation of the data from tests conducted at normal strain levels (above the endurance limit) produce a straight line (Prowell et al. 2010). A fatigue life of 50 million cycles is used to predict the micro-strain level which is equivalent to the fatigue endurance limit. Using Eq. 4.1, and the FEL is determined.

$$FEL = \alpha(N)^{\beta} \tag{4.1}$$

where α and β are regression coefficients, and N = 50 million cycles.

Using the ε-N_f models, the strain which is equivalent to a fatigue life of 50 million cycles is determined. For the field SP-II mixtures, a FEL of 195 με is predicted using N_{f50} criterion and 231 με using ER failure criterion. These FEL values are reasonable considering that fatigue testing of SP-II-L2 sample at 200 με provided an extremely high number of cycles which required extrapolation to determine failure. Furthermore, the FEL values shown for the SP-II mixture in this study are similar to what has been shown for HMA mixtures in previous studies (Prowell et al. 2010).

In terms of the field SP-III mixtures, a FEL of 308 με is predicted using traditional N_{f50} criterion, and 313 με using the ER criterion. These values seem high but not unreasonable. Due to the mixture variables, such as the use of a

modified binder and higher binder content, the FEL can be significantly different from different mixtures. Some studies have shown that the presence of a modified binder in HMA mixtures may improve fatigue resistance (Von Quintas 2004).

4.7.2 FEL Prediction Using the RDEC

In this study, the Ratio of Dissipated Energy Approach (RDEC) approach is used to predict the FEL of HMA mixtures by determining the relationship between the Plateau Value (PV) and the strain amplitude, which is not independent of mixture or temperature. The PV-strain amplitude relationship allowed for the prediction of the strain amplitude that yields a PV of $6.74e^{-09}$ i.e. N_f = $1.1e^{7}$ loading cycles, which is the FEL.

$$PV = \alpha(\varepsilon)^{\beta} \tag{4.2}$$

where ε = strain amplitude, and α and β are regression coefficients (Carpenter and Shen 2005, Underwood and Kim 2009).

Figure 4.10 presents the ε-PV curves for field SP-II and SP-III mixtures. It can be seen here that the mixture with the lower PV corresponding to induced damage for the same strain level has a longer fatigue life; which is the SP-III mixture. The slopes of both curves are very similar which means that the change in percentage of dissipated energy contributing to damage is similar for both mixtures. Using the ε-PV model, the estimated FEL for the field SP-II mixture is 235 με (*ER*) and 222 με (N_{f50}). The FEL of the field SP-III mixture is estimated to be 311 με (*ER*) and 341 με (N_{f50}).

Figure 4.11 presents the PV-N_f relationship for field SP-II and SP-III mixtures and is fitted to a power model (solid line). The dotted line represents Carpenter and Shen's relationship which is fitted to the fatigue test data recorded from this study, using Eq. 4.3, shown below.

$$\text{PV} = 0.4428\,(N_f)^{-1.1102} \tag{4.3}$$

It can be seen here that both relationships are almost identical and follow a similar trend. The PV corresponding to the FEL of 6.74e-09 is also plotted on Figure 4.11.

PV Prediction Model

The PV prediction model, which is initially described in Section 2.3.5, uses material properties such as the flexural stiffness (E), Volumetric Parameter (VP), and the Gradation Parameter (GP) are used to predict the PV. Eq. 4.4 presents the PV model;

$$PV = 44.422\varepsilon^{5.140}E^{2.993}VP^{1.850}GP^{-0.4063} \tag{4.4}$$

Where E = flexural stiffness, VP = Volumetric Parameter;

$$VP = \frac{AV}{AV+V_b} \tag{4.5}$$

where AV = percent air voids, V_b = asphalt content by volume (Roberts et al. 1996),

$$V_b = 100 \times \frac{G_{mb} \times P_{ac}}{G_b} \tag{4.6}$$

G_{mb} = bulk density of HMA, P_{ac} = percent asphalt content by weight, G_b = bulk specific gravity of binder (1.019 for PG 64-22, and 1.020 for PG 70-22), *GP* = Gradation Parameter,

$$GP = \frac{P_{NMS} - P_{PCS}}{P_{200}} \quad (4.7)$$

P_{NMS} = percent aggregate passing nominal maximum size sieve, (NMS is defined as one sieve size greater than the first sieve to retain more than 10 percent of the material), P_{PCS} = percent aggregate passing primary control sieve (PCS = NMS*0.22), and P_{200} = percent aggregate passing #200 sieve.

Table 4.6 shows predicted PV values for field SP-II and SP-III mixtures respectively. PV values based on the predictive model (Eq. 4.4) are compared with those measured from tests and Figure 4.12 shows good consistency, with data points loosely following the line of equality but with some scattering. Therefore, it can be said that the PV model is an alternative method to predict the PV of HMA mixtures using only material properties and load/response parameters.

Using this PV predictive model, the FEL is estimated using material properties such as the flexural stiffness (E), Volumetric Parameter (VP), and the Gradation Parameter (GP).

$$FEL = 0.0123E^{-0.5832}VP^{-0.3599}GP^{0.0790} \quad (4.8)$$

The estimated FEL from the PV model is then compared with FEL predictions provided from the two previous models described in this study, the ε-N_f approach and the ε-PV approach.

Using Eq. 4.8, FEL values of 160 με and 207 με are predicted for field SP-II and SP-III mixtures respectively. Table 4.8 compares FEL values for SP-II and SP-II mixtures predicted using the ε-N_f and ε-PV approaches, as well as those predicted using the material properties (Eq. 7.4). It can be seen here that the FEL values estimated using the PV model, are conservative when compared with the other two approaches (ε-N_f and ε-PV), which is not a bad thing in terms of design consideration.

4.8 The Effect of Polymer-Modified Binder on the FEL of HMA Mixtures

As shown in the literature search, there are very few studies about the effect of polymer-modified binders on the FEL. This study performed fatigue testing on four HMA mixture types with two different binder grades, PG 64-22 and PG 70-22. Figure 4.13 presents ε-N_f curves describing the fatigue behavior of laboratory SP-II mixture. A fatigue life of 50 million cycles is used to predict the strain level which is equivalent to the FEL. From the relationships shown in Figure 4.13(a), and using Eq. 4.1, the FEL of the laboratory SP-II mixture is estimated to be 150 με and 191 με, using traditional N_{f50} criterion and Energy Ratio failure criterion respectively. Figure 4.13(b) presents ε-N_f curves of the SP-II mixture without using log-log scale where the estimated FEL using ER criterion is clearly higher

than the FEL using the N_{f50} criterion. Figure 4.14 describes the ε-N_f curve of the SP-III mixtures from which, the FEL is estimated to be 185 με (N_{f50}) and 202 με ($N_{f(ER)}$).

From the above results, the addition of a modified binder, PG 70-22, to the SP-II mixture, reduced the estimated FEL by 27%. For the SP-III mixture, the use of the neat PG 64-22 binder saw a reduction in the estimated FEL by 30%.

Figure 4.15 presents ε-PV curves describing the fatigue behavior of both laboratory prepared mix types. Once again, the PV of 6.74e-09 is used to estimate the strain level which indicates FEL behavior. Using Eq. 4.2, the FEL of the laboratory SP-II mixture is estimated to be 166 με (N_{f50}) and 213 με ($N_{f(ER)}$). For the laboratory SP-III mixture, the FEL is estimated to be 182 με (N_{f50}) and 170 με ($N_{f(ER)}$). The results show a similar trend to what is found earlier, using the ε-N_f model. The addition of modified binder, PG 70-22, reduced the estimated FEL of the laboratory SP-II mixture by 18%. The FEL of the SP-III mixture containing neat PG 64-22 is almost half (44%) the estimated FEL of the field mixture.

4.9 Laboratory vs. Field Mixture

4.9.1 Fatigue Performance

This section summarizes the fatigue performance of laboratory mixtures and that of field mixtures. Figure 4.16 compares the fatigue life of both laboratory and field mixtures. Figure 4.16(a) shows data points loosely following the line of

unity which indicates similar fatigue life for the SP-II mixture. However, Figure 4.16(b) shows more scatter whereby the fatigue life of the field SP-III mixture seems to be greater than that of the laboratory mixture.

Another way to analyze fatigue life of these mixtures is to compare their PV data. As stated in the literature, the PV represents fatigue life and lower PV indicates longer fatigue life. Figure 4.17 presents PV data for both laboratory and field SP-II and SP-III mixtures. A similar trend to what is shown earlier is also seen here with Figure 4.17(a) showing good consistency, indicating similar fatigue life for laboratory and field mixtures. Figure 4.17(b) confirms the earlier observation that the fatigue life of the field SP-III mixture is much longer than that of the laboratory mixture with lower PV data indicating greater fatigue life.

4.9.2 Predicted FEL

The predicted FEL values for all four mix types are shown in Table 4.8. It can be seen here that the FEL of laboratory mixtures is much lower than that of the field mixes when looking at the ε-N_f and ε-PV results. However, the PV prediction model shows an increased FEL for the laboratory SP-II mixture, suggesting that the higher PG binder grade improves the estimated FEL. Figure 4.18 presents the predicted FEL values for SP-II and SP-III mixtures using ε-N_f and ε-PV models. It can be seen here that predicted FEL values of the laboratory and field SP-II mixture are very similar for both models. However, there is a significant

difference between the predicted FEL values of the field SP-III mixture than those shown for the laboratory SP-III mixture.

Table 4.9 summarizes the predicted FEL values of the SP-II and SP-III mixtures (field and laboratory). It can be seen here that for the field mixes, the SP-III mix shows higher estimated FEL values than the SP-II mix using both N_{f50} and ER failure criterion. This is largely due to the presence of a stiffer binder grade (polymer-modified), smaller aggregate size (1″ NMS), and less stiffness as shown by the dynamic modulus and relaxation modulus results. However, this is not the case for the laboratory SP-II and SP-III mixes where similar estimated FEL values are shown. This may be largely due to the larger size gradation in the SP-II mixture whereby a stiffer binder grade such as PG 70-22 may not be as effective.

Due to its better fatigue performance and higher FEL values, this study recommends using SP-III mixture with PG 70-22 binder grade in the base layer of future asphalt concrete designs. SP-III mix FEL values can be inserted into the MEPDG program whereby the percentage fatigue cracking can be predicted for the design life. An improvement in predicted fatigue performance allows for reduction in design AC layer thickness which is more cost-effective.

4.10 Statistical Analysis

Statistical analysis was done on the initial flexural stiffness results and the fatigue life data of the SP-II and SP-III field mixtures. In addition, analysis is also

performed on SP-II and SP-III fatigue curves using different failure criteria to determine if they are statistically similar.

4.10.1 Flexural Stiffness Data

Due to a large variation in initial flexural stiffness of test samples, additional samples were prepared and tested under similar conditions. SP-II mixture specimens were prepared with strict control on aggregate gradation using the specifications presented in Chapter 3. The neat PG 64-22 binder is also used in the mix design. Cyclic loading is applied for 500 cycles only with strain amplitude varying from 50 to 200 με. In this way, sample stiffness can be analyzed with minimal damage. The percent air voids varied between 3 to 5%. Table 4.10 presents the testing parameters as well as the stiffness ratio results after 500 cycles. It can be seen here that for samples tested from 50 to 150 με, a slight increase in stiffness ratio is observed. This is most likely due to strain hardening during the initial load cycles before sample stabilizes. For samples tested at 200 με, a slight decrease in stiffness ratio is observed due to damage. Figure 4.19 presents the stiffness ratio results after 500 cycles. It can be clearly seen that samples with different percent air voids show similar stiffness. Therefore, it is concluded that even with stricter control on aggregate gradation during the mix design process, it is extremely difficult to achieve identical stiffness with samples compacted to similar density.

4.10.2 Fatigue Life Data

Replicate samples with large variations in fatigue life data are further analyzed in this section. Based on recommendations made in the NCHRP Project 646, samples which showed a difference between log of the fatigue life greater than 0.69, were not considered for further FEL analysis (Prowell et al. 2010).

4.10.3 Fatigue Results Using N_{f50} and ER Criteria

To determine whether two fatigue curves using the traditional (N_{f50}) and Energy Ratio (ER) approaches, from different mixtures are statistically the same, the F-Test is introduced. The hypothesis, H_o, states that the two failure curves are the same, and H_a states that two curves are different. H_o is rejected if the p-value is less than $\alpha = 0.05$. The p-value is the level of significance, which is defined as the probability of obtaining a value of the test statistic that is more likely to reject H_o than the actual observed value of the test statistic. This probability is computed assuming that the null hypothesis is true. Thus, if the p-value is a small value, then the sample data fail to support H_o, and the decision is to reject H_o (Ott 2001).

The F-test is performed on the ε-N_f and PV-ε curves for both SP-II and SP-III mixtures which are shown in Figures 4.7 through 4.9 using Eq. 4.9.

$$F^* = \left(\frac{SSE(R) - SSE(F)}{df(R) - df(F)} \div \frac{SSE(F)}{df(F)}\right) \quad (4.9)$$

where SSE_1 is the error sum of squares for Regression Curve 1 (N_{f50}), SSE_2 is the error sum of squares for Regression Curve 2 (*ER*), SSE(R) is the combined

regression curve from both mixtures, df(F) is the total degrees of freedom df_1 + df_2, and df(R) is the degree of freedom for the combined regression curve.

The p-value is determined using the Excel function of F probability distribution for the two data sets (FDIST):

$$p - value = FDIST(F^*, df_a, df_b) \quad (4.10)$$

where df_a = df(R) − df(F), and df_b = df(F).

For ε-N regression curves through power law, the p-values for SP-II and SP-III mixtures are 7.21e-26 and 0.995 respectively. Because the p-value is greater than α = 0.05 for the SP-III mixture, the H_o hypothesis is not rejected and it is concluded that the two fatigue curves are statistically the same. However, for the SP-II mixture, the p-value is less than 0.05 which means that the two fatigue curves are different. For PV-ε regression curves through power law, the p-values for SP-II and SP-III mixtures are 0.998 and 0.306 respectively. Because the p-values are greater than α = 0.05 for both mixtures, the H_o hypothesis is not rejected and it is concluded that the two fatigue curves are statistically the same.

4.11 Conclusions

The key features of this study found as:

- Majority of fatigue test results show that fatigue failure according to the Energy Ratio criterion occurred after a sample has achieved 50% reduction in stiffness, which is the traditional fatigue criterion.

- Fatigue life extrapolation using the single-stage Weibull function and RDEC approach showed good consistency with fatigue test results of field SP-II and SP-III mixtures, performed at normal strain levels. However, for low strain testing, extremely high fatigue life data is predicted, which suggests that an overestimation of fatigue life.
- Using the traditional ε-Nf relationship, the FEL values of field SP-II and SP-III mixtures are predicted. The FEL of the SP-II mixture is estimated to be 195 με, using traditional failure criterion (N_{f50}), and 231 με using the Energy Ratio failure criterion (ER). For the SP-III mixture, the FEL is estimated to be 308 με (N_{f50}) and 313 με (ER).
- Using the ε-PV approach, the FEL values of field SP-II and SP-III mixtures are predicted. The FEL of the SP-II mixture is estimated to be 235 με (ER) and 222 με (N_{f50}). For the SP-III mixture, the FEL is estimated to be 311 με (ER) and 341 με (N_{f50}).
- PV values predicted using the material property-based PV prediction model showed good consistency with PV values determined from laboratory testing. However, the estimated FEL values using the PV model are much lower than those predicted using the ε-N_f and ε-PV models.
- The effect of polymer modified binder on the FEL of HMA mixtures showed mixed results, with an increase in estimated FEL of SP-III mixture, but reducing the estimated FEL of SP-II mixture.

- The estimated FEL of laboratory mixtures is much lower than that of the field mixes. In particular, the fatigue performance of laboratory SP-II mixtures compares well with that of field SP-II mixtures. However, the laboratory SP-III mixture performs poorly when compared with fatigue performance of the field SP-III mixture.
- The F-test is performed on the ε-N_f and PV-ε curves to determine whether the curves developed using the traditional (N_{f50}) and Energy Ratio (*ER*) approaches are statistically the same. For ε-N regression curves through power law, it is determined that the two fatigue curves are statistically the same for the SP-III mixture. However, the opposite is the case for the SP-II fatigue curves. For the PV-ε curves, the F-Test shows that the fatigue curves are statistically the same using the different fatigue failure approaches.

Table 4.1 Test Matrix for Laboratory Fatigue Testing of SP-II and SP-III Mixtures

HMA Mix Type	PG Binder	Applied Strain (με)	% Air Voids
SP-II	64-22, 70-22	400, 800, 1000, 1200	5-6
SP-III	64-22, 70-22	400, 800, 1000, 1200	5-6

Table 4.2 Laboratory Fatigue Test Results for Field SP-II and SP-III Mixtures

Alternative Beam ID	Beam ID	Strain ε_t (με)	PG Binder	Stiffness E_0 (psi)	% Air Voids	Failure Criteria		Avg. Cycles to Failure	
						N_{f50}	$N_{f(ER)}$	N_{f50}	$N_{f(ER)}$
SP-II MIXTURE									
SPII-F-400-S1-5.2%	N2	400	64-22	646,000	5.2	79,008	69,069	355,377	469,631
SPII-F-400-S2-5.4%	A1	400	64-22	880,310	5.4	263,411	239,818		
SPII-F-400-S3-5.9%	M2	400	64-22	666,158	5.9	723,711	1,100,007		
SPII-F-800-S1-5.1%	I2	800	64-22	471,000	5.1	11,700	10,910	11,100	45,662
SPII-F-800-S2-5.8%	L1	800	64-22	655,716	5.8	10,500	80,412		
SPII-F-1000-S1-4.8%	N1	1000	64-22	853,302	4.8	1,085	1249	2,795	5,795
SPII-F-1000-S2-5.7%	O2	1000	64-22	531,200	5.7	4,504	10,341		
SPII-F-1200-S3-3.5%	K1	1000	64-22	908,661	3.5	1,684	1,547	8,155	7,288
SPII-F-1200-S4-3.0%	K2	1000	64-22	850,501	3.0	14,625	13,029		
SPII-F-1200-S1-4.7%	E1	1200	64-22	680,645	4.7	1,879	4651	1,108	2,599
SPII-F-1200-S2-4.9%	J2	1200	64-22	711,640	4.9	337	547		
SP-III MIXTURE									
SPIII-F-400-S1-4.9%	B1	400	70-22	537,945	4.9	NA	NA	NA	NA
SPIII-F-600-S1-4.9%	C2	600	70-22	557,499	4.9	770,008	748,820	770,008	748,820
SPIII-F-800-S1-4.7%	J1	800	70-22	455,466	4.7	38001	52,926	71,001	174,289
SPIII-F-800-S2-5.9%	M2	800	70-22	415,678	5.9	42,001	46,826		
SPIII-F-800-S3-5.0%	F2	800	70-22	402,190	5.0	114,001	148,576		
SPIII-F-800-S4-3.7%	I1	800	70-22	275,282	3.7	90,001	448,826		
SPIII-F-1000-S1-4.8%	B2	1000	70-22	433,644	4.8	29,801	35,276	25,201	30,276
SPIII-F-1000-S2-4.8%	P1	1000	70-22	582,762	4.8	20,601	25,276		
SPIII-F-1200-S1-5.0%	P2	1200	70-22	485,731	5.0	6,476	7,551	8,026	22,149
SPIII-F-1200-S2-5.8%	Q2	1200	70-22	451,938	5.8	9,576	34,551		
SPIII-F-1200-S3-2.8%	D1	1200	70-22	355,000	2.8	2050	4408	2,095	3,223
SPIII-F-1200-S4-3.0%	D2	1200	70-22	300,000	3.0	2140	2038		

Note: NA=no data available

Table 4.3 Fatigue Test Results of Laboratory Prepared SP-II and SP-III Mixtures

Alternative Beam ID	Beam ID	Applied ε_t ($\mu\varepsilon$)	PG Binder	Stiffness E_0 (psi)	% Air Voids	Failure Criteria		Avg. Cycles to Failure	
						N_{f50}	$N_{f(ER)}$	N_{f50}	$N_{f(ER)}$
SP-II MIXTURE									
SPII-L-400-S1-4.3%	1A	400	70-22	732,504	4.3	71,618	56,907	237,877	544,477
SPII-L-400-S2-4.5%	1B	400	70-22	680,476	4.5	122,008	875,620		
SPII-L-400-S3-5.1%	5B	400	70-22	834,120	5.1	520,004	700,904		
SPII-L-800-S1-4.7%	2A	800	70-22	579,362	4.7	19,494	18,303	15,827	20,715
SPII-L-800-S2-4.5%	2B	800	70-22	476,521	4.5	12,160	23,127		
SPII-L-1000-S1-5.1%	7A	1000	70-22	675,111	5.1	2,363	3,657	2,240	3,195
SPII-L-1000-S2-4.8%	7B	1000	70-22	707,020	4.8	2,117	2,733		
SPII-L-1200-S1-5.0%	8A	1200	70-22	774,222	5.0	718	787	629	661
SPII-L-1200-S2-5.0%	8B	1200	70-22	697,054	5.0	539	535		
SP-III MIXTURE									
SPII-L-400-S1-4.8%	6A	400	64-22	1,040,810	4.8	146,711	131,514	387,008	442,215
SPII-L-400-S2-5.1%	6B	400	64-22	995,268	5.1	627,304	752,915		
SPII-L-800-S1-5.0%	9A	800	64-22	676,177	5.0	2,300	2,869	7,576	6,581
SPIII-L-800-S2-6.3%	9B	800	64-22	709,450	6.3	2,422	3,243		
SPIII-L-800-S3-6.0%	10B	800	64-22	661,054	6.0	18,006	13,631		
SPIII-L-1000-S1-5.0%	8A	1000	64-22	581,865	5.0	7,200	22,685	6,569	17,666
SPIII-L-1000-S2-6.3%	8B	1000	64-22	522,036	6.3	5,937	12,647		
SPIII-L-1200-S1-6.2%	4B	1200	64-22	610,473	6.2	4,205	3,642	2,558	2,451
SPIII-L-1200-S2-6.5%	10A	1200	64-22	592,931	6.5	910	1,260		

Table 4.4 Extrapolated Fatigue Test Results for Field SP-II and SP-III Mixtures

Alternative Beam ID	Beam ID	Applied ε_t (με)	Stiffnes E_0 (psi)	% Air Voids	Cycles Tested	Extrapolated Cycles to N_{f50}		Failure Criteria	
						RDEC	Weibull	N_{f50}	$N_{f(ER)}$
SP-II MIXTURE									
*SPII-F-200-S1-5.4%	L2	200	954,638	5.4	8,479,090	102,493,275	81,486,025	91,989,650[1]	NA
SPII-F-400-S1-5.2%	N2	400	646,000	5.2	79,008	77,779	86,600	79,008	69,069
SPII-F-400-S2-5.4%	A1	400	880,310	5.4	389,811	222,502	220,900	263,411	239,818
SPII-F-400-S3-5.9%	M2	400	666,158	5.9	723,711	877,612	1,335,000	723,711	1,100,007
SPII-F-800-S1-5.1%	I2	800	471,000	5.1	11,700	11,510	11,940	11,700	10,910
SPII-F-800-S2-5.8%	L1	800	655,716	5.8	90,000	25,097	20,650	10,500	80,412
SPII-F-1000-S1-4.8%	N1	1000	853,302	4.8	2,665	1,486	860	1,085	1,249
SPII-F-1000-S2-5.7%	O2	1000	531,200	5.7	17,256	4,797	4,642	4,504	10,341
SPII-F-1200-S1-3.5%	K1	1000	908,661	3.5	13,148	1,788	2,073	1,684	1,547
SPII-F-1200-S2-3.0%	K2	1000	850,501	3.0	18,046	871	407	14,625	13,029
SPII-F-1200-S3-4.7%	E1	1200	680,645	4.7	6,553	1,964	625	1,879	4,651
SPII-F-1200-S4-4.9%	J2	1200	711,640	4.9	1,542	13,697	24,690	337	547
SP-III MIXTURE									
*SPIII-F-400-S1-4.9%	B1	400	537,945	4.9	3,539,851	4.8E+19	1.5E+09	2.4E+19[1]	NA
SPIII-F-600-S1-4.9%	C2	600	557,499	4.9	833,560	89,727	1,110,000	770,008	748,820
SPIII-F-800-S1-4.8%	J1	800	455,466	4.8	106,276	39,303	24,130	38001	52,926
SPIII-F-800-S2-5.9%	M2	800	415,678	5.9	79,176	23,569	29,900	42,001	46,826
SPIII-F-800-S3-5.0%	F2	800	402,190	5.0	150,000	129,567	71,250	114,001	148,576
SPIII-F-1000-S1-4.8%	B2	1000	433,644	4.8	50,701	32,335	21,250	29,801	35,276
SPIII-F-1000-S2-4.8%	P1	1000	582,762	4.8	40,901	20,832	13,110	20,601	25,276
SPIII-F-1200-S1-5.0%	P2	1200	485,731	5.0	12,326	6,962	5,187	6,476	7,551
SPIII-F-1200-S2-5.8%	Q2	1200	451,938	5.8	52,526	9,704	9,230	9,576	36,746
SPIII-F-1200-S3-2.8%	D1	1200	355,000	2.8	13,949	2,159	2,115	2050	4408
SPIII-F-1200-S4-2.8%	D2	1200	300,000	3.0	4,898	1,963	1,928	2140	2038

Note: NA = no data available, *Samples which did not fail, [1]Results averaged using the RDEC and the Weibull Single-Stage approach.

Table 4.5 Control Sieves for Various Asphalt Mixes

	Sieve Size					
NMS mm (in.)	37.5 (1.5)	25 (1)	19 (0.75)	12.5 (0.5)	9.5 (0.375)	4.75 (#4)
PCS mm (in.)	9.5 (0.375)	4.75 (#4)	4.75 (#4)	2.36 (#8)	2.36 (#8)	1.18 (#16)

Note: NMS=Nominal Max Sieve Size, PCS=Primary Control Sieve

Table 4.6 Plateau Value Results for Field SP-II and SP-III Mixtures

Beam ID	Applied ε_t ($\mu\varepsilon$)	Initial E_0 (psi)	% Air Voids	VP	Failure Criteria		Plateau Values		Predicted
					N_{f50}	$N_{f(ER)}$	PV_{f50}	$PV_{f(ER)}$	PV
SP-II MIXTURE									
N2	400	646,000	5.2	0.3305	79,008	69,069	8.3E-06	9.5E-06	5.2E-07
A1	400	880,310	5.4	0.3390	263,411	239,818	3.5E-07	3.8E-07	1.4E-06
M2	400	666,158	5.9	0.3591	723,711	1,100,007	7.2E-08	4.8E-08	6.6E-07
I2	800	471,000	5.1	0.3263	11,700	10,910	3.2E-05	3.4E-05	6.9E-06
L1	800	655,716	5.8	0.3551	10,500	80,412	1.4E-05	1.8E-06	2.2E-05
N1	1000	853,302	4.8	0.3131	1,085	1249	1.7E-04	1.4E-04	1.2E-04
O2	1000	531,200	5.7	0.3512	4,504	10,341	4.0E-05	1.7E-05	3.6E-05
E1	1200	680,645	4.7	0.3086	1,879	4,651	6.0E-05	2.5E-05	1.5E-04
J2	1200	711,640	4.9	0.3175	337	547	5.3E-04	3.5E-04	1.8E-04
K1	1200	908,661	3.5	0.2494	1,684	1,547	5.2E-05	5.7E-05	9.5E-05
K2	1200	850,501	3.0	0.2217	14,625	13,029	2.0E-05	2.2E-05	6.2E-05
SP-III MIXTURE									
B1	400	537,945	4.9	0.3090	NA	NA	NA	NA	2.60E-07
C2	600	557,499	4.9	0.3090	770,008	748,820	1.6E-07	1.7E-07	2.3E-06
J1	800	455,466	4.8	0.3002	38001	52,926	3.1E-06	2.2E-06	5.3E-06
M2	800	415,678	5.9	0.3500	42,001	46,826	3.5E-06	3.1E-06	5.3E-06
F2	800	402,190	5.0	0.3133	114,001	148,576	8.8E-07	6.7E-07	3.9E-06
B2	1000	433,644	4.8	0.3046	29,801	35,276	6.1E-06	5.2E-06	1.5E-05
P1	1000	582,762	4.8	0.3046	20,601	25,276	7.8E-06	6.4E-06	3.6E-05
P2	1200	485,731	5.0	0.3133	6,476	7,551	2.1E-05	1.8E-05	5.6E-05
Q2	1200	451,938	5.8	0.3461	9,576	36,746	1.4E-05	3.7E-06	5.4E-05

Note: VP = Volumetric Parameter, NA = no data available, [1]Less than 6.74E-9 proposed by Carpenter and Shen (2005) as indicative of long fatigue life.

Table 4.7 Plateau Values Results for Laboratory SP-II and SP-III Mixtures

Beam ID	Applied ε_t (με)	Initial E_0 (psi)	% Air Voids	VP	Failure Criteria		Plateau Values		Predicted
					N_{f50}	$N_{f(ER)}$	PV_{f50}	$PV_{f(ER)}$	PV
SP-II MIXTURE									
1A	400	732,504	4.3	0.2914	71,618	56,907	1.2E-06	1.5E-06	6.0E-07
1B	400	680,476	4.5	0.3008	122,008	875,620	8.3E-07	1.2E-07	5.1E-07
5B	400	834,120	5.1	0.3402	520,004	700,904	2.0E-07	1.5E-07	1.2E-06
2A	800	579,362	4.7	0.3101	19,494	18,303	9.4E-06	1.0E-05	1.2E-05
2B	800	476,521	4.5	0.3008	12,160	23,127	1.6E-05	8.4E-06	6.2E-06
7A	1000	675,111	5.1	0.3278	2,363	3,657	9.1E-05	5.9E-05	6.4E-05
7B	1000	707,020	4.8	0.3146	2,117	2,733	1.6E-04	1.3E-04	6.9E-05
8A	1200	774,222	5.0	0.3235	718	787	4.2E-04	3.8E-04	2.4E-04
8B	1200	697,054	5.0	0.3235	539	535	3.4E-04	3.4E-04	1.8E-04
SP-III MIXTURE									
6A	400	1,040,810	4.8	0.3044	146,711	131,514	6.0E-07	6.7E-07	1.8E-06
6B	400	995,268	5.1	0.3174	627,304	752,915	1.8E-07	1.5E-07	1.7E-06
9A	800	676,177	5.0	0.3131	2,300	2,869	1.2E-04	9.6E-05	1.9E-05
9B	800	709,450	6.3	0.3648	2,422	3,243	1.1E-04	8.3E-05	2.9E-05
10B	800	661,054	6.0	0.3536	18,006	13,631	8.5E-06	1.1E-05	2.2E-05
8A	1000	581,865	5.0	0.3131	7,200	22,685	2.5E-05	7.8E-06	3.7E-05
8B	1000	522,036	6.3	0.3648	5,937	12,647	4.6E-05	2.2E-05	3.6E-05
4B	1200	610,473	6.2	0.3609	4,205	3,642	1.0E-04	1.2E-04	1.4E-04
10A	1200	592,931	6.5	0.3721	910	1,260	1.1E-04	7.9E-05	1.4E-04

Note: VP = Volumetric Parameter

Table 4.8 Predicted FEL Values for SP-II and SP-III Mixes

Failure Criteria	SP-II (64-22)			SP-II (70-22)		
	ε-Nf	ε-PV	PV Model	ε-Nf	ε-PV	PV Model
N_{f50}	195	222	160	171	209	171
$N_{f(ER)}$	231	235		218	268	
	SP-III (64-22)			SP-III (70-22)		
	ε-Nf	ε-PV	PV Model	ε-Nf	ε-PV	PV Model
N_{f50}	185	182	160	308	341	207
$N_{f(ER)}$)	202	268		313	311	

Table 4.9 Summary of FEL Performance of SP-II and SP-III Mixtures

	PG Binder Grade	
Mix Type	SP-II	SP-III
Field	PG 64-22	PG 70-22
Laboratory	PG 70-22	PG 64-22

	Predicted FEL Values (N_{f50})	
Mix Type	SP-II	SP-III
Field	$195^1/222^2$	$308^1/341^2$
Laboratory	$171^1/209^2$	$185^1/182^2$

Note: 1=N_{f50} failure criterion, and 2=ER failure criterion

	Predicted FEL Values (ER)	
Mix Type	SP-II	SP-III
Field	$231^1/235^2$	$313^1/311^2$
Laboratory	$218^1/268^2$	$202^1/268^2$

Note: 1=N_{f50} failure criterion, and 2=ER failure criterion

Field Mixtures	
SP-II	SP-III
High E*	Low E*
High E(t)	Low E(t)

Note: E*=Dynamic Modulus, E(t)=relaxation modulus

Table 4.10 Test Parameters and Results of SP-II (PG 64-22) Mixture

SP-II PG 64-22 Beam ID	% Air Voids	Initial E_0 (psi)	Initial E_0 (MPa)	Applied Strain (με)	Cycles Tested	Stiffness Reduction, %
1A	2.6	1,233,225	8,505	50	500	102
1B	2.2	1,575,429	10,865	50	500	103
2A	4	1,099,080	7,580	150	500	100
2B	3.8	1,356,160	9,353	150	500	102
3A	4.1	1,073,744	7,405	200	500	95
3B	3.9	914,264	6,305	200	500	95
5A	4.6	1,028,389	7,092	100	500	101
5B	4.6	1,221,856	8,427	100	500	103

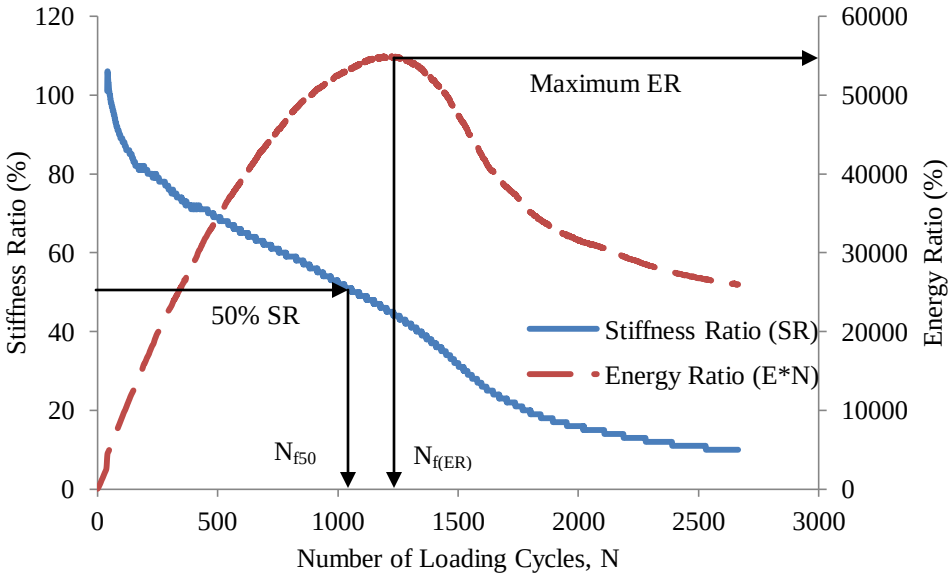

Figure 4.1 Variation of Stiffness Ratio and Energy Ratio with Number of Loading Cycles of SP-II-N1 Sample

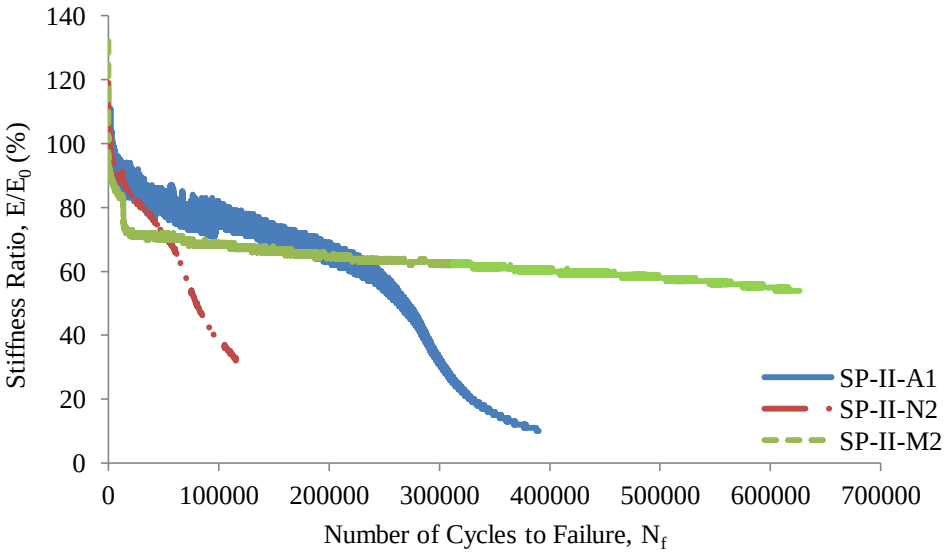

Figure 4.2. Stiffness Ratio Reduction Curves of Replicate SP-II Samples

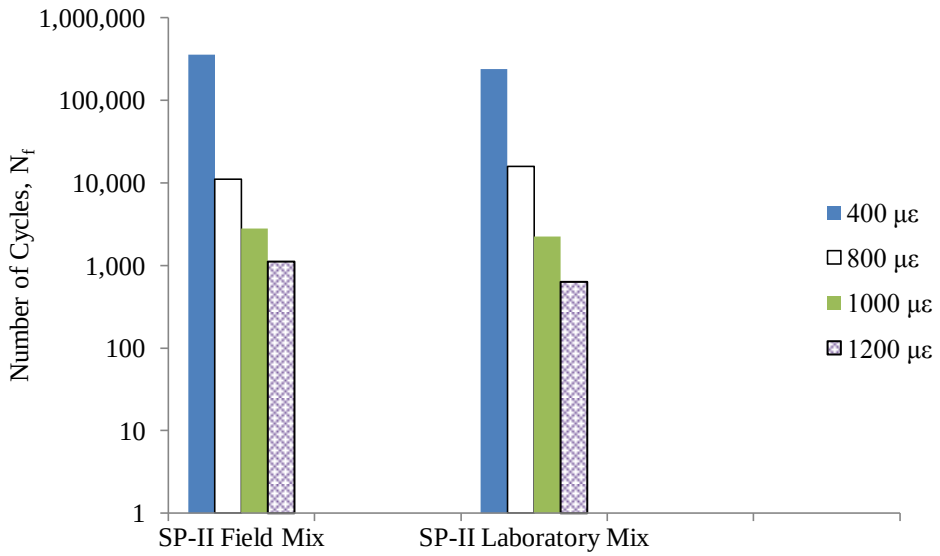

Figure 4.3(a) Comparison of Fatigue Life between Field and Laboratory SP-II Mixtures

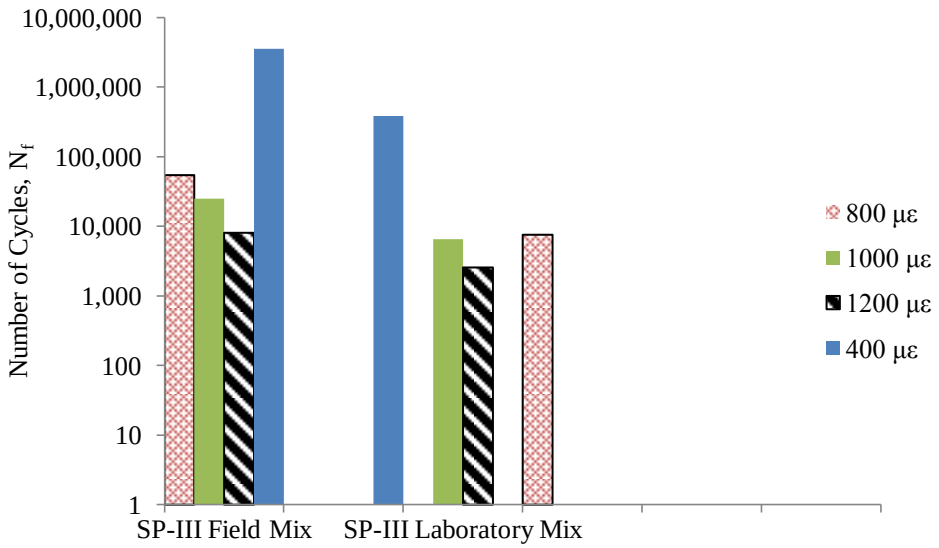

Figure 4.3(b) Comparison of Fatigue Life between Field and Laboratory SP-III Mixtures

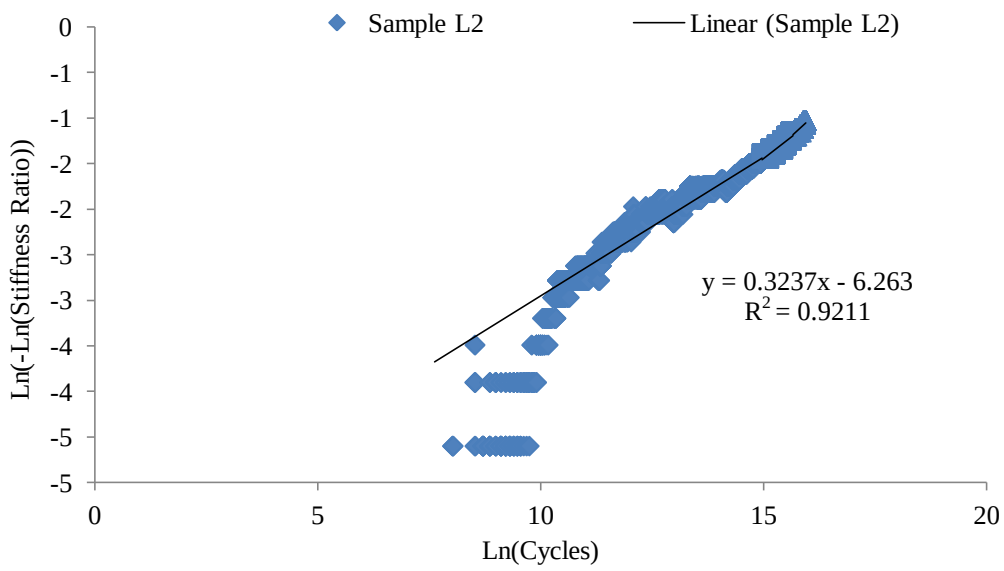

Figure 4.4 Fatigue Curve for SP-II Sample (L2) using Weibull Fuction

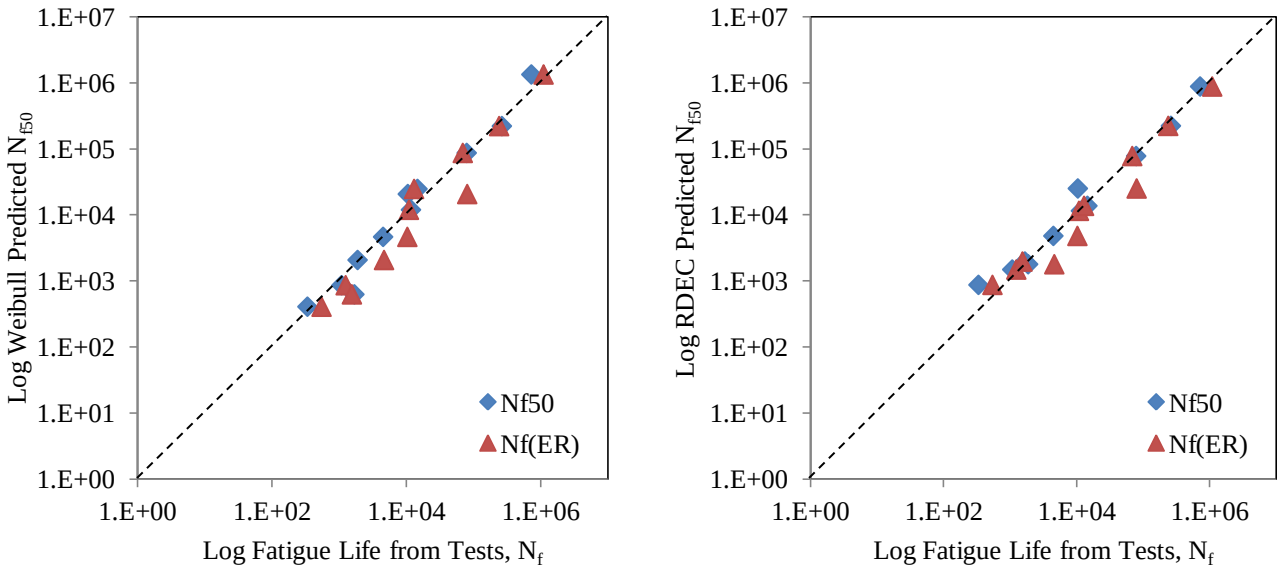

(a) Single-Stage Weibull Function (b) RDEC Approach

Figure 4.5 Comparison of Extrapolated and Tested Fatigue Life Results of Field SP-II Mixtures

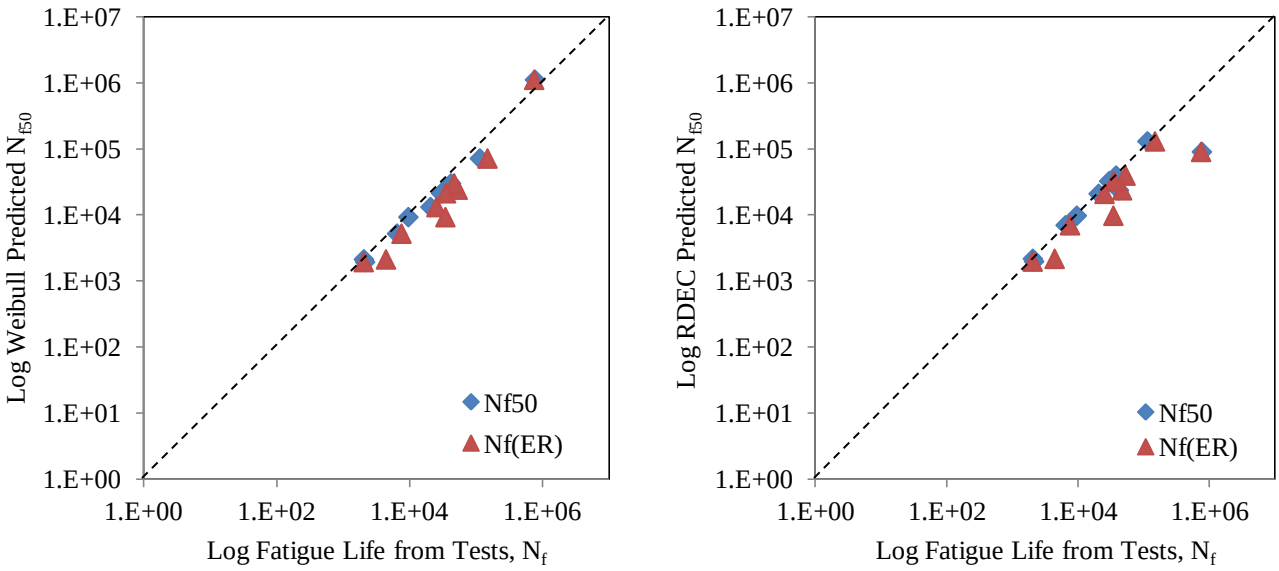

(a) Single-Stage Weibull Function (b) RDEC Approach

Figure 4.6 Comparison of Extrapolated and Tested Fatigue Results of Field SP-III Mixtures

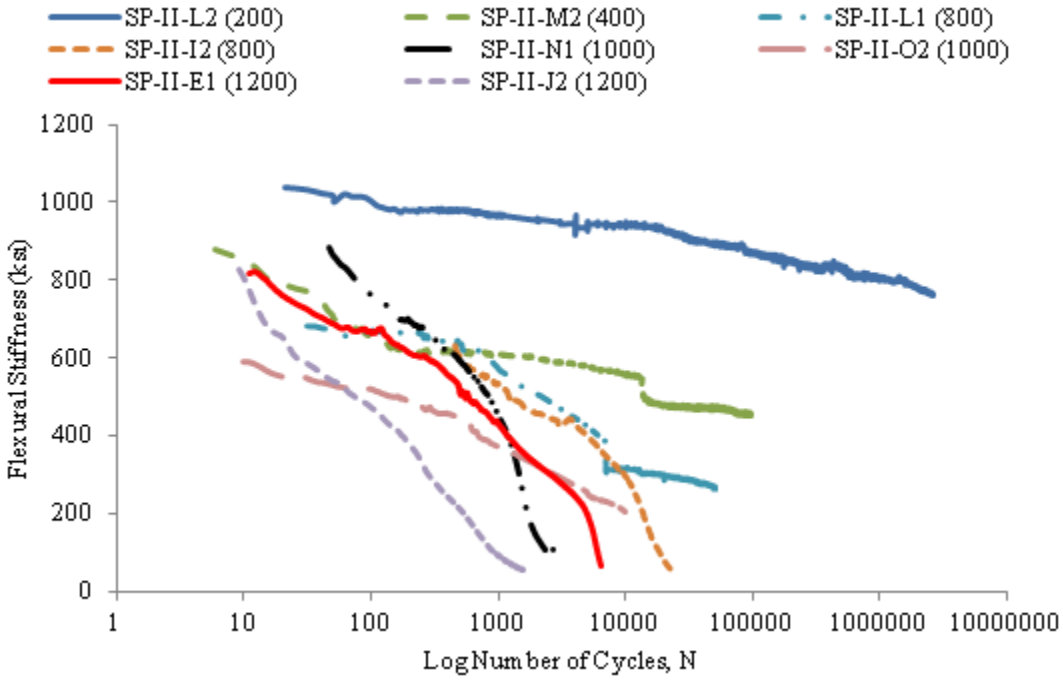

Figure 4.7(a) Flexural Stiffness vs. Loading Cycles for Field SP-II Mixtures

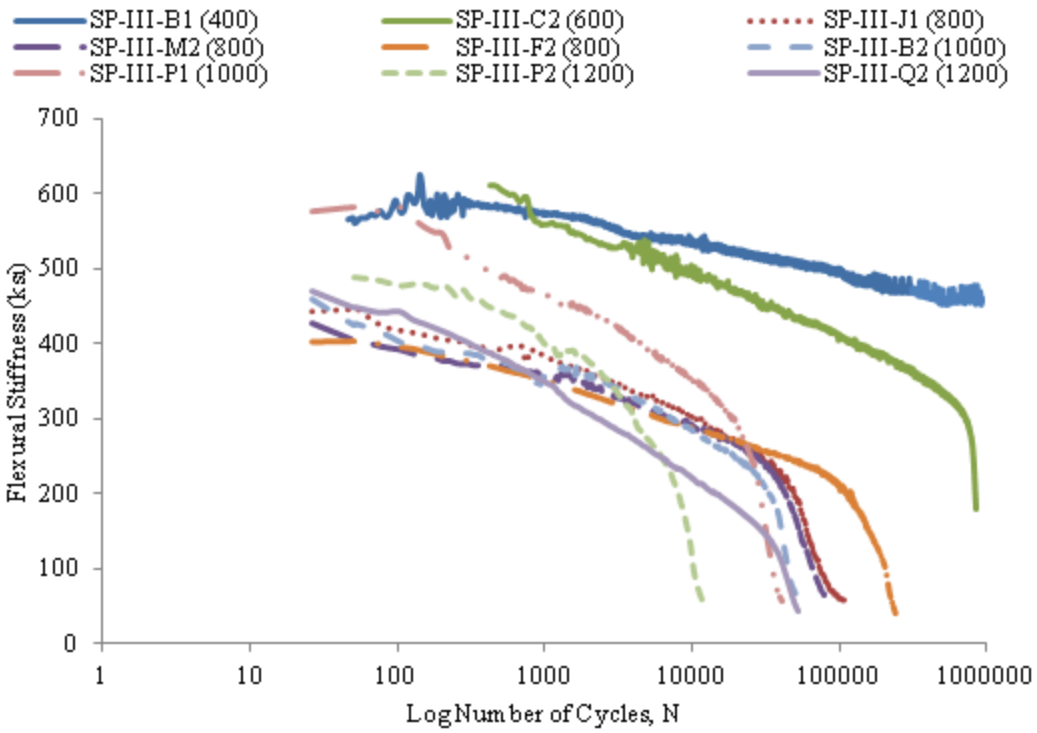

Figure 4.7(b) Flexural Stiffness vs. Loading Cycles for Field SP-III Mixtures

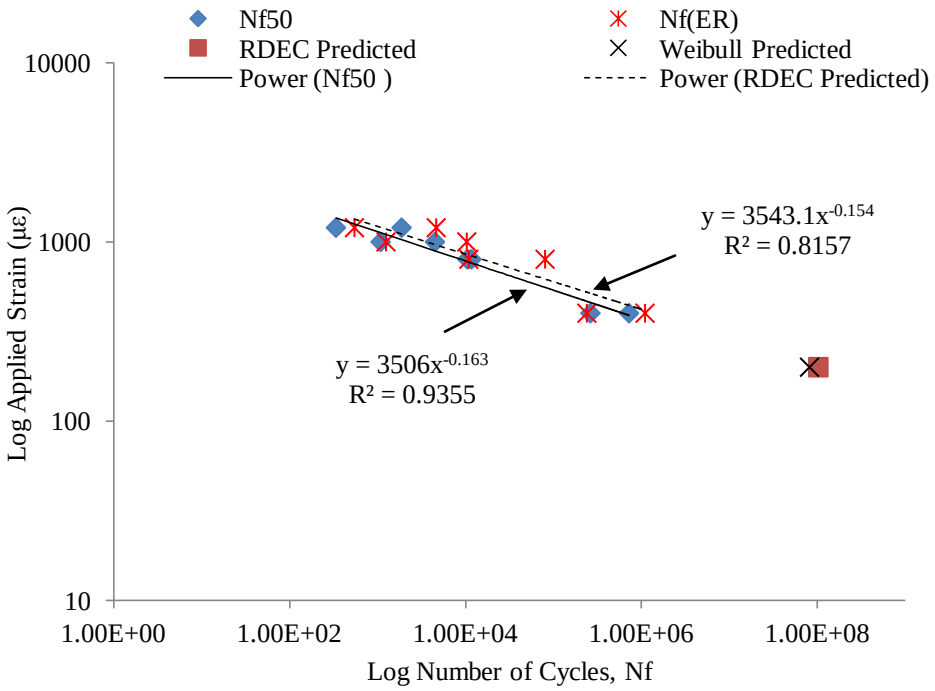

(a) Log-log Plot

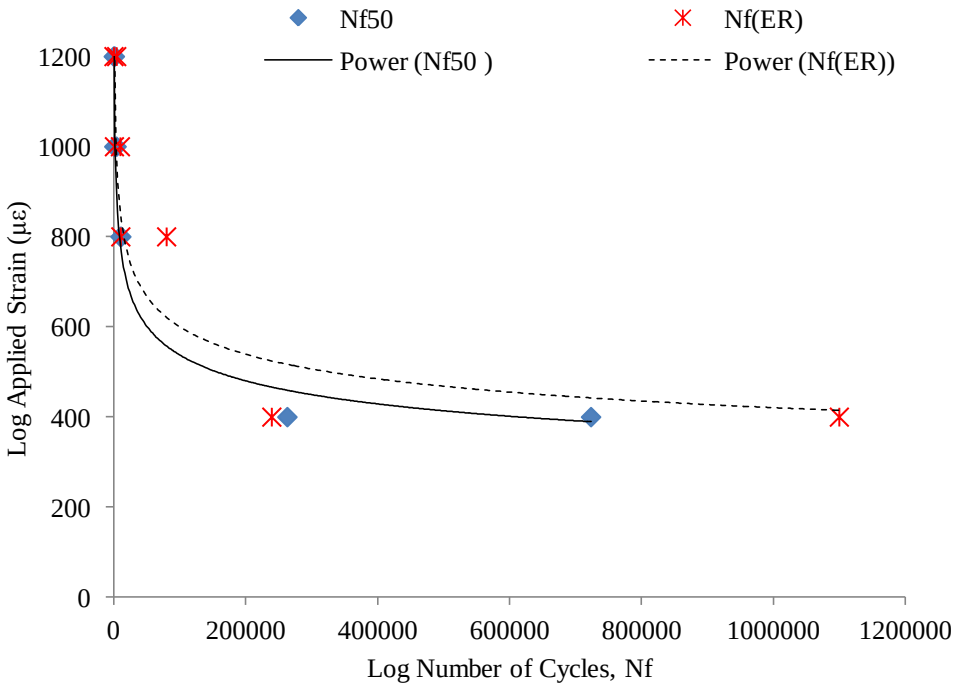

(b) Regular Plot

Figure 4.8 ε-N_f Curve for Field SP-II Mixtures

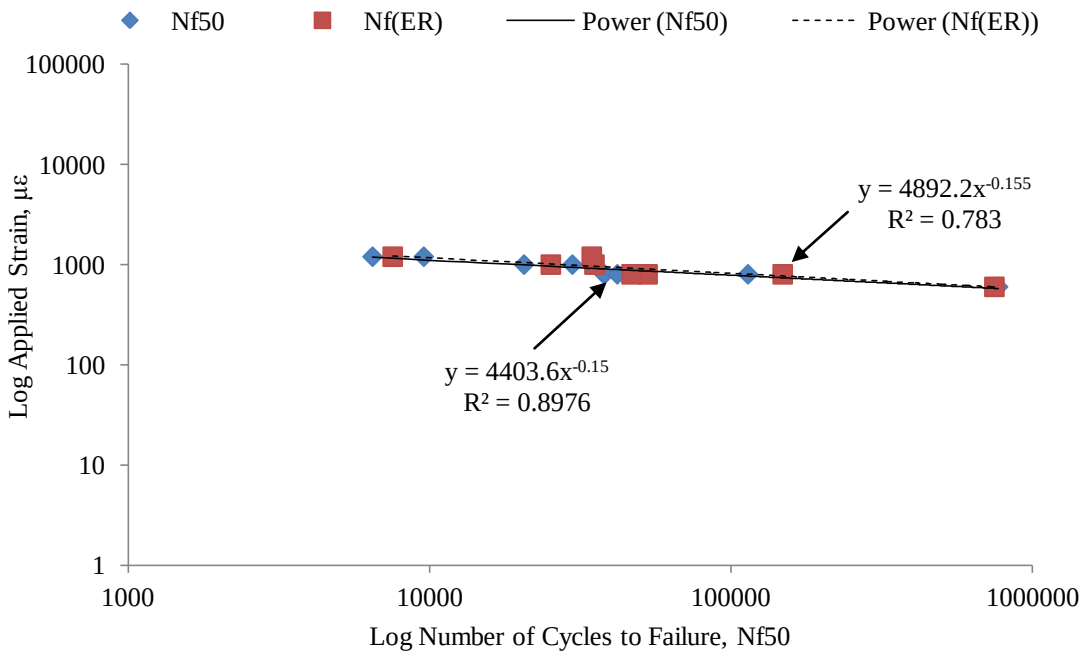

(a) Log-log Plot

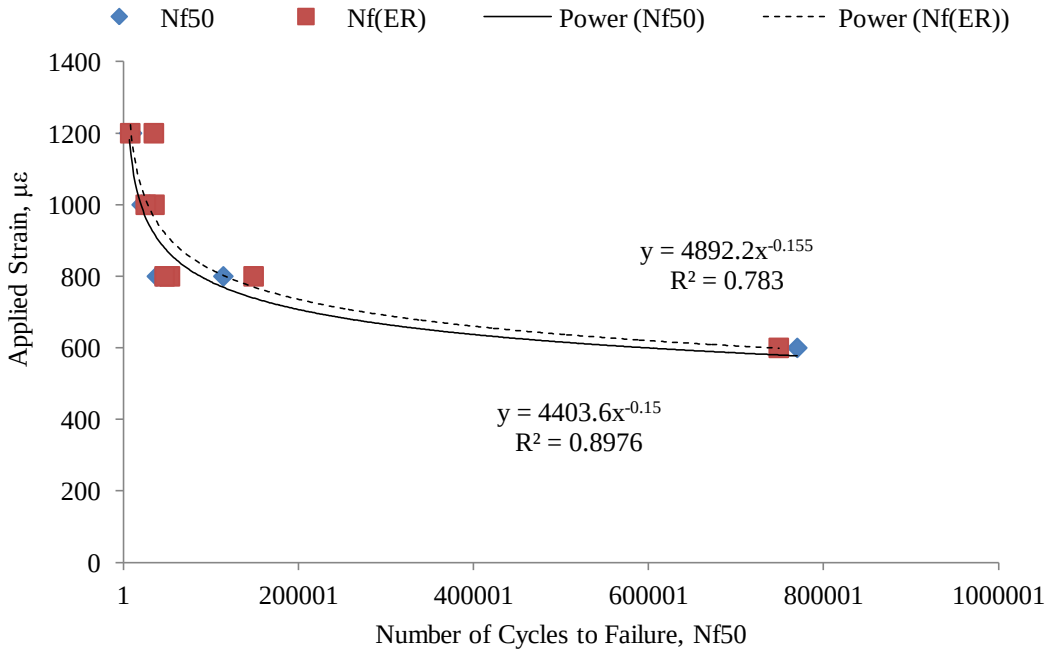

(b) Regular Plot

Figure 4.9 ε-N_f Curve for Field SP-III Mixtures

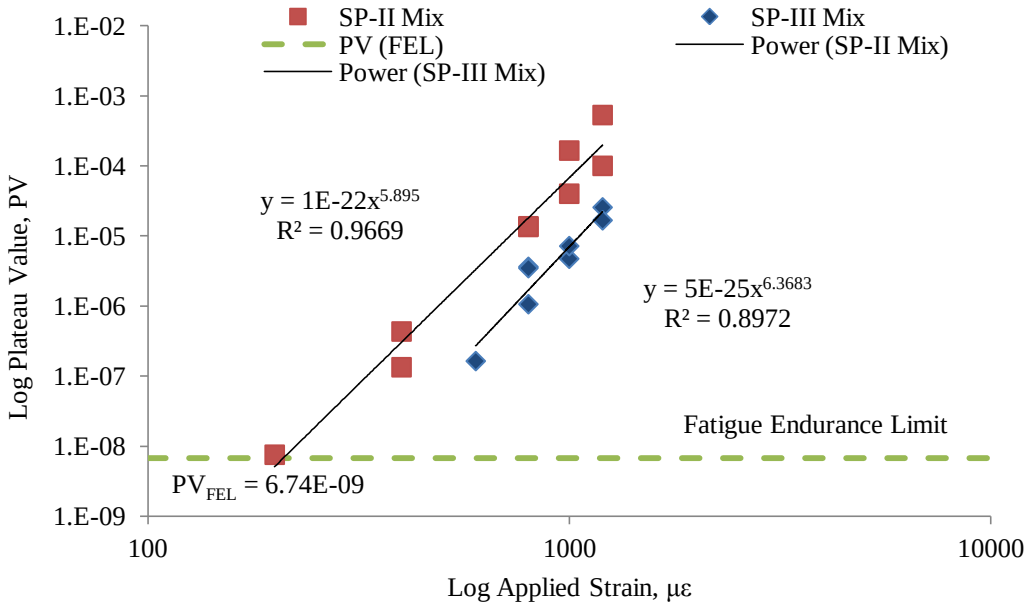

Figure 4.10 Plateau Value vs. Strain Amplitude for Field SP-II and SP-III Mixtures

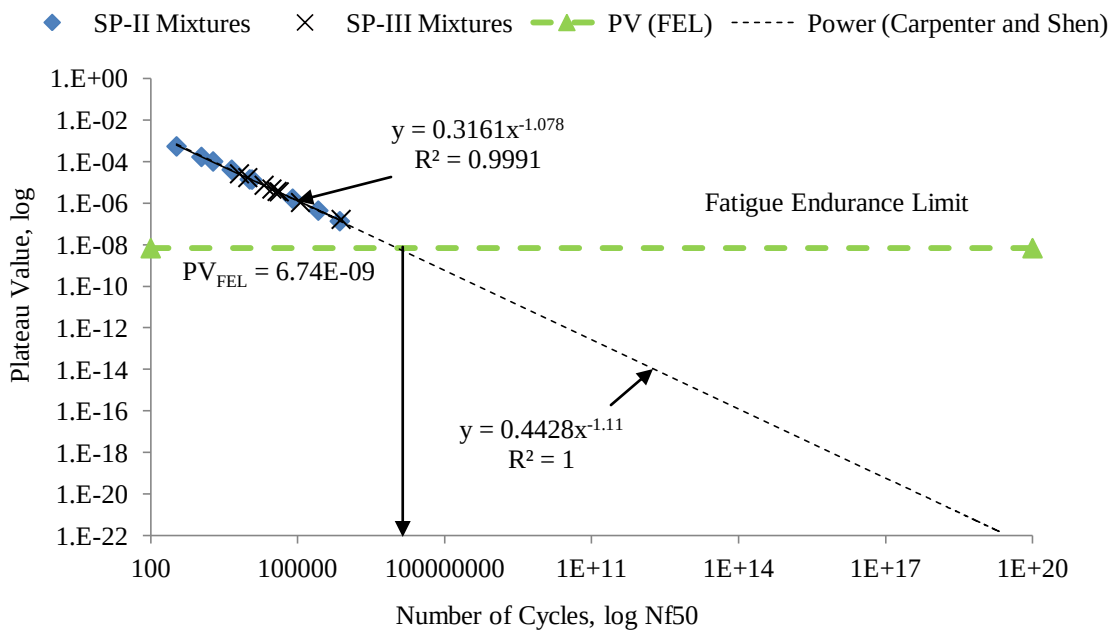

Figure 4.11 Plateau Value vs. Cycles to Failure for Field SP-II and SP-III Mixtures

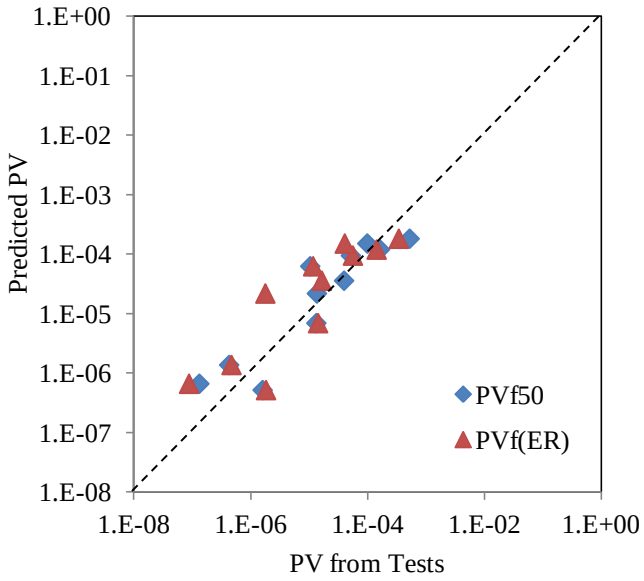

(a) SP-II Mixture

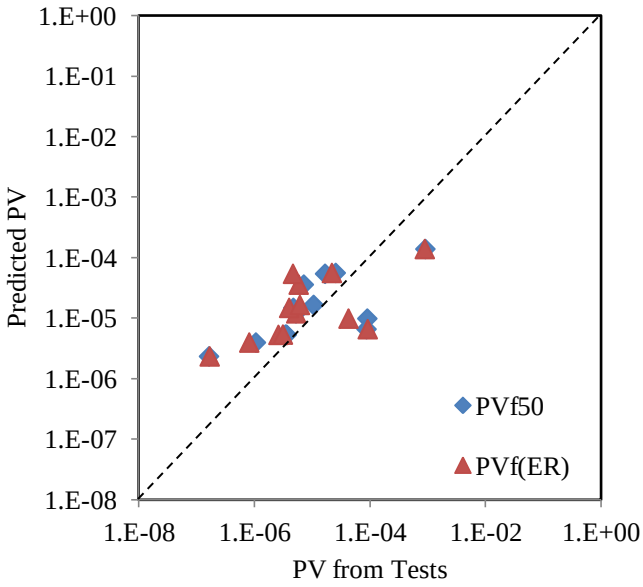

(b) SP-III Mixture

Figure 4.12 Comparison between PV from Model with PV from Test Results for Field Mixtures

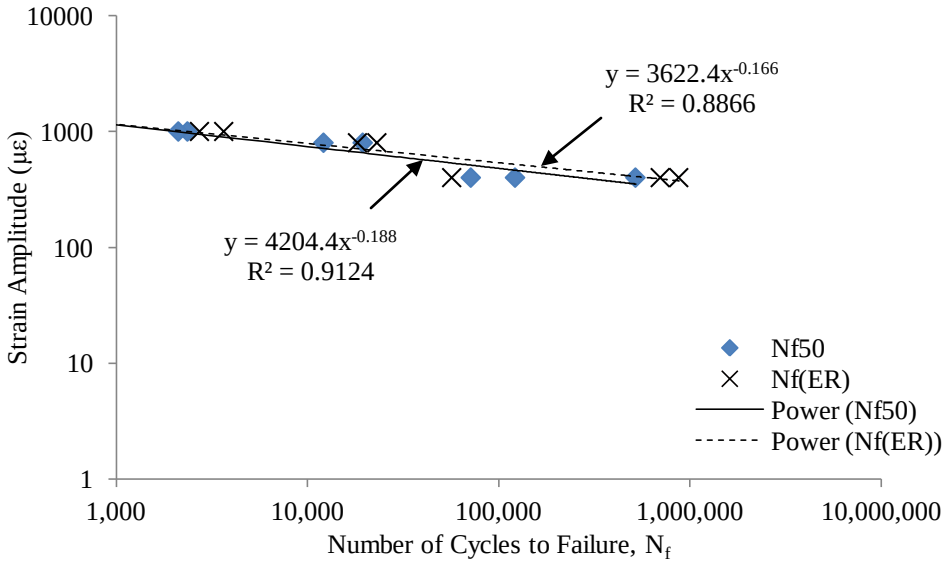

(a) Log-log Plot

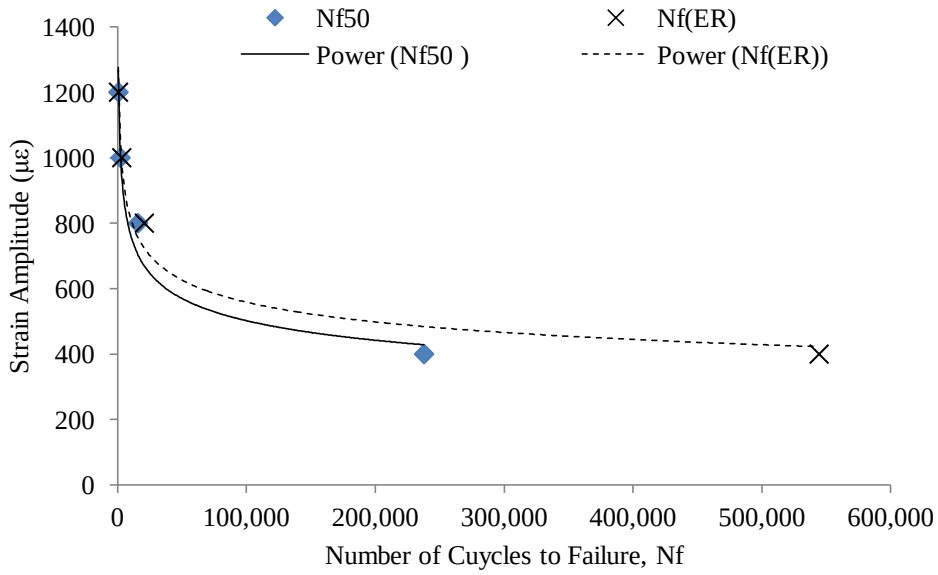

(b) Regular Plot

Figure 4.13 ε-N_f Curves for Laboratory SP-II Mixtures

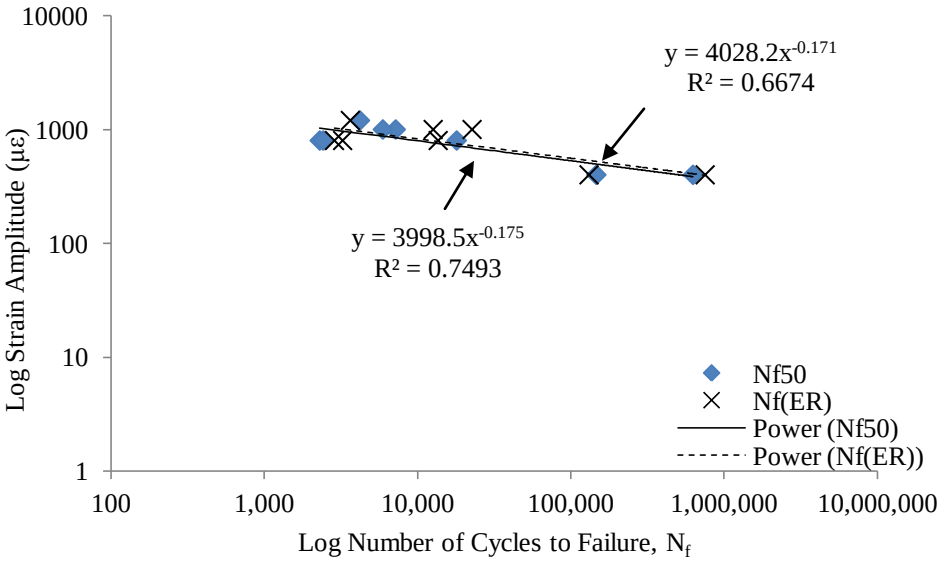

(a) Log-log Plot

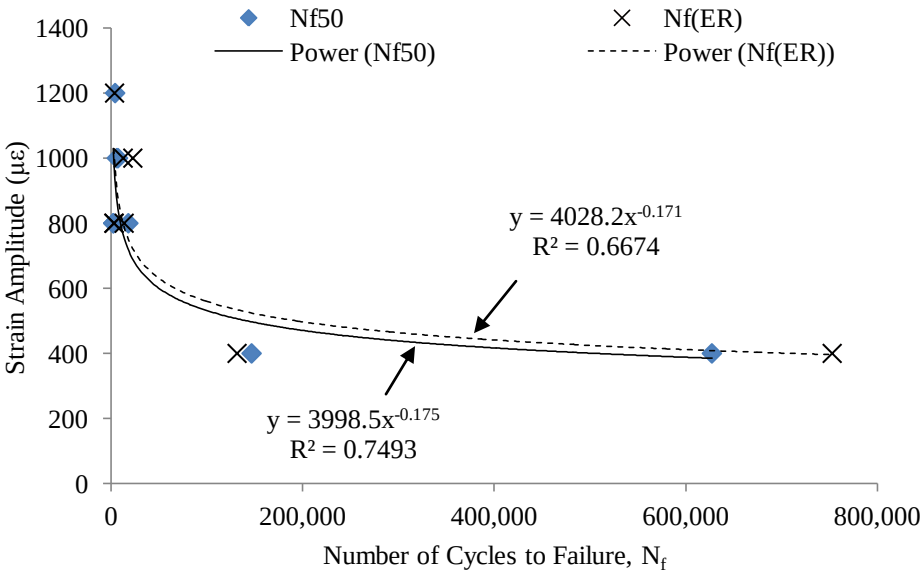

(b) Regular Plot

Figure 4.14 ε-N_f Curve for Laboratory SP-III Mixtures

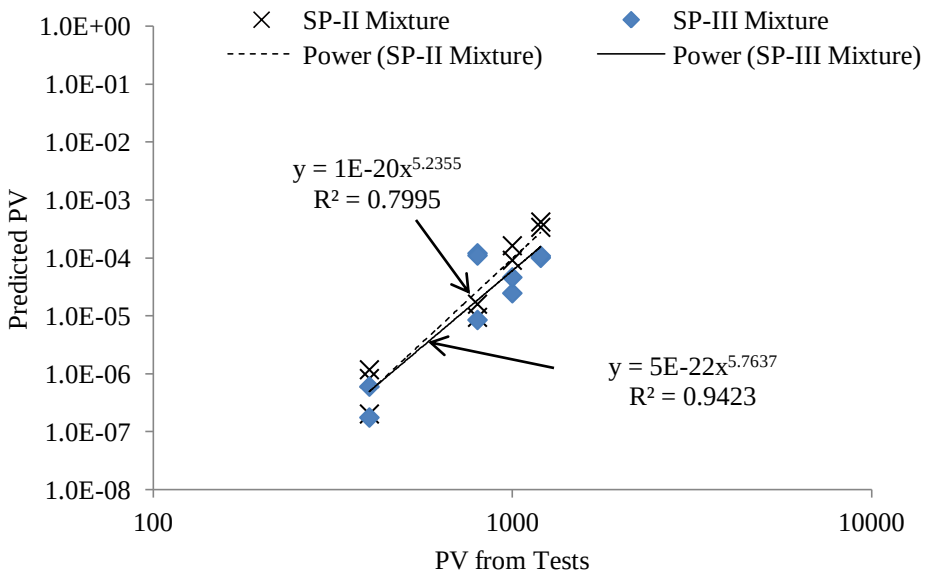

Figure 4.15 ε-PV Curves for Laboratory SP-II and SP-III Mixtures from Laboratory Fatigue Testing

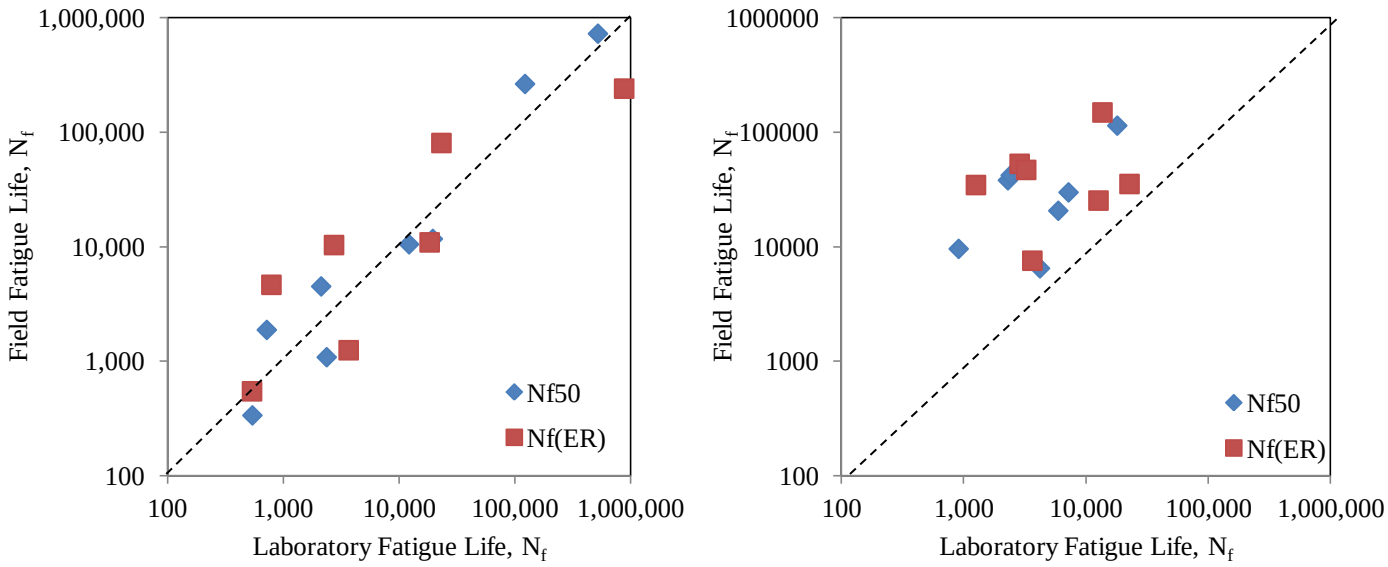

(a) SP-II Mixture (b) SP-III Mixture

Figure 4.16 Comparison of Fatigue Life for Laboratory and Field Mixtures

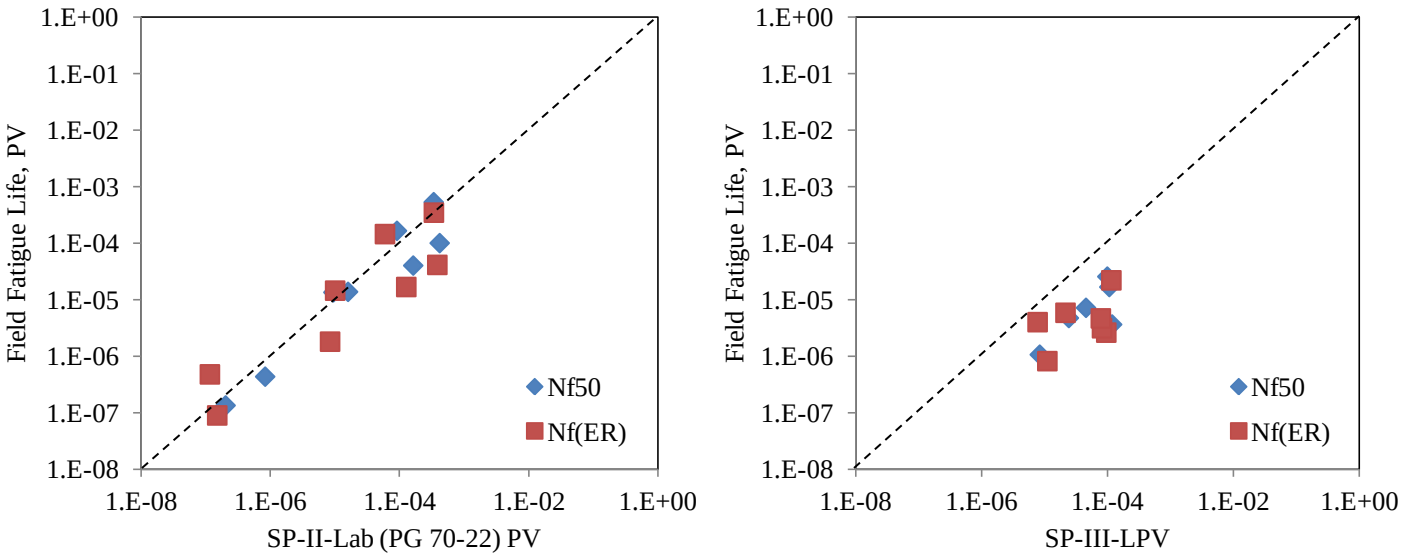

(a) SP-II Mixture (b) SP-III Mixture

Figure 4.17 Comparison of Plateau Values for Laboratory and Field Mixtures

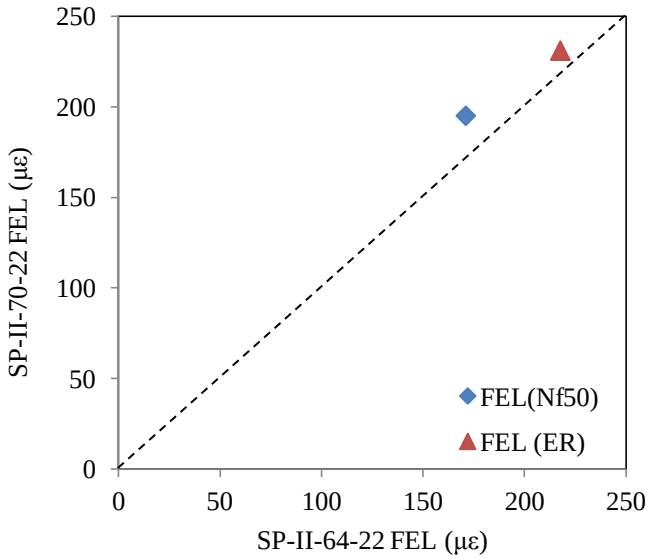

(a) SP-II Mix using ε-N_f Model

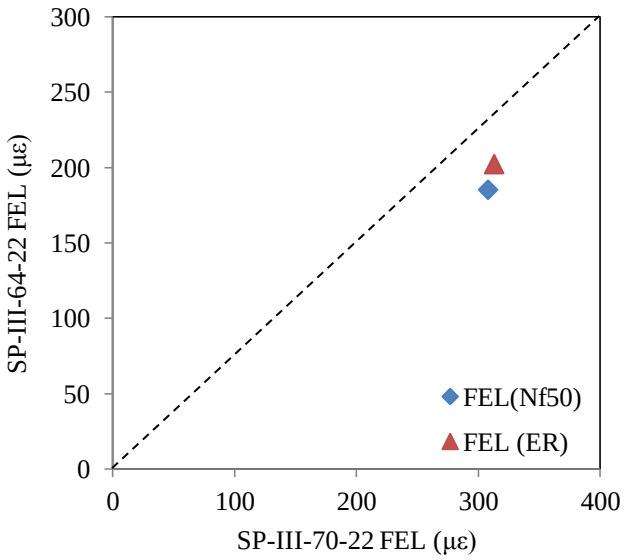

(b) SP-III Mix using ε-N_f Model

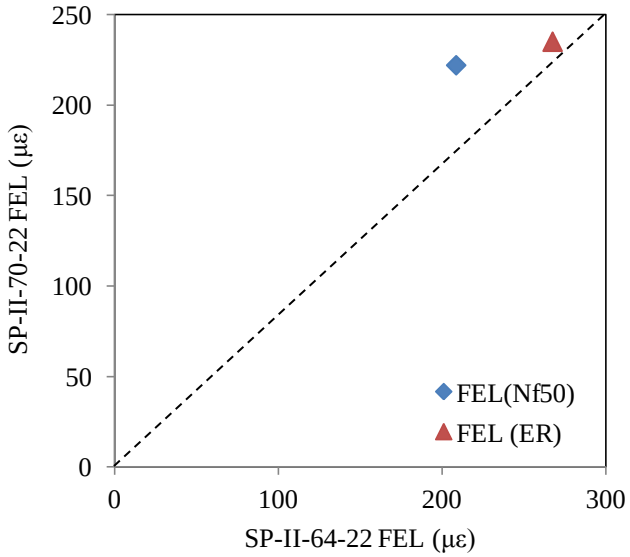

(c) SP-II Mix using ε-PV Model

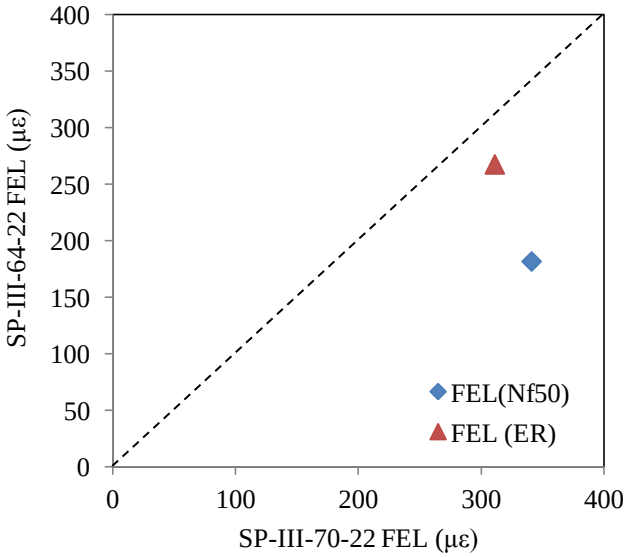

(d) SP-III Mix using ε-PV Model

Figure 4.18 Comparison of Predicted FEL Values for SP-II and SP-III Mixtures

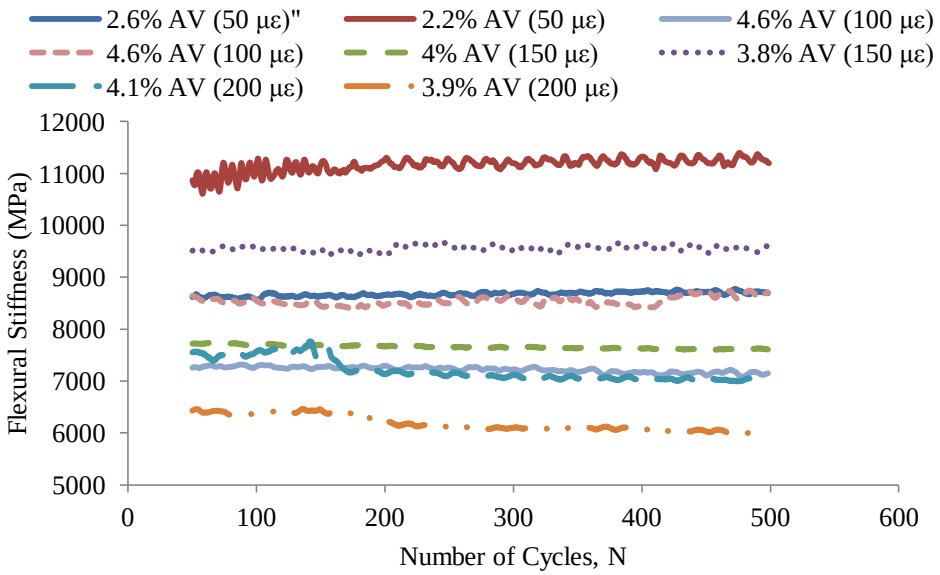

Figure 4.19 Stiffness Results for SP-II (PG 64-22) Samples with Varying Air Void Contents

CHAPTER V

COMPARISON OF DIFFERENT FAILURE CRITERA FOR FATIGUE TESTING

5.1 Introduction

Traditionally, third point loaded beam fatigue has been used to characterize fatigue performance under laboratory conditions (AASHTO T 321-07). This includes subjecting beams to damage inducing cyclic loading (displacement control) and monitoring its stress history. Using the beam geometry, applied displacement and measured load, strain and stress in beam are calculated. Further, stiffness of material is calculated using stress and strain history. Then, the number of cycles at 50% reduction in stiffness is recorded as failure of the beam. This procedure is repeated at other strain levels to obtain relation between applied strain and number of cycles to failure. The same relation is given in Equation 5.1. Sometimes, initial stiffness of material is also incorporated into fatigue model and is given in Equation 5.2.

$$N_f = k_1 \left(\frac{1}{\varepsilon}\right)^{k_2} \tag{5.1}$$

$$N_f = k_1 \left(\frac{1}{\varepsilon}\right)^{k_2} \left(\frac{1}{E}\right)^{k_3} \tag{5.2}$$

where N_f = number of cycles at failure, ε = maximum tensile strain in beam, E = initial stiffness and k_i = regression coefficients.

Under controlled displacement mode of loading, the stress in beam reduces with increase in number of cycles. Due to testing difficulties, it is difficult to monitor development and propagation of cracks in the beam. Often, it takes a large number of repetitions of load to see a macrocrack in the beam. Due to nature of loading, measured load might not decrease beyond certain value. Also, 50% reduction in stiffness has been arbitrarily defined as failure point. Such an approach might not indicate better utilization of material and time resources available.

Several researchers have proposed energy based approaches to analyze fatigue data. Among them dissipated energy, cumulative dissipated energy and dissipated energy ratio approaches are popular among pavement engineering community due to its simplistic nature. However these approaches fail to account for viscoelastic nature of asphalt concrete. On the other hand viscoelastic continuum damage approach has shown promising results in terms of robustness, efficient utilization of available resources.

In summary, this study compared fatigue failure criterion developed using stiffness based approach with viscoelastic continuum damage approach. Such a comparison can aid phenomenological approach in describing fatigue performance in a rational manner.

5.2 Background on Current Fatigue Failure Criteria

As mentioned previously, in phenomenological approach failure is defined as number of cycles at which stiffness of material decreases by 50% (AASHTO T 321). Initial stiffness of beam is measured at 50^{th} loading cycle. This is to account for initial setting of beam. However one might expect stiffness reduction from first cycle itself. Thus in this approach damage in initial few cycles is ignored. This often leads to unrealistic values especially at higher strain amplitude levels.

Other researchers have used dissipated energy to model fatigue behavior (Van Dijk and Vesser 1977, Rowe 1993, Pronk and Hopman 1990, Pronk 1997). Dissipated energy is defined as energy lost during each cycle of loading. This includes energy lost due to damping, viscoelastic effects and damage growth. Dissipated energy can be calculated by calculating area within stress-strain curve. Mathematically, dissipated energy in each cycle i is given by Equation 5.1. Further dissipated energy in each cycle is summed to obtain cumulative dissipated energy as shown in Equation 5.2.

$$w_i = \pi \sigma_{amp} \varepsilon_{amp} \sin \varphi \tag{5.1}$$

$$W_i = \sum_1^N w_i \tag{5.2}$$

where w_i = dissipated energy in cycle i, σ_{amp} = stress amplitude, ε_{amp} = strain amplitude, φ = phase angle between stress and strain and W_i = cumulative dissipated energy up to cycle i.

Van Dijk and Vesser (1977) found a strong relation between numbers of cycles and cumulative dissipated energy. Pronk and Hopman (1990) refined dissipated energy approach by defining energy ratio to check for linearity. Energy ratio is defined as ratio of initial dissipated energy to dissipated energy in cycle i multiplied by number of cycles. Deviation from straight line in plot of energy ratio against number of cycles indicates development of macrocrack in beam. However deviation from straight line is subjected to individual judgment.

Guzlan and Carpenter (2000) used the Dissipated Energy Ratio (DER) to quantify relative change in dissipated strain energy. Dissipated energy ratio is defined as Chapter 2 where Guzlan and Carpenter (2000) found a strong relationship between DER and number of cycles to failure. A plot of dissipated energy ratio vs. number of cycles indicates three distinct regions, as described earlier in Chapter 2. Research by Shen and Carpenter (2005) indicated a linear relationship between the plateau value and number of cycles to 50 percent initial stiffness (semi-log scale). However due to overly sensitive dissipated energy difference, plot of dissipated energy ratio vs. number of cycles indicates scatter. Thus it is difficult to interpret failure location visually as well as mathematically.

Rowe and Bouldin (2000) introduced Energy Ratio for modeling fatigue behavior and is described in detail in Chapter 2. The Energy Ratio is obtained by multiplying stiffness (kPa) by the corresponding number of cycle. The Energy Ratio is cross plotted against number of cycles to determine the failure location.

The peak value in this plot indicates the transition from micro-cracking to macro-cracking.

In all above cases, material is considered to be elastic. However asphalt concrete exhibits rate dependent and temperature dependent behavior. Kim (1988) successfully applied the elastic-viscoelastic correspondence principle for modeling sand-asphalt mixture behavior under multi level cyclic loading. Kim (1988) found that the secant pseudo stiffness (stress corresponding to maximum pseudo strain divided by maximum pseudo strain in each cycle) value decreases with increasing damage. Daniel (Daniel 2001, Daniel and Kim 2002) found that the relationship between the normalized pseudo stiffness ($C1$) and the damage parameter ($S1$) is unique for a given asphalt concrete mix (hereafter referred to as damage characteristic curve) under uniaxial mode of loading. Swamy (2011) extended viscoelastic continuum damage mode to flexure mode of loading and found that damage characteristic curve is unique at given temperature under flexure mode of loading. Swamy and Daniel (2011) found a point of inflection in the damage characteristic curve beyond which the material loses its structural integrity at faster rate. Also, it is observed that normalized pseudo stiffness at this inflection point is dependent on mixture properties.

In this study, traditional four point bending beam fatigue testing apparatus is used. AASHTO T321 standards are used for fatigue testing. For determining viscoelastic properties, displacement controlled cyclic loading mode is used.

5.3 Laboratory Testing

Initially, prepared specimen is tested for its viscoelastic properties and subsequently tested for its fatigue properties. During the determination of viscoelastic properties, specimen is subjected to low strain amplitude cyclic loading to obtain its dynamic modulus and phase angle fingerprint at different temperatures and frequencies. The maximum strain in specimen is limited to 75 microstrain. Dynamic modulus and phase angle measurements are obtained at -10°C to 30°C in 10°C increments. Within each temperature, frequencies of 15, 10, 5, 2, 1, 0.5, 0.2, and 0.1 Hz are used. Using time-temperature superposition principle, dynamic modulus and phase angle mastercurves are constructed. Using dynamic modulus and phase angle mastercurve coefficients, relaxation modulus mastercurve is obtained using the inter-conversion technique proposed by Park and Kim (1999).

In second stage, fatigue testing is conducted on specimens to obtain fatigue properties on mixture. All specimens are tested at damage inducing strain level. In this research strain amplitudes used are in range of 400-1200 microstrain. Using the deflection history, load response history, and geometry of test specimen, the maximum strain and stress in specimen are calculated using Eq. 5.3 and 5.4, respectively.

$$\varepsilon = \frac{12\,h\,\delta}{3L^2 - 4a^2} \tag{5.3}$$

$$\sigma = \frac{P\,L}{b\,h^2} \tag{5.4}$$

Where P = Load applied by actuator at time t, b =average specimen width and h =average specimen height, δ = deflection at center of beam at time t, a = distance between inside clamps and L = distance between outside clamps.

5.4 Analysis procedure

The relaxation modulus mastercurve is obtained using dynamic modulus and phase angle mastercurve coefficients through the inter-conversion technique. Dynamic modulus mastercurves and relaxation modulus for both mix types are presented in Appendix B. Using computed strain history and relaxation modulus mastercurve, pseudo strain is computed using Eq. 5.5. This pseudo strain accounts for all viscoelastic effects and separates effects of damage and healing within the specimen.

$$\varepsilon^R(t) = \frac{1}{E_R}\int_0^t E\,(t-\tau)\frac{d\varepsilon}{d\tau}\,d\tau \tag{5.5}$$

where E_R = reference modulus, $E(t)$ = relaxation modulus, ε = computed physical strain, t = elapsed time between the time loading began and the time of interest and τ = time variable.

In a fatigue test, loops are seen in cross plot of measured stress vs. pseudo strain. Further the slope of these loops decreases as testing progresses. The secant pseudo stiffness (S_i^R) in any cycle i is calculated by dividing measured stress by maximum pseudo strain in cycle i. To account for specimen to specimen variation, secant pseudo stiffness is divided by secant pseudo stiffness in first cycle of loading (I). From here onwards for simplicity, this value will be referred

to as normalized pseudo stiffness ($C1$). Due to continuous growth of damage, numerical value of normalized pseudo stiffness continuously decreases (has value of 1 at undamaged condition, 0 at complete failure). The variation of normalized pseudo stiffness during a fatigue test is shown in Figure 5.1. Using the histories of normalized pseudo stiffness and computed physical strain, damage parameter is computed. The equation to compute damage parameter is presented in Eq. 5.6.

$$S1_i \cong \sum_{i=1}^{N} \left[\frac{I}{2}\left(\varepsilon_{max,i}^{R}\right)^2 (C1_{i-1} - C1_i)\right]^{\frac{\alpha}{1+\alpha}} (t_i - t_{i-1})^{\frac{1}{1+\alpha}} \quad (5.6)$$

Where $\varepsilon_{max,i}^{R}$ = maximum pseudo strain in cycle i, $C1_i$ = normalized pseudostiffness in cycle i, $S1_i$ = damage parameter in cycle i, α = material constant and t = time to maximum pseudo strain in cycle i.

Due to continuous growth of damage, numerical value of damage parameter continuously increases (with initial value of 0). Further, the normalized pseudo stiffness is plotted against the damage parameter to obtain damage characteristic curve. This curve is fitted with generalized exponential model presented in Eq. 5.7.

$$C1 = e^{k_1 \times (S1)^{k_2}} \quad (5.7)$$

Where $C1$ = normalized pseudostiffness, $S1$ = damage parameter and k_i = regression coefficients.

Visual examination of actual damage characteristic curve and predicted values from generalized exponential model indicated that generalized exponential model

over-predicted at lower normalized pseudo stiffness values. Thus using data points below which deviation is seen is fitted with second order polynomial. The composite mode consisting of generalized exponential model and second order polynomial is used for further analysis. The point of intersection of generalized exponential model and second order polynomial referred to point of inflection. Characteristic damage curve obtained for SP-II-K2 specimen (SP-II mixture) is shown in Figure 5.2. The number of cycles corresponding to this inflection point has been documented as failure criterion by Swamy and Daniel (2011). The same figure shows fitted generalized exponential model and second order polynomial. More details about viscoelastic continuum damage approach as applied to flexure mode of loading can be found elsewhere (Swamy 2011, Swamy and Daniel 2011).

Using the computed strain and stress, stiffness in each cycle of loading is computed. Further stiffness ratio is computed using initial stiffness, stiffness corresponding to number of cycles. The formula to compute stiffness ratio is Eq. 5.8. The variation of the stiffness ratio with number of cycles is shown in Figure 5.1. During the course of the fatigue test, stiffness ratio increases initially and then decreases. Number of cycles corresponding to maximum stiffness ratio has been considered to be failure point by researchers (Rowe and Bouldin 2000).

$$SR = \left(\frac{S_i}{S_0}\right) N_i \tag{5.8}$$

Where SR = stiffness ratio, S_i = stiffness in cycle N_i, and S_0 = initial stiffness.

5.5 Results

Damage characteristic curves for SP-II and SPIII mixtures using alpha =1 +1/n are shown in Figure 5.3 and Figure 5.4, respectively. Alpha is a material constant, used to determine the relaxation modulus master curve, E_R, shown in Eq. 5.5. The slope of the $E_R = n$. If the material's fracture energy and failure stress are constant, then the material constant, α, equals 1+1/n. On the other hand, if the fracture process zone size and fracture energy are constant, the material constant, α equals 1/n. Lee and Kim (1998b) suggested that material constant forms α = 1+1/n, and α = 1/n, are more suitable for controlled strain amplitude test and controlled stress amplitude test, respectively.

5.6 Comparison of Parameters at Maximum Stiffness Ratio

The number of cycles to 50% reduction in stiffness is compared with number of cycles at maximum energy ratio for SP-II and SP-III mixtures in Figure 5.5 and Figure 5.6, respectively. In general, number of cycles at maximum energy ratio is higher than number of cycles to 50% reduction in stiffness.

The number of cycles at inflection point in damage characteristic curve (using alpha = 1 + 1/n) is compared with number of cycles at maximum energy ratio for SP-II and SP-III mixtures in Figure 5.7 and Figure 5.8, respectively. In general, a strong correlation is found between number of cycles at inflection point in damage characteristic curve and number of cycles at maximum energy ratio.

Further, number of cycles at inflection point in damage characteristic curve is always less than number of cycles at maximum energy ratio.

5.7 Comparison of CD Method with Traditional Method

Scatter plot of number of cycles at inflection point in damage characteristic curve vs. number of cycles at 50% reduction in stiffness for SP-II and SP-III mixtures are presented in Figure 5.9 and Figure 5.10, respectively. Coefficient of correlation (with power fit, both on log scales) is in range of 0.6575 to 0.9245. R^2 values and visual interpretation indicates a strong correlation between these two parameters.

5.8 Effect of Strain Amplitude

Effect on strain amplitude on number of cycles is investigated for SP II and SP III mixture. Criterion like 50% reduction in stiffness, maximum stiffness ratio and inflection point in damage characteristic curve is used in evaluation. The plots for SP-II and SP-III mixtures are shown in Figure 5.11 and Figure 5.12, respectively.

In case of SP-II mixture, with decrease in strain amplitude, the number of cycles increased for all three cases. However this is not the case for SP-III mixture. In case of SP-II mixture, R^2 value is 0.797, 0.738 and 0.8195 for 50% reduction in stiffness, maximum stiffness ratio and inflection point in damage characteristic curve, respectively. For SP-III mixture, R^2 value is 0.219, 0.403 and 0.5904 for 50% reduction in stiffness, maximum stiffness ratio and inflection point in

damage characteristic curve, respectively. This indicates that there is better correlation between strain amplitude and the number of cycles at inflection point in the damage characteristic curve.

5.9 Summary

This section summarizes compared fatigue failure criterion developed using stiffness based approach with viscoelastic continuum damage approach, as performed in this study:

- Dynamic modulus testing is performed on asphalt beam samples to determine the dynamic modulus and phase angle master curves. Using mastercurve coefficients, a relaxation modulus mastercurve is obtained whereby the pseudo-strain is computed for each test.
- The secant pseudostiffness (stress corresponding to maximum pseudostrain divided by maximum pseudostrain in each cycle) value is found to decrease with increasing damage. The damage characteristic curve describes the relationship between the normalized pseudostiffness (C1) and the damage parameter (S1).
- Using the VCDM approach, a point of inflection is identified in the damage characteristic curve beyond which the material loses its structural integrity at faster rate. This point is considered the fatigue failure of the sample.
- A strong correlation is found between the VCDM criterion and the Energy Ratio criterion. Further, the fatigue life of the VCDM approach is always less than Energy Ratio fatigue life.

- A strong correlation is also found between the VCDM criterion and the traditional criterion (N_{f50}).
- The effect of strain amplitude on the fatigue life of SP-II and SP-III mixtures is analyzed using the three different failure approaches. In case of the SP-II mixture, with decrease in strain amplitude, the number of cycles increased for all three cases. However this is not the case for SP-III mixture. Higher R^2 values for the inflection point in damage characteristic curve suggest that there is better correlation between strain amplitude and number of cycles at inflection point in the damage characteristic curve.

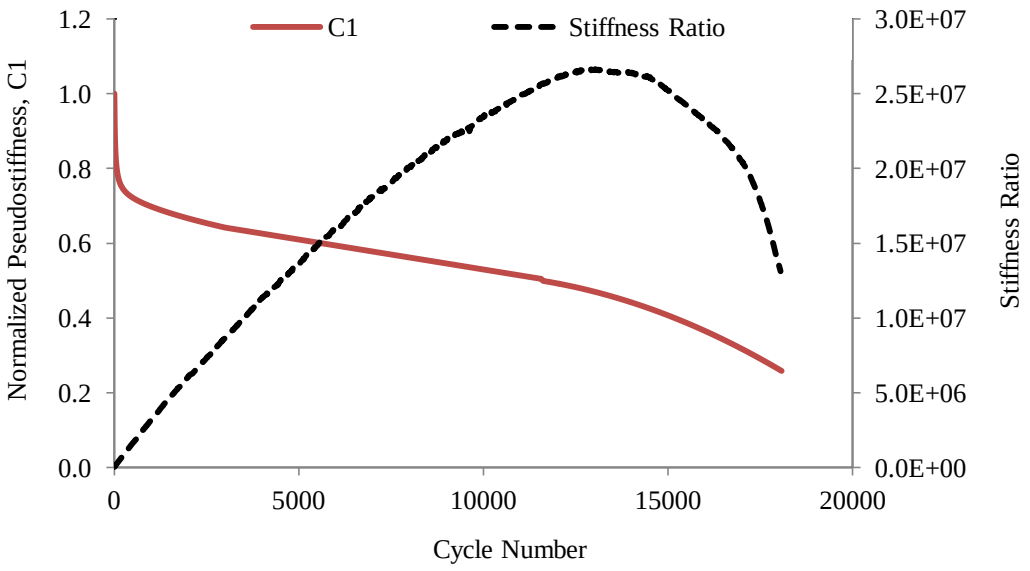

Figure 5.1 Variation of Normalized Pseudo Stiffness and Stiffness Ratio with Number of Repetitions

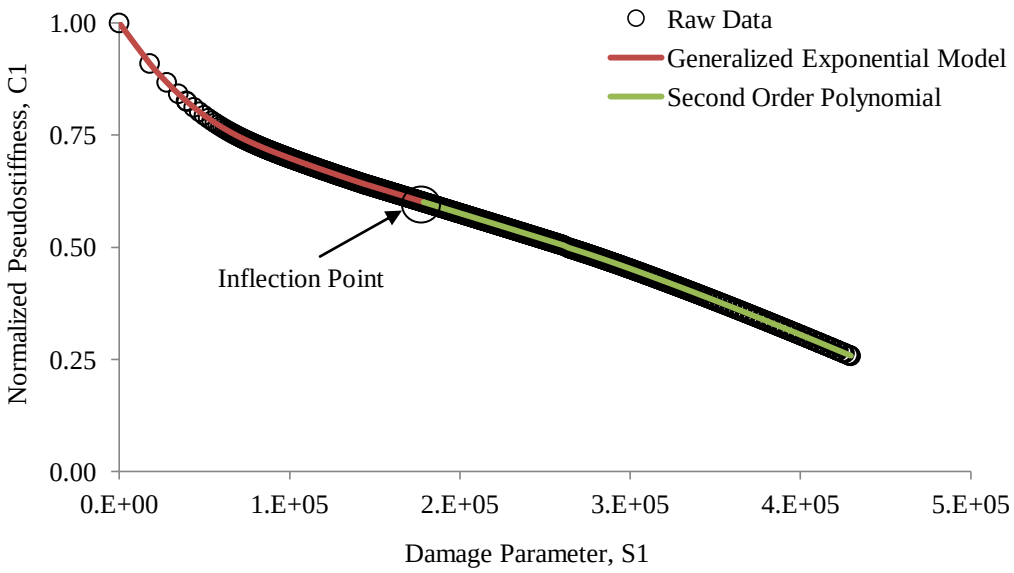

Figure 5.2 Damage Characteristic Curve for SP-II-K2 Specimen

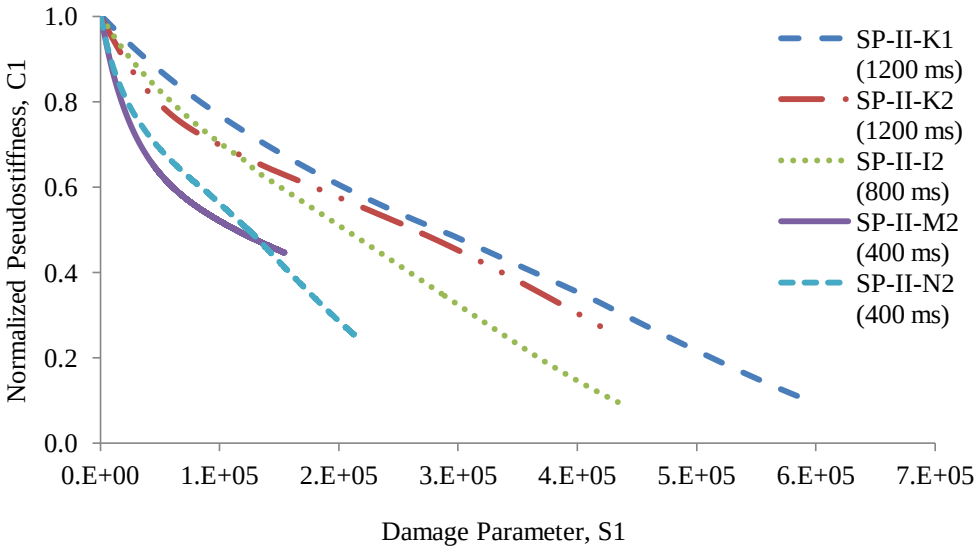

Figure 5.3 Damage Characteristic Curves for SP-II Mixture

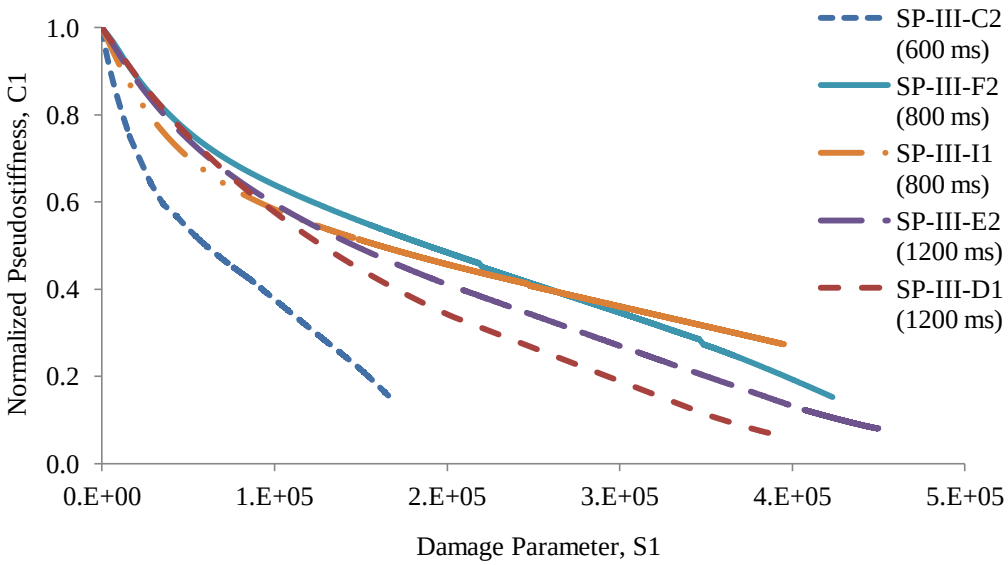

Figure 5.4 Damage Characteristic Curves for SP-III Mixture

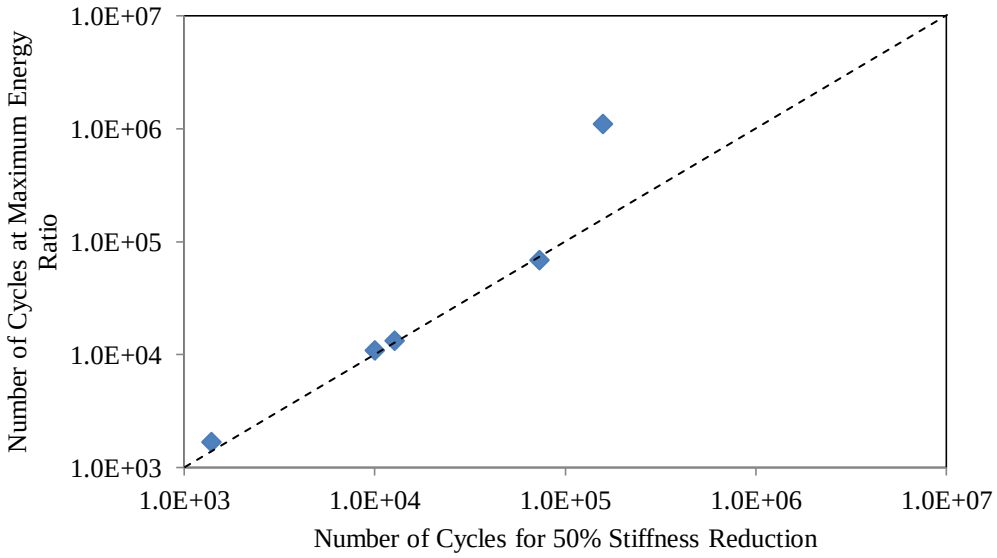

Figure 5.5 Comparison of number of cycles at maximum energy ratio and number of cycles for 50% stiffness reduction for SP II mixture

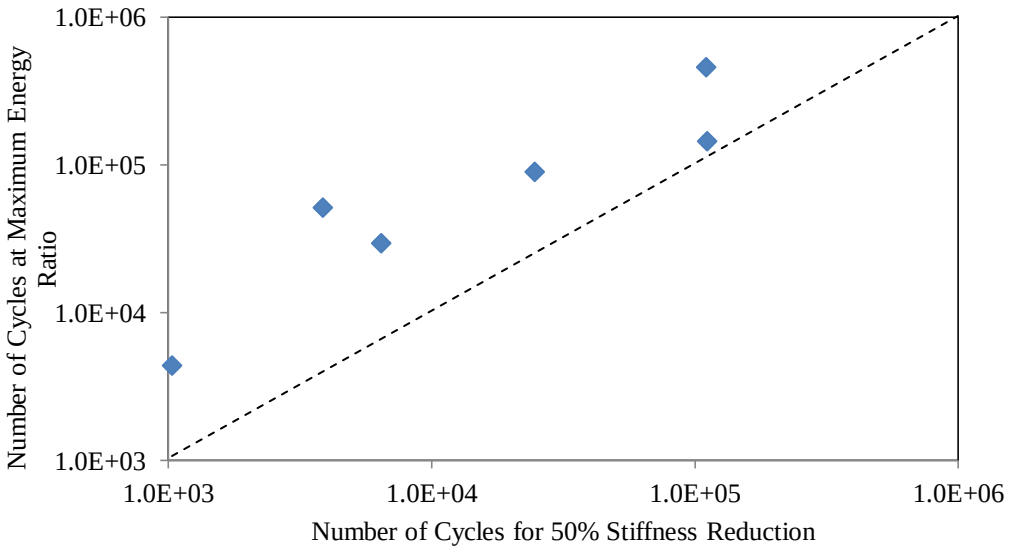

Figure 5.6 Comparison of Number of Cycles at Maximum Energy Ratio and Number of Cycles for 50% Stiffness Reduction for SP-III Mixture

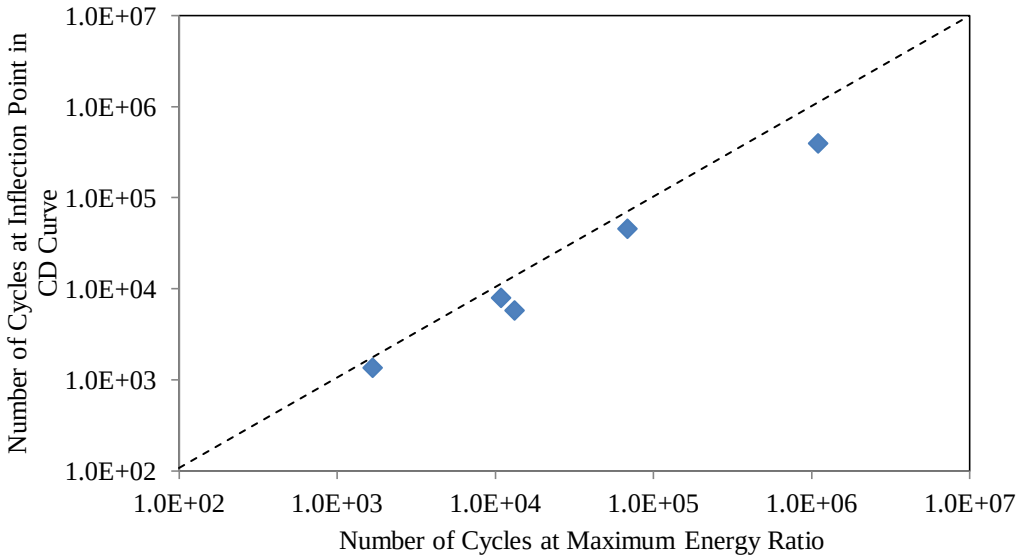

Figure 5.7 Comparison of Number of Cycles at Inflection Point and Number of Cycles at Maximum Energy Ratio for SP-II Mixture

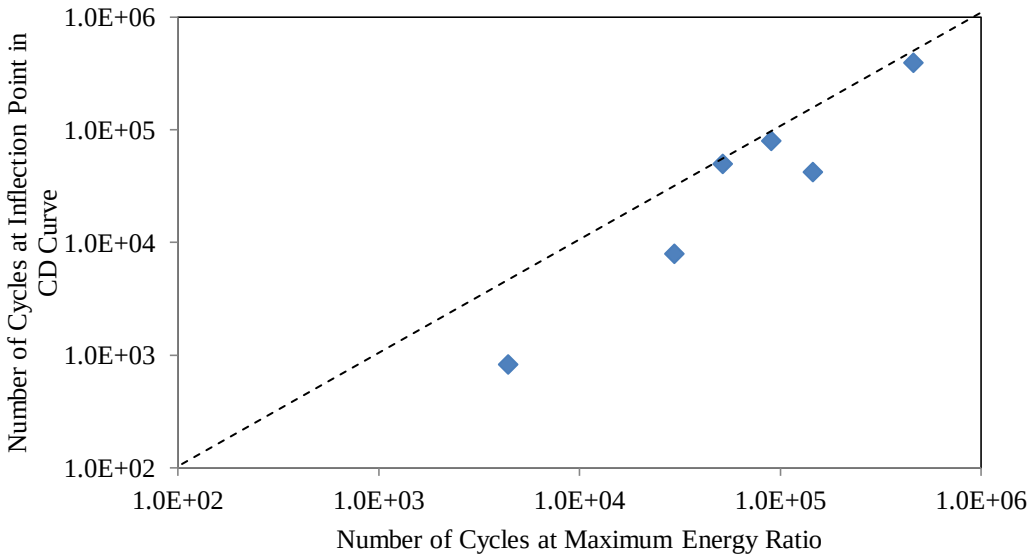

Figure 5.8 Comparison of Number of Cycles at Inflection Point and Number of Cycles at Maximum Energy Ratio for SP-III Mixture

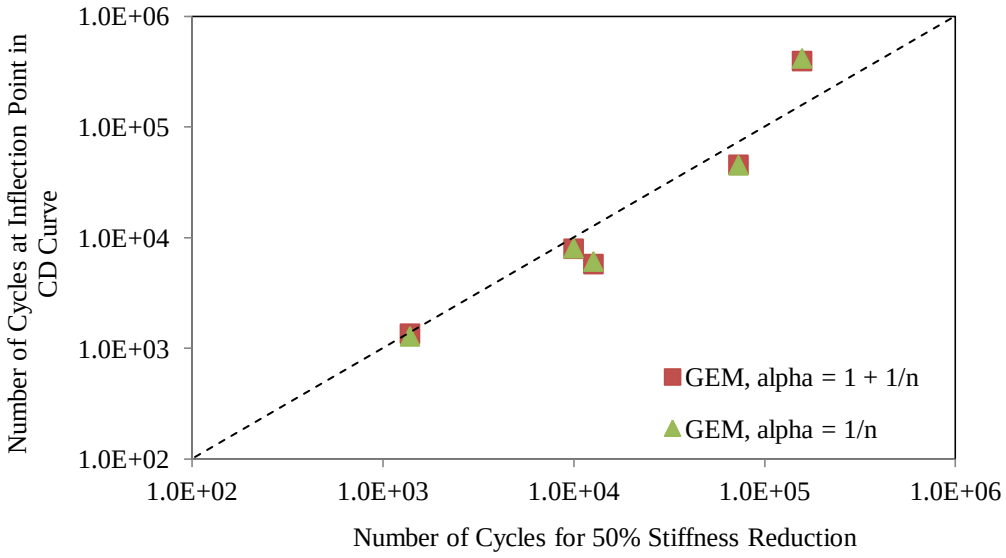

Figure 5.9 Comparison of Number of Cycles at Inflection Point and Number of Cycles for 50% Stiffness Reduction for SP-II Mixture

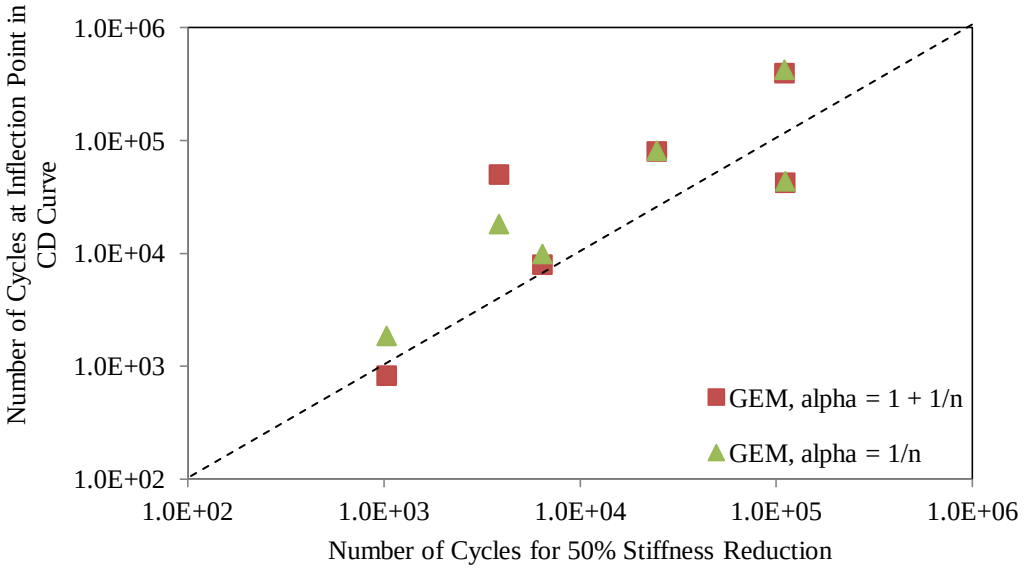

Figure 5.10 Comparison of Number of Cycles at Inflection Point and Number of Cycles for 50% Stiffness Reduction for SP-III Mixture

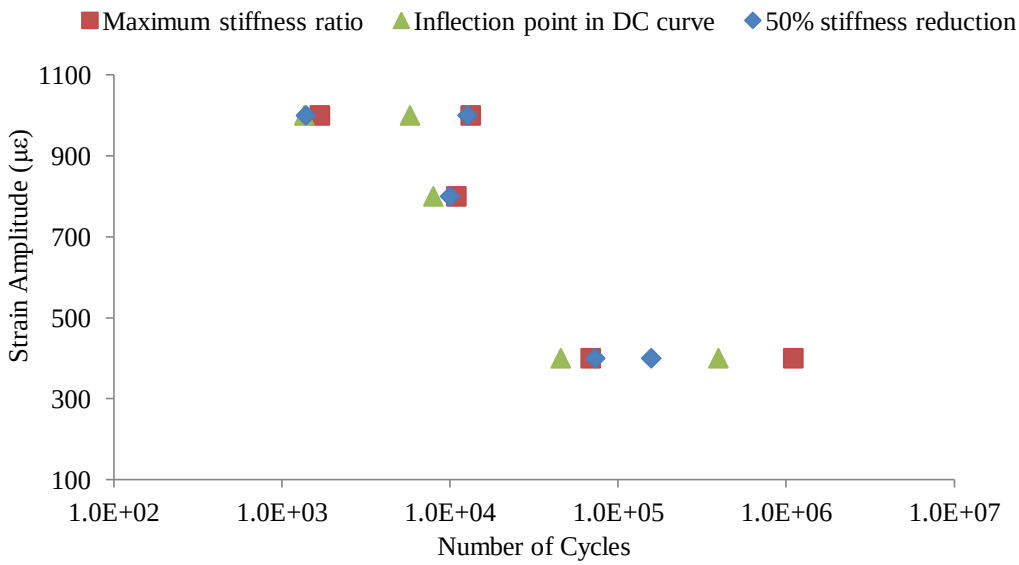

Figure 5.11 Effect of Strain Amplitude on Failure Criteria for SP-II Mixture

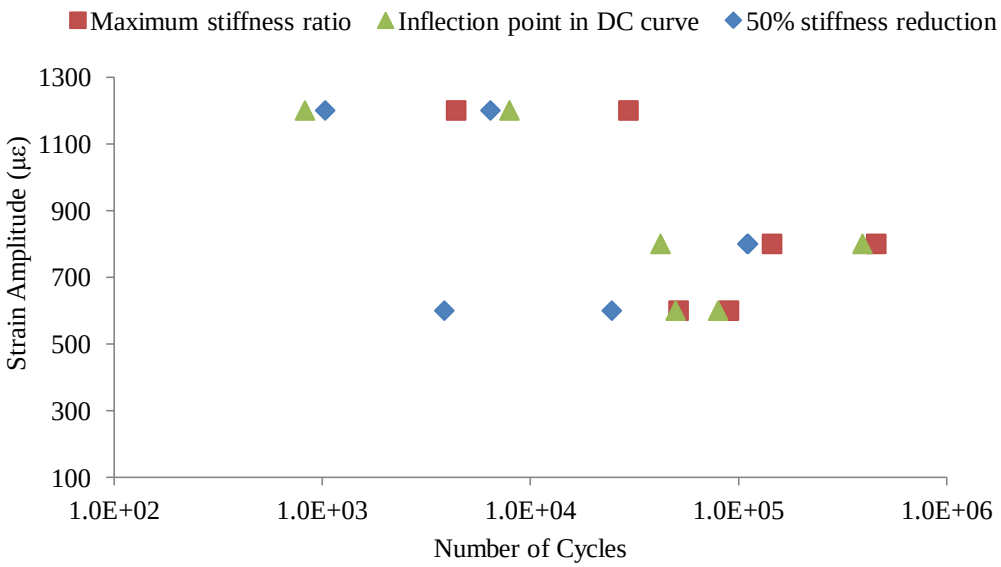

Figure 5.12 Effect of Strain Amplitude on Failure Criteria for SP-III Mixture

CHAPTER VI
FATIGUE CRACK PROPAGATION IN HMA MIXTURES

6.1 Introduction

It has been well documented that fatigue cracking has three stages; crack initiation, propagation, and rapid failure (Kravchenko 1964). Under controlled displacement flexural mode of loading, the stress in the beam reduces with increase in loading cycles. Due to testing difficulties, it is difficult to monitor development and propagation of cracks in the beam. Often, it takes a large number of load repetitions to see a macrocrack in the beam. For this study, traditional four-point bending is performed on HMA beam specimens and the resulting fatigue cracking is analyzed. Fatigue testing is conducted in an environmental chamber where the temperature is kept constant at 20°C. At the end of each test, each beam is examined and where visible, cracks are highlighted and photographed. In addition, crack lengths are measured using a scale roller pen, and separated into three categories, depending on where the location of the crack existed: within the asphalt mastic, through aggregates, and at the interface between aggregate and asphalt mastic.

The mastic is a the mixture of fine aggregate passing the #200 sieve and asphalt binder, which is a viscoelastic composite that has adhesive and cohesive properties capable of withstanding tensile forces (Kias 2008). The interface is

defined as the surface that is the boundary between the binder, or mastic, and the aggregate. The aggregate consists of coarse particulate matter that is coated with binder and forms the load-bearing skeleton of the HMA. Cracks can initiate and propagate through any of these three phases. The objective of this paper is to determine a pattern or trend, if any, of crack initiation and propagation in HMA materials, as well as understand why fatigue results may differ under similar testing conditions.

6.2 Background

Traditional mechanistic-empirical approaches for predicting fatigue of HMA mixtures require controlled stress (strain) laboratory testing, usually dictated by a single temperature over a range of applied stress (strain) levels. The number of cycles to failure is then recorded along with the critical stress (strain) level and a plot of this relationship describes the fatigue behavior of a HMA mixture. Usually, replicate samples are required for testing at different stress or strain levels. Results of fatigue testing of replicate samples should in theory be similar. However, this is not always the case as it is virtually impossible to recreate two to three identical samples. Aggregate alignment and distribution vary with each sample prepared, and because of that, crack initiation and propagation rates change with each test. Therefore, it can only be assumed that the fatigue life differs from one sample to another, despite similar testing conditions.

Many test factors can be controlled such as mixture type, sample stiffness, percentage air voids, temperature, frequency, and aggregate gradation. However, due to the limited sample size, factors which are nearly impossible to control are the location and distribution of large size aggregates (greater than ½ inch). Beam sample size for fatigue testing is 15″ x 2.5″ x 2.0″ (AASHTO T321-07). Within these boundaries, larger size aggregates can congregate, which may lead to poor a density gradient, and ultimately premature fatigue failure. As stated earlier, fatigue failure has three stages; crack initiation, propagation, and failure. The presence of larger-size aggregates within close proximity of each other may induce crack initiation, as well as affect crack propagation rates.

There are numerous studies of crack behavior in metallic materials, yet crack initiation, crack path and propagation are not well understood in asphalt concrete. One particular study characterized crack initiation and propagation through HMA materials. In particular, crack pathways are evaluated by micro-mechanical testing of the phases of asphalt concrete in tension, compression, and shear, Results showed that the interface phase is preferential for crack initiation and propagation (Kias 2008). However, notched samples are tested under monotonic loading only. This study investigates cracking due to fatigue failure on un-notched HMA samples and the effects of the chosen crack path on the associated fatigue life.

6.3 Fatigue Test Results

6.3.1 SP-II Mixture

Table 6.1 presents the fatigue test results of SP-II mixture samples. The applied strain and initial stiffness of the beam (taken at 50 load cycles) are shown, as well as the percent air voids and fatigue life of each test specimen. The fatigue life is the number of cycles required to achieve failure. AASHTO T321-07 standards require that a sample achieve 50% reduction in initial stiffness (N_{f50}) before considered failed. However, this may only lead to minor cracking, even micro-cracking which may not be visible to the naked eye. Therefore, beam samples are tested until they achieved 80-90% reduction in initial stiffness, whereby macro-cracking can be easily identified. Also listed in Table 6.1 is the failure criterion ($N_{f(ER)}$) defined by the Energy Ratio method. The Energy Ratio approach is based on a stress-controlled study by Hopman et al. (1989) which claims to identify the point at which micro-cracking becomes a macro-crack (defined as fatigue failure). The Energy Ratio is obtained by multiplying stiffness by corresponding number of cycle. The point at which the maximum value of *ER* occurs is defined as the fatigue failure. The peak in the curve indicates the transition point between micro-crack formation and propagation of a macroscopic crack. The Energy Ratio is defined in Equation 6.1:

$$\textit{Energy Ratio (ER)} = \textit{Cycle Number}^{*}\ \textit{Stiffness} \tag{6.1}$$

where *E* is the flexural stiffness (kPa) and *N* is the number of cycles.

Table 6.1 shows that the strain range varied from 200 to 1000 με. Sample SP-II-L2 is tested at 200 microstrain (με) for 10 days, achieving 8.5 million cycles, yet flexural stiffness reduced by only 30%. Therefore, testing is stopped and the applied strain is increased to 400 με for the next test.

Table 6.2 presents crack lengths measured for each SP-II sample. Crack lengths are measured as they pass through the asphalt mastic, aggregate, and interface phases. Each sample face is labeled clearly; Faces 1 and 3 are the sides of the beam, while Faces 2 and 4 are the bottom and top sides respectively. Micro and macro-cracking usually occurs at the base of the sample (Face 2) first, due to the presence of the maximum tensile strain, which is induced during flexure. The cracking propagates upward through the beam until it eventually appears on the topside of the beam. This process basically simulates the behavior of fatigue cracking in the field.

Replicate samples which are tested under similar conditions are analyzed. Samples SP-II-A1, SP-II-M2, and SP-II-N2 are tested at 400 με. All tests are conducted at the same frequency (10 Hz) and temperature (20°C), and contain similar air voids (5-6%). Sample SP-II-A1 failed after 263,111 cycles (N_{f50}). Table 2.2 shows that sample SP-II-A1 had a total crack length of 3 inches. The majority of the crack length occurred along the interface (93%), whereas the remaining cracks propagated through the asphalt mastic (3%) and aggregates (4%).

Figure 6.1 illustrates the cracking in the base of sample SP-II-A1 and shows that the crack path propagates at the interface between large size aggregates and asphalt mastic. The crack then propagated towards the topside of the beam, as shown in Figure 6.2. However, when compared with replicate test samples, the fatigue life data differs. It can be seen from Table 2.1 that sample SP-II-M2 is of same mix type, contained similar air voids, but had slightly lower flexural stiffness. SP-II-M2 is also tested at 400 με but yielded a far greater fatigue life.

Figure 6.3 shows the crack path in sample SP-II-M2. The data shown in Table 6.2, shows that only 33% of the crack length occurred at the interface, with the majority, 52%, passing through aggregates. As expected, the crack propagation rate is reduced when cracks pass through aggregates, therefore extending the fatigue life of the material. This scenario may explain the superior fatigue life of sample SP-II-M2 when compared with sample SP-II-A1.

The last replicate sample, SP-II-N1, is shown in Figure 6.4. Little or no cracking is evident in the sample, except for minor cracking which is visible at the interface of a large aggregate in the base of the sample. The reason for low cracking in sample SP-II-N1 is because the test is stopped after achieving only 70% reduction in stiffness, whereas 80-90% usually initiates unstable macro-cracking. However, the sample SP-II-N1 achieved 50% reduction in stiffness (failure) well before samples SP-II-A1 and SP-II-M2. The remaining SP-II

samples described in Table 6.1 all show similar results (N_{f50} data) to their replicate test samples.

6.3.2 SP-III Mixture

Table 6.3 presents fatigue test results of SP-III mixture samples. Once again, sample name, applied strain, sample stiffness, percent air voids, and fatigue life of each test specimen are shown. The applied strain varied from 70 to 1200 με. Once again, initial test samples, SP-III-A1 and SP-III-B1, experienced 25 and 3.5 million cycles respectively, without achieving failure. Therefore, testing is continued at higher strains and the results are analyzed. In general, with increasing strain, fatigue life reduces. This trend is shown in Table 6.3, when looking at the average number of cycles to failure for each strain level.

As with the SP-II mixtures, fatigue results from replicate samples tested at the same applied strain are analyzed and discussed. Samples SP-III-F2, SP-III-J1, and SP-III-M2 are tested at 800 με, under identical conditions. Table 6.4 presents crack lengths measured for each SP-III sample. Crack lengths are measured as they pass through the asphalt mastic, aggregate, and interface phases. Each sample face is labeled clearly; Faces 1 and 3 are the sides of the beam, while Faces 2 and 4 are the bottom and top sides respectively.

Figure 6.5 shows multiple cracking primarily located at the interface of aggregates and asphalt mastic of sample SP-III-F2. Table 6.3 confirms this

observation with 80% of total cracking occurring at the interface. From Figure 6.6, cracks are highlighted propagating upwards through sample SP-III-F2 from the bottom side. The crack follows a path along the interface of a large aggregate whereupon it stops about halfway through the beam. The fatigue life of sample SP-III-F2 is 114,000 cycles. When compared with replicate sample SP-III-J1, which has a much shorter fatigue life, it can be seen that almost 90% of the cracking occurred at the interface also. Figure 6.7 shows the crack path in the base of sample SP-III-J1. Large air voids are visible which may have initiated cracking, and almost certainly increased the crack propagation rate. Therefore, the fatigue life of sample SP-III-J1 with 38,000 cycles, is much shorter than that of sample SP-III-F2.

Finally, sample SP-III-M2 showed a fatigue life similar to that of sample SP-III-J1, with 42,000 cycles. Once again, Table 6.4 shows that 60% of the crack path is located at the interface. Figure 6.8 shows some air voids present between large size aggregates, but surprisingly, the crack path did not pass through the air voids. Instead, the crack followed a path along the interface between two large aggregates. This suggests that the effect of air voids is minimal on cracking in this sample. When comparing all three samples, each show similar values in terms of flexural stiffness, ranging between 400-450 ksi, and percentage air voids varying from 5 to 6%. Therefore, judging by the photographic evidence of cracking highlighted in each sample, the distribution of large-size aggregates seems to play a vital role. Sample SP-III-F2 has a much better distribution of large size

aggregates within the asphalt mastic than that shown in samples SP-III-J1 and SP-III-M2. In addition, the presence of voids does not necessarily cause crack initiation or even propagation. Rather, the presence of larger size aggregates close to one another, and crack propagation along the interface of these aggregates may reduce the fatigue life in the HMA materials.

From this study, the measured crack lengths from fatigue test results of SP-II and SP-III mixtures show that the majority of the cracking occurred at the interface. 54% and 70% of the total fatigue crack lengths in SP-II and SP-III samples are measured at the interface phase. This finding concurs with other studies which showed that the interface phase is preferential for crack initiation and propagation (Kias 2008).

6.4 Conclusions

The conclusions being made here are:

- HMA mixture samples of similar mix design which are tested under similar conditions did not necessarily show similar fatigue lives. HMA fatigue life depends greatly on the ability of the material to withstand crack propagation. This study shows that the location and distribution of large size aggregates within the asphalt matrix affects crack propagation, whereby crack paths often propagate at the interface of the large aggregates and asphalt mastic.

- Failure due to fatigue cracking most often occurred at the interface of HMA samples where 54% and 70% of the total fatigue crack lengths in SP-II and SP-III samples are measured at the interface phase.
- Approximately 30% and 20% of the total fatigue crack lengths are measured in the mastic phase, and 17% and 10% are measured in the aggregate phase, of SP-II and SP-III samples.

Table 6.1 Flexural Fatigue Test Results for SP-II Mixture Samples

Beam ID	Applied ε_t ($\mu\varepsilon$)	Initial E_0 (psi)	% Air Voids	Cycles Tested	Failure Criteria		Avg. Cycles to Failure	
					N_{f50}	$N_{f\ (ER)}$	N_{f50}	$N_{f(ER)}$
L2	200	954,638	5.4	8,479,090	NA	NA	NA	NA
N2	400	646,000	5.2	115,101	79,008	69,069	355,377	469,631
A1	400	880,310	5.4	389,811	263,411	239,818		
M2	400	666,158	5.9	1,535,746	723,711	1,100,007		
I2	800	471,000	5.1	23,612	11,700	10,910	11,100	45,661
L1	800	655,716	5.8	156,076	10,500	80,412		
N1	1000	853,302	4.8	2,665	1,085	1249	2,795	5,795
O2	1000	531,200	5.7	17,256	4,504	10,341		

Table 6.2 Crack Lengths in Failed SP-II Samples

Sample	Sample	Fatigue Cracking (in)				Crack Location (%)		
I2	Side	Mastic	Aggregate	Interface	Total	Mastic	Aggregate	Interface
Side 1	Face 1	0.3	0.77	1.07	2.1	14.0	36.0	50.0
Bottom	Face 2	1.29	1.84	2.01	5.1	25.1	35.8	39.1
Side 2	Face 3	0	0	0.55	0.6	0.0	0.0	100.0
Top	Face 4	0	0	0	0.0	NA	NA	NA
M2	Face 1	0.52	0.45	1.89	2.9	18.2	15.7	66.1
	Face 2	0.55	1.84	1.17	3.6	15.4	51.7	32.9
	Face 3	0.45	0	1.74	2.2	20.5	0.0	79.5
	Face 4	1.86	0	0.42	2.3	81.6	0.0	18.4
L1	Face 1	0.25	0	0.6	0.9	29.4	0.0	70.6
	Face 2	0.89	0	1.61	2.5	35.6	0.0	64.4
	Face 3	0	0	0.79	0.8	0.0	0.0	100.0
	Face 4	0	0	0	0.0	NA	NA	NA
N2	Face 1	0	0	0	0.0	NA	NA	NA
	Face 2	0	0	1.17	1.2	0.0	0.0	100.0
	Face 3	0	0	0	0.0	NA	NA	NA
	Face 4	0	0	0	0.0	NA	NA	NA
N1	Face 1	0.4	0	0.17	0.6	70.2	0.0	29.8
	Face 2	0.22	1.19	1.6	3.0	7.3	39.5	53.2
	Face 3	0.72	0	1.32	2.0	35.3	0.0	64.7
	Face 4	0	0	0	0.0	NA	NA	NA
A1	Face 1	0.25	0.22	0.12	0.6	42.4	37.3	20.3
	Face 2	0.1	0.12	2.8	3.0	3.3	4.0	92.7
	Face 3	1.14	0	0	1.1	100.0	0.0	0.0
	Face 4	0	0.15	0.79	0.9	0.0	16.0	84.0
O2	Face 1	0.45	0	0.77	1.2	36.9	0.0	63.1
	Face 2	0.92	0.37	1.07	2.4	39.0	15.7	45.3
	Face 3	1.07	0	0	1.1	100.0	0.0	0.0
	Face 4	0	0	0	0.0	NA	NA	NA
TOTAL		11.38	6.95	21.66	40.0	28.5	17.4	54.2

Table 6.3 Flexural Fatigue Test Results for SP-III Mixture Samples

Beam ID	Applied ε_t (με)	Initial E_0 (psi)	% Air Voids	Cycles Tested	Failure Criteria		Avg. Cycles to Failure	
					N_{f50}	$N_{f(ER)}$	N_{f50}	$N_{f(ER)}$
A1	70	437,320	9.9	20,741,011	NA	NA	NA	NA
B1	400	537,945	4.9	3,539,851	NA	NA	NA	NA
C1	600	557,499	4.9	833,560	770,008	748,820	770,008	748,820
J1	800	455,466	4.8	106,276	38,001	52,926	64,668	82,776
M2	800	415,678	5.9	79,176	42,001	46,826		
F2	800	402,190	5	150,000	114,001	148,576		
B2	1000	433,644	4.8	50,701	29,801	35,276	25,201	30,276
P1	1000	582,762	4.8	40,901	20,601	25,276		
P2	1200	485,731	5	12,326	6,476	7,551	8,026	22,149
Q2	1200	451,938	5.8	52,526	9,576	36,746		

Table 6.4 Crack Lengths in Failed SP-III Samples

Sample	Sample	Fatigue Cracking (in)				Crack Location (%)		
P1	Side	Mastic	Aggregate	Interface	Total	Mastic	Aggregate	Interface
Side 1	Face 1	0.32	0	1.29	1.61	19.9	0.0	80.1
Bottom	Face 2	0.87	0.94	1.53	3.34	26.0	28.1	45.8
Side 2	Face 3	0.27	0.22	0.57	1.06	25.5	20.8	53.8
Top	Face 4	0	0	0	0	NA	NA	NA
M2	Face 1	0	0.34	0.57	0.91	0.0	37.4	62.6
	Face 2	0.72	0.17	1.32	2.21	32.6	7.7	59.7
	Face 3	0.25	0	0.65	0.9	27.8	0.0	72.2
	Face 4	0	0	0	0	NA	NA	NA
B1	Face 1	0	0	0	0	NA	NA	NA
	Face 2	0.25	0.47	0.92	1.64	15.2	28.7	56.1
	Face 3	0	0	0.27	0.27	0.0	0.0	100.0
	Face 4	0	0	0	0	NA	NA	NA
F2	Face 1	0	0	0.52	0.52	0.0	0.0	100.0
	Face 2	0.35	0.42	3.13	3.9	9.0	10.8	80.3
	Face 3	0	0	1.59	1.59	0.0	0.0	100.0
	Face 4	0	0	0	0	NA	NA	NA
Q2	Face 1	0.65	0.2	0.97	1.82	35.7	11.0	53.3
	Face 2	0.46	0.63	1.29	2.38	19.3	26.5	54.2
	Face 3	0	0	0.49	0.49	0.0	0.0	100.0
	Face 4	1.41	0	0.94	2.35	60.0	0.0	40.0
J1	Face 1	0	0	1.12	1.12	0.0	0.0	100.0
	Face 2	0.42	0	2.97	3.39	12.4	0.0	87.6
	Face 3	0.41	0	0.55	0.96	42.7	0.0	57.3
	Face 4	0	0	0	0	NA	NA	NA
B2	Face 1	0	0	0.62	0.62	0.0	0.0	100.0
	Face 2	0.46	0	0.2	0.66	69.7	0.0	30.3
	Face 3	0	0	0	0	NA	NA	NA
	Face 4	0	0	0	0	NA	NA	NA
P2	Face 1	0.27	0.12	0.5	0.89	30.3	13.5	56.2
	Face 2	0.19	0.22	2.26	2.67	7.1	8.2	84.6
	Face 3	0	0	0.65	0.65	0.0	0.0	100.0
	Face 4	0	0	0	0	NA	NA	NA
TOTAL		7.3	3.73	24.92	36	20.3	10.4	69.3

Figure 6.1 Fatigue Cracking in HMA Beam Sample SP-II-A1

Figure 6.2 Fatigue Crack Propagating Upwards in HMA Beam Sample SP-II-A1

Figure 6.3 Fatigue Cracking in HMA Beam Sample SP-II-M2

Figure 6.4 Fatigue Cracking in HMA Beam Sample SP-II-N2

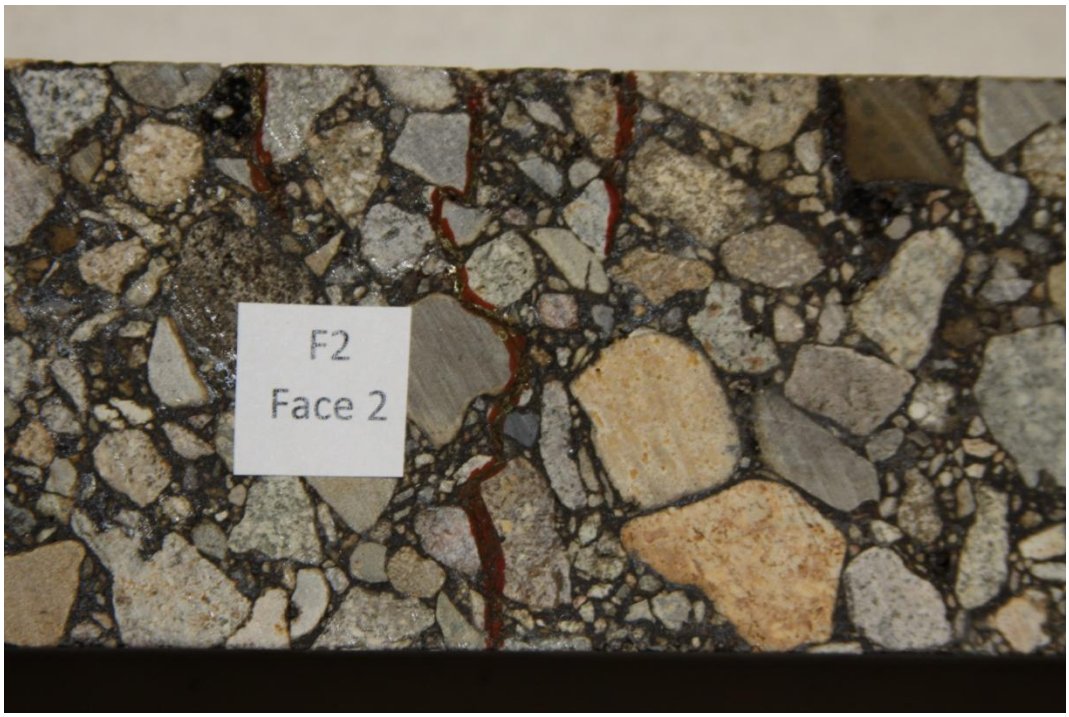

Figure 6.5 Fatigue Cracking in HMA Beam Sample SP-III-F2

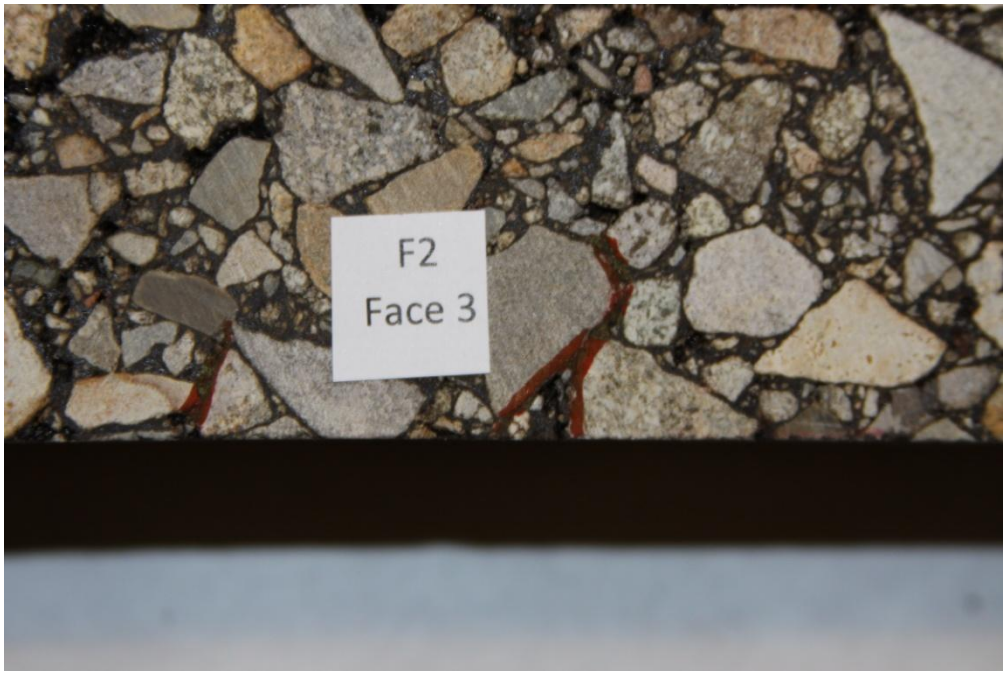

Figure 6.6 Fatigue Crack Propagating Upwards in HMA Beam Sample SP-III-F2

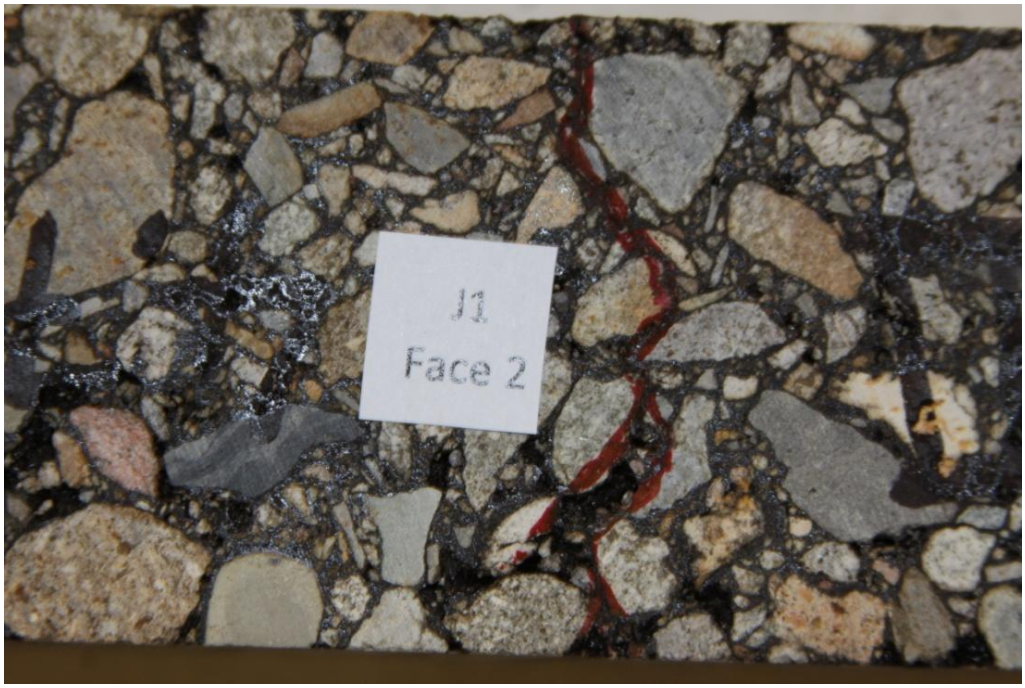

Figure 6.7 Fatigue Cracking in HMA Beam Sample SP-III-J1

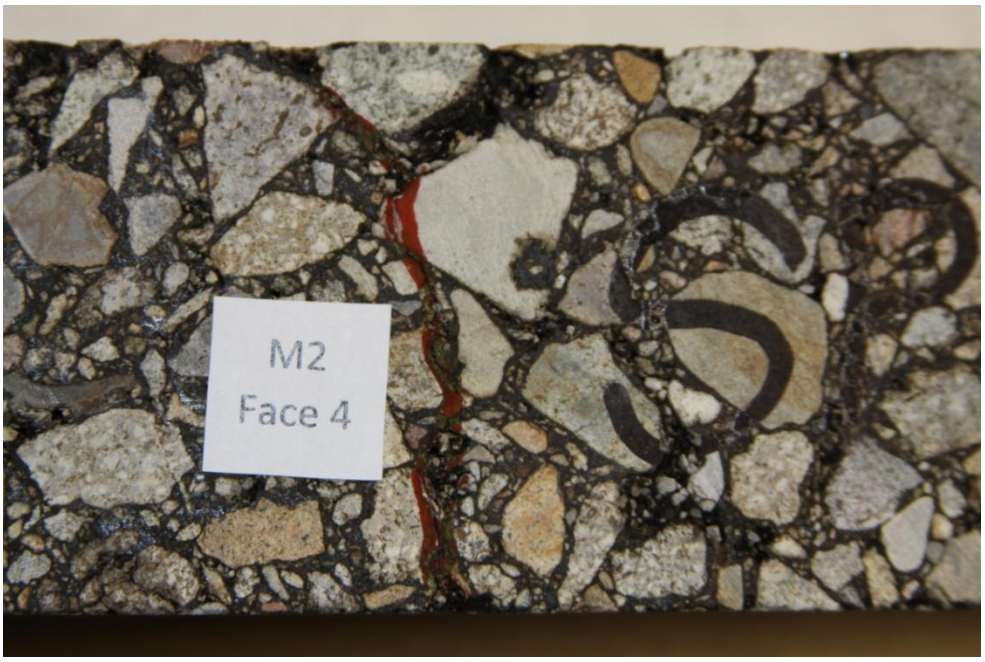

Figure 6.8 Fatigue Cracking in HMA Beam Sample SP-III-M2

CHAPTER VII

CONCLUSIONS AND RECOMMENDATIONS

7.1 Summary

This thesis documents an extensive laboratory investigation of fatigue endurance limits in asphalt concrete. In addition, alternative fatigue failure criteria are compared, as well as the effect of crack propagation paths, and polymer-modified binder, on the fatigue life of asphalt concrete. The fatigue endurance limit is defined as the strain level below which a material sustains an infinite fatigue life without accumulating damage. Although, an infinite fatigue life for an asphalt pavement is not practical for design, a design life of 50 years or more is considered extraordinary long. Such a structure is termed a perpetual pavement, and is considered the future of pavement design. Although most of study focuses on laboratory fatigue failure of asphalt concrete, attempts are made to relate the findings with the field asphalt concrete fatigue, which can be incorporated in current pavement design methods.

Fatigue failure, especially in asphalt concrete, is poorly understood problem as described in Chapter 1. The main problem with the past studies on identifying fatigue endurance limits is that those studies are mostly based on the phenomenological approach which relates the number of loading cycles to fatigue failure with applied tensile strain and initial stiffness of material. However,

asphalt concrete is a viscoelastic material, which means that fatigue failure is temperature dependent. Chapter 1 formulates the problem statement.

Chapter 2 covers previous studies done to investigate the fatigue endurance limit as well as their limitations. A number of laboratory test methods developed in the past to determine fatigue failure are described. Very few studies, if any, address the fatigue failure of asphalt concrete from viscoelastic point of view. Hence the use of viscoelastic damage mechanics is recommended in addressing the current problem in asphalt concrete for fatigue failure.

Chapter 3 presents the experimental work performed in this study. In order to facilitate current standards, fatigue testing is performed using AASHTO T321-07. Four point bending is applied to beams using controlled strain loading for a range of strain amplitudes. In addition, a dynamic modulus testing is conducted to determine the linear viscoelastic range of asphalt concrete which is represented by dynamic modulus and phase angle mastercurves as well as the relaxation modulus. Dynamic modulus testing is usually performed on cylindrical samples (6 in. tall) under compression. On contrary, dynamic modulus testing of beam samples under flexural loading may be more useful as sample slabs (2-3 in. tall) can be extracted from the field and then directly tested, once they are cut to size. Laboratory sample preparation also included compaction using a linear kneading compactor, sample sizing using a stone-cutting saw, and finally sample

conditioning using an environmental chamber. Each fatigue test at a certain strain level required additional replicate samples (2-3) to be tested.

The results of laboratory fatigue testing at normal and low strain levels are presented in Chapter 4. Failure is defined as 50% reduction in stiffness and the majority of tests are conducted until sample stiffness has reduced by 80-90% in order to identify fatigue cracking. Beam samples which did not fail had their fatigue life determined using extrapolation techniques. In this way, a more complete picture of the fatigue behavior of asphalt concrete is described. Although previous studies have shown that an endurance limit does exist for HMA mixtures, an established value is yet to be determined, with values varying from 70-300 microstrain (με) based on mixture variability. Chapter 4 determines the FEL of HMA mixtures using the phenomenological approach as well as a fundamental energy based approach, the dissipated energy concept. Furthermore, two different stiffness-based fatigue failure criteria are compared, as well as their effect of the estimated FEL of HMA materials. In addition, the effect of certain mixture variables on the FEL is investigated. Starting from last one and half decades, polymer has been a part of asphalt binder. Therefore this study includes fatigue behavior of a polymer modified binder as well as that of base asphalt binder which is described in Chapter 4. Polymer-modified PG 70-22 and unmodified PG 64-22 binders are investigated for their effect on FEL of asphalt concrete.

Flexural fatigue testing has been used by the asphalt pavement industry for several decades. Various approaches have been used to relate fatigue performance with parameters such as stiffness, dissipated energy, cumulative dissipated energy, pseudostiffness and so on. Traditional fatigue relation testing relates the number of loading cycles to failure with applied tensile strain and initial stiffness of material. Furthermore, the number of loading cycles to failure is defined as that number of cycles at which the stiffness of a material reduces by 50%. Also, approaches based on cumulative dissipated energy require visual interpretation of plots and often ignore viscoelastic effects. On the other hand, approaches based on viscoelastic continuum damage have shown promising results. This approach has considerable advantages like reduction in testing time and resources, and is based on fundamental energy based approach. Therefore a viscoelastic damage mechanics model is very appropriate to examine fatigue failure in asphalt concrete. Chapter 5 compares stiffness based failure criterion with failure criterion based on viscoelastic continuum damage approach.

For this study, fatigue testing of HMA mixtures required controlled strain laboratory testing of replicate samples at various strain amplitudes. The number of cycles to failure is recorded along with the critical strain level and this relationship is used to describe the fatigue behavior of asphalt concrete. Replicate samples are tested at each strain level. However, fatigue test results of replicate samples did not always provide similar results. It is impossible to recreate two to three identical samples, hence crack paths in failed samples vary considerably.

Chapter 6 presents a study on the effect of the crack path on the fatigue life of asphalt concrete. Fatigue cracks are highlighted and photographed in each failed specimen. Crack lengths are separated into three categories, depending on where the crack existed; (1) within the asphalt mastic, (2) through the aggregates, and (3) at the interface between aggregate and asphalt mastic. Fatigue life data of replicate samples are analyzed using the crack path data as a means to understand inconsistent results.

7.2 Conclusions

The viscoelastic nature of asphalt concrete influences the fatigue life of laboratory tested asphalt beam samples. Therefore the viscoelastic continuum damage mechanics (VCDM) model can be considered a tool to determine the fatigue failure in AC. A comparison of selected fatigue analysis approaches, a summary of mixture fatigue results and the effects of polymer-modified binder on HMA mixture fatigue resistance are summarized in this section.

- Fatigue test results show that fatigue failure according to the Energy Ratio criterion most often occurred after a sample has achieved 50% reduction in stiffness, which is the traditional fatigue criterion.
- Fatigue life extrapolation using the single-stage Weibull function and RDEC approach showed good consistency with fatigue test results of SP-II and SP-III mixtures, performed at normal strain levels. However, for low strain testing, extremely high fatigue life data is predicted, which suggests that an overestimation of fatigue life.

- The FEL values of field SP-II and SP-III mixtures are predicted using the traditional ε-N relationship. The FEL of the SP-II mixture is estimated to be 195 με, using traditional failure criterion (Nf_{50}), and 231 με using the Energy Ratio failure criterion (*ER*). For the SP-III mixture, the FEL is estimated to be 308 με (Nf_{50}) and 313 με (*ER*), as shown in Table 7.1.
- The FEL values of field SP-II mixture using the ε-PV approach are estimated to be 235 με (*ER*) and 222 με (N_{f50}), and for the field SP-III mixture, the FEL is estimated to be 311 με (*ER*) and 341 με (N_{f50}), as shown in Figure 7.1.
- PV values predicted using the material property-based PV prediction model showed good consistency with PV values determined from laboratory testing. However, the estimated FEL values using the PV model are much lower than those predicted using the ε-N_f and ε-PV models.
- The effect of polymer modified binder on the FEL of HMA mixtures showed mixed results, with an increase in estimated FEL of SP-III mixture, but reducing the estimated FEL of SP-II mixture.
- The FEL of laboratory mixtures is much lower than that of the field mixes. In particular, the fatigue performance of laboratory SP-II mixtures compares well with that of field SP-II mixtures. However, the laboratory SP-III mixture performs poorly when compared with the fatigue performance of the field SP-III mixture.

- The F-test is performed on the ε-Nf and PV-ε curves to determine whether the curves developed using the N_{f50} and *ER* failure criteria are statistically the same. For ε-N regression curves through power law, it is determined that the two fatigue curves are statistically the same for the SP-III mixture. However, the opposite is the case for the SP-II fatigue curves. For the PV-ε curves, the F-Test shows that the fatigue curves are statistically the same using the different fatigue failure approaches.
- Using the VCDM approach, a point of inflection is identified in the damage characteristic curve beyond which the material loses its structural integrity at faster rate. This point is considered the fatigue failure of the sample.
- A strong correlation is found between the VCDM criterion and the stiffness-based failure criteria.
- Asphalt concrete beam samples of similar mix type which are tested under similar conditions did not necessarily show similar fatigue lives. The fatigue life depends greatly on the chosen crack path. This study showed that the path of least resistance i.e. the interface of the aggregates and asphalt mastic, greatly affected the associated fatigue life.

7.3 Recommendations for Future Work

Recommendations for future work based on this study are shown below:

- Perform tensile static load tests on asphalt concrete beams for both SP-II and SP-III mixtures to determine the maximum tensile strength of each mix type. These results can then be compared with initial flexural stiffness of test samples. Samples that have similar tensile strength values can then be selected for subsequent fatigue testing.
- The large variation in fatigue life data shown in this study may be due to human error introduced during the mixing or compaction process. In order to account for this, additional test samples were prepared using strict gradation control measures and tested for 500 loading cycles at low strain amplitudes. Results show that stiffness values were similar for samples with different percent air voids. In addition, stiffness variations were observed in samples of similar percent air voids. Therefore, it is recommended that emphasis be placed on achieving similar sample stiffness as well as similar air void content in future testing.

Table 7.1 Summary of FEL Performance of SP-II and SP-III Mixtures

	PG Binder Grade	
Mix Type	SP-II	SP-III
Field	PG 64-22	PG 70-22
Laboratory	PG 70-22	PG 64-22

	Predicted FEL Values (ε-N_{f50})	
Mix Type	SP-II	SP-III
Field	$195^1/222^2$	$308^1/341^2$
Laboratory	$171^1/209^2$	$185^1/182^2$

Note: 1=predicted from ε-N_{f50} model, and 2=predicted from ε-PV model

	Predicted FEL Values (ε-PV)	
Mix Type	SP-II	SP-III
Field	$231^1/235^2$	$313^1/311^2$
Laboratory	$218^1/268^2$	$202^1/268^2$

Note: 1=predicted from ε-N_{f50} model, and 2=predicted from ε-PV model

Field Mixtures	
SP-II	SP-III
High E*	Low E*
High E(t)	Low E(t)

Note: E*=Dynamic Modulus, E(t)=relaxation modulus

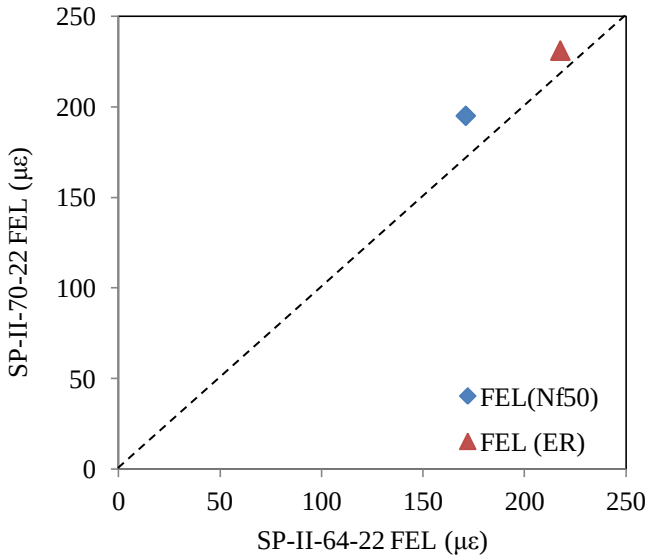

(a) SP-II Mix using ε-N_f Model

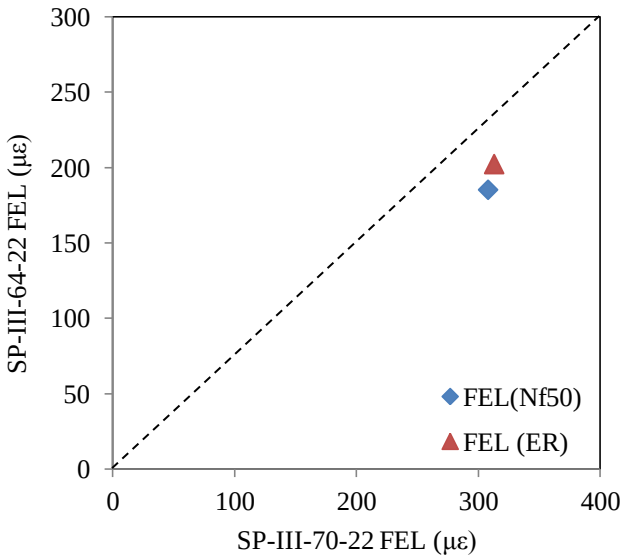

(b) SP-III Mix using ε-N_f Model

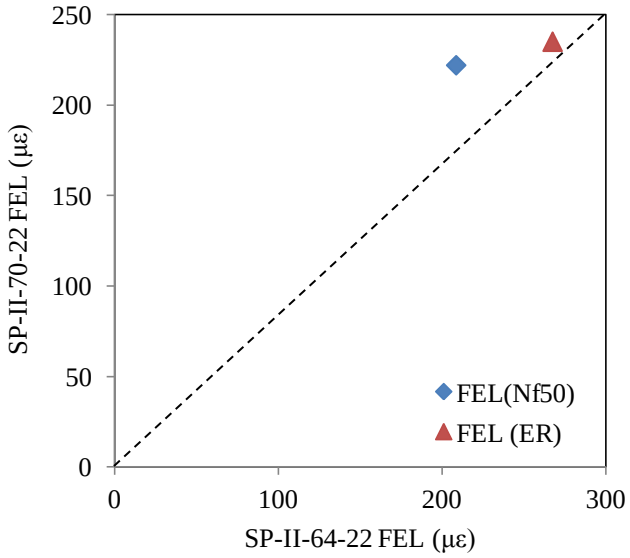

(c) SP-II Mix using ε-PV Model

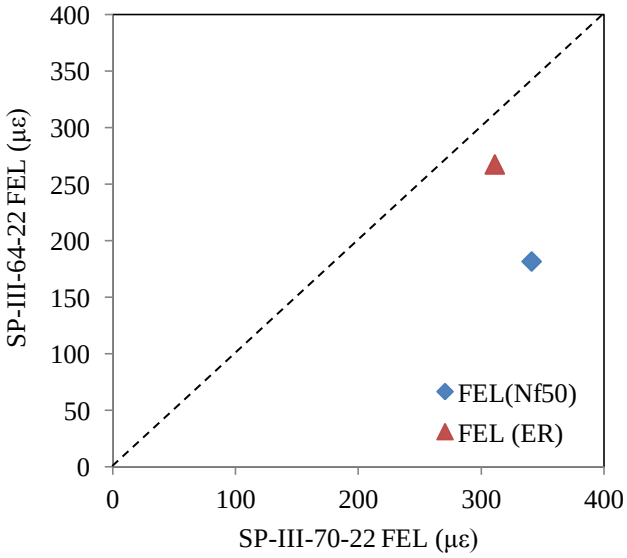

(d) SP-III Mix using ε-PV Model

Figure 7.1 Comparison of Predicted FEL Values for SP-II and SP-III Mixtures

REFERENCES

AASHTO T 166-07. "Standard Method of Test for Bulk Specific Gravity of Compacted Hot Mix Asphalt (HMA) Using Saturated Surface-Dry Specimens." *American Association of State Highway and Transportation Officials* (AASHTO), Washington D.C., (2007).

AASHTO T 168-07. Standard Test Method for Sampling Bituminous Paving Mixtures, *American Association of State Highway and Transportation Officials* (AASHTO), Washington D.C., (2007).

AASHTO T 209-07. Standard Method of Test for Theoretical Maximum Specific Gravity and Density of Hot Mix Asphalt (HMA), *American Association of State Highway and Transportation Officials* (AASHTO), Washington D.C., (2007).

AASHTO T 269-07. "Standard Method of Test for Percent Air Voids in Compacted Dense and Open Asphalt Mixtures." *American Association of State Highway and Transportation Officials* (AASHTO), Washington D.C., (2007).

AASHTO T 30-08. Standard Method of Test for Mechanical Analysis of Extracted Aggregate, *American Association of State Highway and Transportation Officials* (AASHTO), Washington D.C., (2008).

AASHTO T 308-08. Standard Method of Test for Determining the Asphalt Content of Hot-Mix Asphalt (HMA) by the Ignition Method, *American*

Association of State Highway and Transportation Officials (AASHTO), Washington D.C., (2008).

AASHTO T 312-07. Standard Method of Test for Preparing and Determining the Density of Hot Mix Asphalt (HMA) Specimens by Means of the Superpave Gyratory Compactor, *American Association of State Highway and Transportation Officials* (AASHTO), Washington D.C., (2007).

AASHTO T321-07. "Standard Test Method for Determining the Fatigue Life of Compacted Hot-Mix Asphalt (HMA) Subjected to Repeated Flexural Bending." *American Association of State Highway and Transportation Officials* (AASHTO), Washington D.C., (2007).

ASTM D7460-10. "Standard Test Method for Determining Fatigue Failure of Compacted Asphalt Concrete Subjected to Repeated Flexural Bending." ASTM International, West Conshohocken, PA, (2010).

Advanced Asphalt Technologies, LLC (2008). "Developing a Plan for Validating an Endurance Limit for HMA Pavements: HMA Endurance Limit Validation Study," National Cooperative Highway Research Program Project 9-44.

Bonnaure, F.P., Huibers, A.H.J.J., Boonders, A. (1982). "A Laboratory Investigation of the Influence of Rest Periods on the Fatigue Response of Bituminous Mixes," *Proceedings, Association of Asphalt Paving Technologists*, Vol. 51, Kansas City, Missouri.

Brown, S. F., Hakim, B. and Thom, N. H., (2004). "Performance and Rehabilitation of Heavy-Duty Pavements in the UK: Some Case Studies."

Proceedings of the International Symposium on design & construction of long lasting asphalt pavement. Auburn, Alabama. pp. 811-829.

Carpenter, S. H., Ghuzlan, K. A., and Shen, S. (2003). "Fatigue Endurance Limit for Highway and Airport Pavement." *Transportation Research Record*, No. 1832, pp. 131-138.

Carpenter, S. H., and Shen, S. (2005). "Application of the Dissipated Energy Concept in Fatigue Endurance Limit Testing." *Transportation Research Record*, No. 1929, pp. 165-173.

Carpenter, S. H., and Shen, S. (2006). "Dissipated Energy Approach to Study Hot-Mix Asphalt Healing in Fatigue." *Transportation Research Record*, No. 1970, pp. 178-185.

Carpenter, S. H. and Shen, S. (2009). "Effect of Mixture Variables on the Fatigue Endurance Limit for Perpetual Pavement Design." *Proceedings International Conference on Perpetual Pavements*. Columbus, Ohio 2009.

Chehab, G. R., Kim, Y. R., Schapery, R. A., Witczak, M. W., and Bonaquist, R. (2003). "Characterization of Asphalt Concrete in Uniaxial Tension Using a Viscoelastoplastic Continuum Damage Model." *Journal of the Association of Asphalt Paving Technologists*, Vol. 72: 315-355.

Clear, C. A. (1985). "The Effect of Autogenous Healing upon Leakage of Water Through Crack Initiation and Arresting in Epoxy." *International Journal of Fracture*, Vol. 55(3): 209-222.

Daniel, J.S. (2001). "Development of a Simplified Fatigue Test and Analysis Procedure Using a Viscoelastic, Continuum Damage Model and its

Implementation to WesTrack Mixtures." Doctoral dissertation, North Carolina State University, Raleigh, NC.

Daniel J.S. and Kim, Y.R. (2002). "Development of a Simplified Fatigue Test and Analysis Procedure Using a Visco-Elastic Continuum Damage Model." *Journal of the Association of Asphalt Paving Technologists*, Vol. 71: 619-650.

Edvardsen, C (1999). "Water Permeability and Autogenous Healing of Cracks in Concrete." *ACI Materials Journal*, Vol. 96(4): 448–454.

Epps, A. L., Harvey, J. T., and Monismith, C. L. (1999). "Performance Characteristics of Mixes Containing Asphalt Cements and Crumb Rubber Modified Binders." *Symposium on Asphalt, Number One Thermoplastic Polymer as part of the 217th American Chemical Society Meeting*, Anaheim, California, March 1999.

Freund, L. B., and Suresh, S. (2003). *Thin Film Materials: Stress, Defect Formation and Surface Evolution.* Cambridge University Press, Cambridge, United Kingdom.

Ghuzlan, K., and Carpenter, S. H. (2000). "Energy-Derived, Damage-Based Failure Criterion for Fatigue Testing." *Transportation Research Record*, No. 1723, pp. 141–149.

Ghuzlan, K (2001). "Fatigue damage analysis in asphalt concrete mixtures based upon dissipated energy concepts," thesis, presented to University of Illinois at Urbana-Champaign, IL, in partial fulfillment of the requirements for the degree of Doctor of Philosophy.

Goodrich, J.L. (1988). "Asphalt and Polymer Modified Asphalt Properties Related to the Performance of Asphalt Concrete Mixes." *Proceedings of Association of Asphalt Paving Technologists Technical Sessions*, Vol. 57, Williamsburg, VA, pp. 116–175.

Harvey, J. T., Deacon, J.A., Taybali, A.A., and Leahy, R.B. (1997). "A Reliability-Based Mix Design and Analysis System for Mitigating Fatigues Distress." *Proceedings of the 8th International Conference on Asphalt Pavements*, Vol. 1. University of Washington, Seattle, WA, pp. 301-323.

Hibbeler, R.C. (2005). *Mechanics of Materials*. Prentice-Hall, Inc., Upper Saddle River, NJ.

Jud, K., and Kausch, H. H. (1979). "Load Transfer Through Chain Molecules After Interpenetration at Interfaces." *Polymer Bulletin*, Vol. 1, pp. 697–707.

Kias, E.M.C. (2008). "Laboratory Evaluation of Cracking in Asphalt Concrete." Master's Thesis, University of New Mexico, Albuquerque, NM.

Kim, Y.R. (1988). "Evaluation of Healing and Constitutive Modeling of Asphalt Concrete by Means of Theory of Nonlinear Viscoelasticity and Damage Mechanics." Doctoral dissertation, Texas A & M University, College Station, TX.

Kim, Y. R., Lee, H. J., and Little, D. N. (1997a). "Fatigue Characterization of Asphalt Concrete using Visco-Elasticity and Continuum Damage Theory."

Journal of the Association of Asphalt Paving Technologists, Vol. 66, pp. 520-569.

Kim, Y. R., Lee, H. J, Kim, Y, and Little, D. N. (1997b). "Mechanistic evaluation of fatigue damage growth and healing of asphalt concrete: Laboratory and field experiments." *Proceedings of the 8th International Conference on Asphalt Pavements*, ISAP, Seattle, Washington, August 10-14, 1089-1107.

Kim, Y., Allen, D. H., and Little, D. N. (2005). "Damage-induced Modeling of Asphalt Mixtures through Computational Micromechanics and Cohesive Zone Fracture." *Journal of Materials in Civil Engineering*, ASCE, 17(5), pp. 477-484.

Kim, Y.R. (2008). *Modeling of Asphalt Concrete*. McGraw-Hill Professional, New York.

Kravchenko, P.E. (1964). *Fatigue Resistance.* Oxford; Pergamon Press, New York.

Leahy, R.B., Hicks, R.G., Monismith, C.L., and Finn, F.N. (1995). "Framework for Performance-Based Approach to Mix Design and Analysis." *Proceedings of the Association of Asphalt Paving Technologists*, Vol. 64, pp 431-473.

Lee, H.J., Daniel, J.S., Kim, Y.R. (2000). "Continuum Damage Mechanics-Based Fatigue Model of Asphalt Concrete." *Journal of Materials in Civil Engineering*, Vol. 12(2), pp. 105-112.

Lee, H. J., J. Y. Choi, Y. Zhao, and Y. R. Kim (2002). "Laboratory Evaluation of the Effects of Aggregate Gradation and Binder Type on Performance of

Asphalt Mixtures." *In Proceedings of the Ninth International Conference on Asphalt Pavements,* Copenhagen, Denmark. 2002.

Little, D. N., Lytton, R. L., Williams, D., and Kim, Y. R. (1999). "An Analysis of the Mechanism of Microdamage Healing Based on the Applications of Micromechanics First Principles of Fracture and Healing." *Journal of the Association of Asphalt Paving Technologists*, Vol. 68, pp. 501–542.

Lytton, R.L. (2000). "Characterizing Asphalt Pavements for Performance." *Transportation Research Record*, No. 1723, pp. 5–16.

Matthews, J., Monismith, C. L., and Craus, J. (1993). "Investigation of Laboratory Fatigue Testing Procedures for Asphalt Aggregate Mixtures." *Journal of Transportation Engineering*, Vol. 119, pp. 634-654.

Mechanistic-Empirical Pavement Design Guide – A Manual of Practice (Interim Edition). *American Association of State Highway and Transportation Officials* (AASHTO), Washington D.C., (2008).

Monismith, C. L., and Epps, J. A. (1970). "Asphalt Mixture Behavior in Repeated Flexure." *Report No. TE 70-5*, Institute of Transportation and Traffic Engineering, University of California, Berkley.

Mun, S., Guddati, M. N., and Kim, Y. R. (2004). "Fatigue Cracking Mechanisms in Asphalt Pavements with Viscoelastic Continuum Damage Finite-Element Program." *Transportation Research Record*, No. 1896, pp. 96-106.

Park, S.W., Kim, Y. R., and Schapery, R.A. (1996). ‘‘A Viscoelastic Continuum Damage Model and its Application to Uniaxial Behavior of Asphalt Concrete.’’ *Mechanics of Materials*, Vol. 24(4), pp. 241–255.

Petersen, J. C. (1984). “Chemical Composition of Asphalts Related to Asphalt Durability: State of the Art.” *Transportation Research Record*, No. 999, pp. 13–30.

Pierce, L. M. and Mahoney, J.P. (1996). “Asphalt Concrete Overlay Design Case Studies.” *Transportation Research Record*, No. 1543, pp 3-9.

Priest, A.L. (2006). “Methodology and Calibration of Fatigue Transfer Functions for Mechanistic-Empirical Flexible Pavement Design.” *NCAT Report 06-03*, National Center for Asphalt Technology, Auburn University, Alabama.

Pronk, A.C., and P.C. Hopman (1990). “Energy Dissipation: The Leading Factor of Fatigue.” Highway Research: Sharing the Benefits, *Proceedings of the Conference, the United States Strategic Highway Research Program (SHRP)*, London.

Pronk, A.C., “Comparison of 2 and 4-Point Fatigue Tests and Healing in 4-Point Dynamic Bending Test based on the Dissipated Energy Concept.” *Proceedings of the 8th International Conference on Asphalt Pavements*, Seattle, Washington, USA, 1997.

Prowell, B., Brown, E. R., Daniel, J., Bhattacharjee, S., Von Quintus, H., Carpenter, S. H., Shen, S., Anderson, M., Swamy, A. K., and Maghsoodloo, S. (2008). “Endurance Limit of Hot Mix Asphalt Mixtures

to Prevent Fatigue Cracking in Flexible Pavements." *Updated Draft Final Report, NCHRP 9-38*, National Cooperative Highway Research Program, Washington, D.C.

Prowell, B., Brown, E. R., Anderson, M., Daniel, J., Swamy, A. K., Von Quintus, H., Shen, S., Carpenter, S. H., Bhattacharjee, S., and Maghsoodloo, S. (2010). "Validating the Fatigue Endurance Limit for Hot Mix Asphalt." *NCHRP Report 6-46*, National Cooperative Highway Research Program, Washington, D.C.

Romero, P., Stuart, K.D., and Mogawer, W. (2000). "Fatigue Response of Asphalt Mixtures Tested by the Federal Highway Administration's Accelerated Loading Facility." *Journal of the Association of Asphalt Paving Technologists*, Vol. 69, pp. 212-235.

Roberts, F.L., Kandhal, P.S., Brown, E.R., Lee, D.Y., and Kennedy, T.W. (1996). *Hot mix asphalt materials, mixture design, and construction*. NAPA Education Foundation, Lanham, MD.

Rowe, G.M. (1993). "Performance of the Asphalt Mixtures in the Trapezoidal Fatigue Test." *Journal of Association of Asphalt Paving Technologists*, 62, 344-384.

Rowe, G.M. and Bouldin, M.G. (2000). "Improved Techniques to Evaluate the Fatigue Resistance of Asphaltic Mixtures." *Proceedings of 2nd Eurasphalt & Eurobitumen Congress*, Barcelona, Spain 2000.

Schapery, R. A. (1984). “Correspondence Principles and a Generalized J-integral for Large Deformation and Fracture Analysis of Viscoelastic Media.” *International Journal of Fracture*, Vol. 25, pp. 195–223.

Schapery, R. A. (1990). “A Theory of Mechanical Behavior of Elastic Media with Growing Damage and Other Changes in Structure.” *Journal of the Mechanics and Physics of Solids*, Vol. 38, pp. 215–253.

Shen, L. and Carpenter, S. H. (2005). “Application of Dissipated Energy Concept in Fatigue Endurance Limit Testing,” *Transportation Research Record*, No. 1929, pp. 165-173.

Stavrinidis, B., and Holloway, D. G. (1983). “Crack Healing in Glass.” *Physics and Chemistry of Glasses*, Vol. 24(1), pp. 19–25.

Sukhotskaya, S. S., Mazhorava, V. P., and Terekhin, Y. N. (1983). “Effect of Autogenous Healing of Concrete Subjected to Periodic Freeze–Thaw Cycles.” *Journal of Hydrotechnical Construction*, Vol. 17(6), pp. 295–296.

Swamy, A. K. (2011). “Evaluating Mode of Loading Effect and Laboratory Fatigue Performance of Asphalt Concrete using Viscoelastic Continuum Damage Mechanics.” Doctoral dissertation, University of New Hampshire, Durham, NH, 2011.

Swamy, A. K. and J. S. Daniel. (2011). “Modeling Flexural Fatigue Behavior using Viscoelastic 19 Continuum Damage Mechanics Principles.” *Proceedings of Engineering Mechanics Institute 2011*, Boston, USA.

Tangella, R., Craus, J., Deacon, J.A., and Monismith, C.L. (1990). "Summary Report of Fatigue Response of Asphalt Mixtures." *SHRP-A/IR-90-011*, Institute of Transportation Studies, University of California, Berkley.

Tarefder, R. A. and Bateman, D. (2010) "Future Design of Perpetual Pavements for New Mexico," *Final Report*, Submitted to Research Bureau, New Mexico Department of Transportation, 2010.

Tayebali, A. A., Deacon, J. A., Coplantz, J. S., Harvey, J. T., and Monismith, C. L. (1992). "Fatigue Response of Asphalt-Aggregate Mixes." *Report No. SHRP A-404*, Strategic Highway Research Program, National Research Council, Washington, D.C.

Thompson, M.R., ad Carpenter, S.H. (2004). "Design Principles for Long Lasting Pavement," *Proceedings, International Symposium of Design and Construction of Long Lasting Asphalt Pavements*, National Center for Asphalt Technology, Auburn, AL.

Thompson, M. and Carpenter, S.H. (2006). "Considering Hot-Mix-Asphalt Fatigue Endurance Limit in Full-Depth Mechanistic-Empirical Pavement Design." *Proceedings International Conference on Perpetual Pavement Design* (CD-ROM), Columbus, OH.

Thompson, M. and Carpenter, S.H. (2009). "Perpetual Pavement Design: An Overview." *Proceedings of the 2009 International Conference on Perpetual Pavement*, Columbus, OH, 2009.

Timm, D., H., and Young, J., B. (2004). "Effects of Load Spectra and Variability on Perpetual Pavement Design." *Proceedings, International Symposium of*

Design and Construction of Long Lasting Asphalt Pavements, National Center for Asphalt Technology, Auburn, AL.

Underwood, B.S. and Kim, Y.R. (2009). "Analytical Techniques for Determining the Endurance Limit of Hot Mix Asphalt Concrete," *Proceedings of the 2009 International Conference on Perpetual Pavement*, Columbus, OH 2009.

Van Dijk, W., and Vesser, W. (1977). "The Energy Approach to Fatigue for Pavement Design." *Journal of Association of Asphalt Paving Technologists*, Vol. 46, pp. 1–40.

Von Quintus, H.L., Mallela, J., and Jiang, J. (2004). "Quantifications of the Effects of Polymer-Modified Asphalt for Reducing Pavement Distress." *ER-215*, Asphalt Institute, Lexington, KY.

Walubita, L. (2006). "Comparison of Fatigue Analysis Approaches for Predicting Fatigue Lives of Hot-Mix Asphalt Concrete (HMAC) Mixtures." Thesis, presented to University of Texas A&M, TX, in partial fulfillment of the requirements for the degree of Doctor of Philosophy.

Willis, J.R. and Timm, D.H. (2009). "A Comparison of Laboratory Fatigue Thresholds to Measured Strains in Full-Scale Pavements." *Proceedings, International Conference on Perpetual Pavements*, Columbus, Ohio 2009.

Zhou, F., Hu, S., Chen, D., and Scullion, T. (2007). "Overlay Tester: Simple Performance Test for Fatigue Cracking." *Transportation Research Record*, No. 2001, pp. 1-8.

APPENDICES

APPENDIX A1

DESIGN OF OPTIMAL PERPETUAL PAVEMENT

Design of Optimal Perpetual Pavement Structure

Rafiqul A. Tarefder[1], and Damien Bateman[2]

Abstract

In this study, combinations of layer, stiffness, and thickness that produce an optimal perpetual pavement are determined for implementation on New Mexico State highways. Using a number of trial designs in the Mechanistic Empirical Pavement Design Guide (MEPDG), pavement performances are determined and analyzed for 50 year design life. It is shown that the required thickness of perpetual pavement varies from 10 to 15 in. for moderate to high truck traffic roads. One example is a pavement that has a 3 in. surface layer containing a fine asphalt mix and a 7 in. intermediate layer that uses a coarse asphalt mix. This perpetual pavement carries up to 180 million equivalent single axle loads (ESALs) over its 50 year design life. Low bottom-up fatigue cracking (< 12%) as

[1] Assistant Professor, Department of Civil Engineering, University of New Mexico, MSC01 1070, Albuquerque, NM 87131, Phone: (505) 277 6083, Fax: (505) 277 1988, Email: tarefder@unm.edu; Corresponding Author.

[2] Graduate Research Assistant and Ph.D. Candidate, Department of Civil Engineering, University of New Mexico, MSC01 1070, Albuquerque, NM 87131, Phone: (505) 277 3222, Fax: (505) 277 1988, Email: bateman@unm.edu

well as little or no top-down cracking (< 0.2 ft/mi) are observed at the end of 50 years. Rutting in the intermediate layer is also low (< 0.05 in.) at the end of the 10-year maintenance cycle. Overall, fatigue cracking is not a major concern in the design of perpetual pavements for New Mexico's conditions, rather rutting is more of a concern. For implementation of the perpetual pavements, a resurfacing plan is recommended to remove rutting (if > 0.1″) in the top surface every 10 year. Additionally, perpetual pavements with and without rich binder layers (RBLs) are examined in this study. Recommends are made for using a perpetual pavement that does not include a RBL based on life cycle cost analysis. Another factor that is investigated in this study is de-bonding of Hot Mix Asphalt (HMA) layers. Analysis shows that 88% of the perpetual pavements may fail by top-down cracking if de-bonding occurs between two HMA layers. Bottom-up cracking increases significantly in a de-bonded environment.

Key Words

Perpetual pavement, MEPDG, stiffness, de-bonding, rutting, fatigue, HMA, top-down cracking, design, ESAL, rich binder layer.

[1] Associate Professor, Department of Civil Engineering, University of New Mexico, MSC01 1070, Albuquerque, NM 87131, Phone: (505) 277 6083, Fax: (505) 277 1988, Email: tarefder@unm.edu; Corresponding Author.

[2] Graduate Research Assistant and Ph.D. Candidate, Department of Civil Engineering, University of New Mexico, MSC01 1070, Albuquerque, NM 87131, Phone: (505) 277 3222, Fax: (505) 277 1988, Email: bateman@unm.edu

Introduction

Traditionally, asphalt pavements have been designed for a 20-year life, whereas perpetual pavements are expected to perform for 50 years or more (Newcomb 2002, Nunn and Ferne 2001, Mahoney et al. 2007). Perpetual pavement in this study is defined as an asphalt pavement designed and built to last 50 years or more without requiring major structural rehabilitation or reconstruction. With perpetual pavements, the potential for traditional fatigue cracking is reduced, and pavement distress is typically confined to the upper layer of the structure (Walubita and Scullion 2007). Thus, when surface distress reaches a critical level, an economical solution is to remove and replace the top layer (Prowell et al. 2006). The perpetual pavement concept can be used for any pavement structure where it is desirable to minimize rehabilitation and reconstruction costs as well as minimize closures to traffic. These considerations are especially important on high-traffic volume freeways where user delay costs may be prohibitive. In particular, in urban areas where new roads are being built, use of perpetual pavements may minimize future costs due to user delays and construction. Perpetual asphalt pavement is a very appealing alternative to concrete pavements, especially for large metropolitan areas (Scholz et al. 2006, Merrill et al. 2006).

Perpetual pavement has been around for long time (Romanoschi 2008). While there are some successes with perpetual pavements, there is a big gap in our understanding the design of this pavement (Harvey 2004, Yang 2006). The main issue with the current perpetual pavement design method is that it does not ensure

optimum structure and/or layers that have yet to satisfy 50 year design periods. However, through a sound scheme of varying layer, thickness, and stiffness of pavement layers, it is possible to obtain optimal asphalt pavement structures that will last 50 years or more requiring only periodic top surface replacement. Such scheme should include mechanistic pavement design methodology, materials selection to improve rutting and fatigue resistance, prediction of performance, and life-cycle cost analysis (Tarefder et al. 2009).

Another critical issue with perpetual pavement design is that some of the most important factors related to pavement longevity are not adequately addressed by existing design approaches. In particular, the effects of interlayer de-bonding can be principal factor in reduction of pavement performance over time, yet this effect is only accounted for in a relatively crude manner (Tarefder et al. 2009, Scullion 2006). Thus, another goal of this study is to examine the effects of bonding/de-bonding on the design life of perpetual pavements. Having de-bonded layers within the HMA structure, fatigue cracking may initiate at the de-bonded interface, which may results in more severe the consequences on the pavement's fatigue life.

Yet another important issue regarding perpetual pavement design is the possibility of using perpetual pavement designs with binder 'rich bottom layer' or so called rich binder layer (RBL). Conceptually, this layer is softer or flexible than traditional binder layer so as to accommodate higher number of load repetition

without showing up any bottom-up cracking. Another way to prevent this bottom-up cracking is just by reducing the magnitude of the tensile strain at the bottom of the binder layer through use of thicker layer. Whether RBL layer has been associated with moisture infiltration issue, the thicker layer is related to cost issues (Walubita and Scullion 2007, Wills and Timm 2006). To this end, it is attempted in this study whether a perpetual pavement can be design without RBL and if so, then how economical it will be.

Objectives and Scope

The specific objectives of this study are to:

- Determine the optimal perpetual pavement structure using the mechanistic-empirical design approach to develop and evaluate design alternatives based on pavement layer, stiffness, and thickness. Also, perform a Life Cycle Cost Analyses (LCCA) to assess the most economic design among the alternative designs which pass the design life criteria of 50 years or more.
- Examine whether there is a need for a RBL in the design of perpetual pavement structure in New Mexico.
- Examine the behavior of the layers' interface due to non-bonding and bonding environments.

Structure of a Perpetual Pavement

A perpetual pavement a wear-resistant and renewable top layer, a rut-resistant intermediate layer, and a fatigue-resistant base layer (Asphalt Institute 2004, Hass et al. 2006). Figure 1 shows the structure of the perpetual pavement that is used in this study. It contains treated subgrade, granular base and a thick asphalt mat on top. The asphalt mat comprises of three different asphalt layers: surface course, intermediate course, and base course.

HMA Surface Layer: The choice of the HMA surface layer depends on the functional requirements, which could be a combination of comfort, durability, stability, skid resistance and noise reduction. There may be additional requirements like surface water drainage or very low water impermeability. A wide range of bituminous surface layer products can be considered appropriate depending on specific requirements. In some instances, the use of a conventional dense-graded Superpave mixture is adequate (Christopher and McGuffey 1997). In very high-traffic areas, the use of Stone Matrix Asphalt (SMA) may be attractive. In other instances, an Open Graded Friction Course (OGFC) is used to reduce splash and spray and to provide better skid resistance during rainstorms (Martin et al. 2001). An OGFC is considered to be a non-structural layer and therefore, it is not used pavement performance calculations in this study (MEPDG Interim Guide 2008). Rather, a dense-graded fine Superpave mix is considered as a surface layer.

HMA Intermediate Layer: HMA intermediate layer is the middle layer designed specifically to carry most of the traffic load. Therefore, it must be rut-resistant and durable. Rut resistance can best be provided by using stone-on-stone contact in the coarse aggregate and using binders having appropriate high-temperature properties such as high performance grade (PG) binders (Sides and Uzzan 2009, Timm and Newcomb 2006).

HMA Base layer: HMA base layer is designed specifically to resist fatigue cracking. Two approaches can be used to resist fatigue cracking in the base layer. First, the total pavement thickness can be made great enough such that the tensile strain at the bottom of the base layer is insignificant. Alternatively, the HMA base layer could be made using an extra-flexible HMA. This can be most easily accomplished by increasing the asphalt content of the base layer. As such, the base layer is called rich binder layer (RBL). Recently, the need for the rich bottom fatigue layer has been questioned especially when the total HMA thickness is greater than 12 inches (Tarefder et al. 2008, Sargand 2009).

Review of Current Practices

There have been several state DOT, FHWA, and AASHTO studies involving the design, construction, and testing of existing perpetual pavements (Powers 2007, Rowe et al. 2001, AMEC 2007, Scholz et al. 2007, Mahoney 2001, Krebs 2008, Battaglia 2009, Green 2008, Renteria 2008, Scullion 2006). In this study, these all the state DOTs are contacted through email, fax, and phone (not survey) to collect

perpetual pavement data such as the number of pavement layer, thickness, and stiffness, design method, and field performance. Table 1 shows 17 states' perpetual pavement data. This is not an exhaustic list. There are states and agencies which have perpetual pavements but very little to no information on the perpetual pavements are available. However, the current list suffices the purpose of data gathering, which is to have a sense of mean and range of layer thickness, stiffness, and number of layers used in perpetual pavements. Table 1 presents the perpetual pavement sections built by their respective state highway agency, surface course life, design life, traffic volume, layer thickness, stiffness, and performance grade (PG) binder. Also shown in Table 1 is some statistical analysis of the data. The mean layer thickness is determined as well as the range (standard deviation) of thicknesses for each asphalt layer. This information is used in the Section 5 to determine an optimal perpetual pavement structure based on layer, thickness, and stiffness. From Table 1, it can be seen that polymer modified binders are more commonly used in surface and intermediate layers, in order to prevent rutting. The use of polymer-modified binders in base layers is rare. Based on the literature reviewed, only one state DOT (i.e., Illinois DOT) out of 17 has used a polymer-modified binder in its base layer.

In perpetual pavement design concept, the tensile strain at the bottom of the asphalt layer is kept so small that the fatigue life of the base layer becomes virtually infinite (Prowell et at. 2006, Von Quintus 2006). The limiting strain that leads to this infinite fatigue life is called endurance limit. An endurance limit or

limiting strain of 70 με (micro-strain) is the most common value used (Garcia and Thomas 2008, Carpenter 2006). To ensure limiting strain, currently two main approaches are used. The first approach is the construction of a bottom lift for the base layer with rich in binder content (i.e., RBL layer). The second approach is the increase of the total thickness of asphalt layers. Table 2 presents state DOTs that use a RBL in their perpetual pavements. Some DOTs decided against using a RBL as the potentially higher permeability of Superpave mixtures might allow moisture to infiltrate and become entrapped and this would lead to premature stripping of the HMA (Mueller 2007, Tarefder et al. 2005, AMEC 2007, Maupin 2001, Harm 2001). Maryland and Oregon DOTs do not include a RBL in their respective perpetual pavements, I-695 and I-5 (Scholz et al. 2006, Renteria 2008, Powers 2007). Texas, California and Ohio DOTs use both RBLs and polymer modified binders in their respective base and upper asphalt layers, to prevent fatigue cracking and rutting (Walubita and Scullion 2007, Martin et al. 2001, Green 2008).

Also shown in the last column of Table 2 is the design method used for each state perpetual pavement. Many US states still use AASHTO 1993 Pavement Guide for the design of perpetual pavements, such as Kansas, Washington, Oregon and New Jersey (Romanoschi 2008, Mahoney 2001, Scholz et al. 2006, Rowe et al. 2001). Several states have come up with their own mechanistic empirical design method such as California, Illinois and Texas, while others are in the process of developing a mechanistic-empirical method (Asphalt Institute 2004, Walubita and

Scullion 2007, Harvey et al. 2004). In this study, AASHTO's Mechanistic Empirical Pavement Design Guide (MEPDG) is used to analyze perpetual pavement design alternatives.

Perpetual Pavement Design Alternatives

Design alternatives are developed based on a test matrix of varying design parameters used as inputs to MEPDG. Design trials are created based on layer stiffness and thickness. Traffic volume, climate, and pavement distress criteria are selected to represent traffic and climatic conditions of New Mexico. Pavements that pass the predefined performance criterion are considered perpetual pavements. In addition, HMA mixes used in successful perpetual pavements are analyzed with particular emphasis on performance in the intermediate and rich binder layers. LCCA is employed for final selection of perpetual pavements.

Input Matrix

An input matrix is devised to combine these parameters as level 3 input to MEPDG. Table 3 presents the input matrix. This input matrix is created to determine how a perpetual pavement performs based on the individual layer thicknesses, HMA mix design, and PG-binder grades. Traditionally, NMDOT allows only one type of materials in untreated base course, which are granular materials or granular base (GB). The thickness of the granular base in New Mexico traditionally varies from 6 to 10 inches. The granular base thickness is set

to 6 in. to reduce the trial designs. The thickness of the treated subgrade layer is 12 in.

Review of NMDOT projects reveal that most of the NMDOT flexible pavement thicknesses fall below 15 inches (Tarefder and Damien 2010). Therefore, the maximum thickness of HMA layer is set to 15 in. The surface layer thickness varies from 1.5 to 3 inches. The RBL thickness varies from 3 to 7 inches all over the United States (Tarefder and Damien 2009). A RBL layer thickness of 5 inches is the mean thickness taken from 38 perpetual pavement data collected. From this data the standard deviation is also calculated and used to determine the range of thicknesses of the rich-binder layers. The thicknesses of the intermediate layer are calculated based on the total HMA layer thickness minus the surface and RBL layers. An additional 2 and 4 inches are subtracted from the resulting intermediate layer thickness to account for total thickness of 11 and 13 inches. Adjustments are made here to reduce the total thickness so as to produce more feasible alternatives for NMDOT.

Other parameters that are varied in the matrix are the mix design and the binder's Performance Grade (PG). Two modified PG binders are used in the surface and intermediate layers. These are PG 76-22 and PG 70-22 binders. PG 64-22 is used in the rich binder layer for flexibility. The input matrix contains 3213 runs. The number of runs is calculated using the formula below:

$$Input\ Matrix = Surface \times Intermediate \times RBL \times Mix\ type\ \times Binder\ PG$$

$$= (T_1 \times 3) \times (T_3 \times 3) \times (15 - T_1 - T_3) \times (13 - T_1 - T_3)$$

$$\times (11 - T_1 - T_3) \times (Mix_1^2) \times (Mix_2^3) \times (Mix_3^3) \times (PG_1^2) \times (PG_2^2)$$

where T_1 = thickness of surface layer, T_3 = thickness of rich binder layer, 15-T_1-T_3 = thickness of intermediate layer, SuperPave (SP) Mix_1 = SP-II, Mix_2 = SP-III, Mix_3 = SP-IV, PG_1 = PG 70-22, and PG_2 = PG 76-22, and *SP* = SuPerPave (Superior Performing Pavement).

Table 4 shows Superpave mix gradations used by NMDOT. Mix SP-II is a coarse mix. Mixes SP-III and SP-IV are fine mixes. As it can be seen from Table 4, mix SP-IV contains higher percentage of fine aggregates (% passing < #200 sieve) than mix SP-III. Therefore, mixes SP-III and SP-IV are used in the surface course. The intermediate and RBL layers use mix type SP-II, SP-III, and SP-IV. The percentage air voids and effective binder content are shown in Table 4. They are set to the criterion specified by the NMDOT for these mixes. The surface and intermediate HMA mix designs contain 6% air voids. In New Mexico, HMA mixes are compacted at 6±1% air voids in the field but designed at 4±1% air voids. The RBL contains 3% air voids. In general, rich binder layers use a higher percentage of binder than traditional surface mix. The extra binder fills the voids in the mineral aggregate and thus creates a low air-void mix.

Design Simulations

The MEPDG Version 1.0 is used for running design simulations. The MEPDG is based on mechanistic-empirical principles, where mechanistic part assumes that

pavement can be modeled as a multi-layered elastic structure and the empirical part related stress-strain to common term pavement distresses such as rutting, fatigue cracking, roughness (NCHRP 2008). There are three levels of inputs in the MEPDG analyses. In Level 1, materials properties such as dynamic modulus of asphalt concrete and resilient modulus of soils and aggregate are obtained from laboratory tests. In Level 2, these properties are determined using existing or local correlation equations. In Level 3, the dynamic and resilient moduli are calculated from index properties such as soil classification, plasticity, aggregate gradation, binder content, etc. using nationally calibrated correlations or equations. The MEPDG's level 3 analysis is calibrated to nationwide standards. However, it would be more beneficial if level 1 analysis is used where the MEPDG is calibrated to meet local highway standards (NCHRP 2008). Unfortunately, this has yet to be done in New Mexico. So level 3 analysis is performed in this study to determine optimal perpetual pavement structure.

There are options available in MEPDG when considering fatigue cracking. One option is including a fatigue endurance limit for the pavement. A fatigue endurance limit considers the tensile strain experienced at the bottom of the HMA layer under traffic loading. If the tensile strain remains below the endurance limit, the pavement will have an infinite fatigue life. The fatigue endurance limit of NMDOT mixes are not known yet. Therefore, this study did not use fatigue endurance limit criteria. Rather, it uses the nationally calibrated fatigue model

which predicts the percentage fatigue cracking (MEPDG 2008, MEPDG Interim Guide 2008).

Traffic and Climatic Data

The functional classification of traffic, appropriate traffic class and growth factors are selected for designing perpetual pavements to last 50 years or more for major highways in New Mexico. The basic required MEPDG input data is Annual Average Daily Traffic (AADT), percentage of trucks in the design direction and on the design lane, operational speed, and traffic growth rate (MEPDG 2008, MEPDG Interim Guide 2008). For this study, all other required traffic inputs, such as monthly and hourly truck distribution, truck class distribution, axle load distributions, and some other general traffic inputs, are derived from the design guide level 3 or default values. Table 5(a) presents the traffic volumes used in this study. Table 5(a) also shows the equivalent number of ESALs to enhance the understanding of design traffic for 50+year perpetual pavements. The AADTTs used are 1750, 5000, and 10000 with a truck traffic classification (TTC) factor of 1, which considers predominantly single trailer trucks (Class 9 traffic). Traffic growth is similar to typical New Mexico interstate traffic growth which is 4%. Two lanes and 50 percent trucks in the design direction, operational speed of 70 mph, and vehicle tire pressure of 120 psi are used in this study.

Climate conditions may play a significant role in the performance of perpetual pavements. Pavements located in semi-arid regions require specific design criteria

to withstand the extreme temperature changes. The climatic data used in this study is taken from the weather station at Albuquerque, New Mexico. The water-table depth is known to below 10 ft depth. Variations in climatic inputs are not considered for perpetual pavement design in this study.

Base and Subgrade Input Data

The granular base consisted of compacted crushed gravel with a resilient modulus (M_R) of 20000 psi. The natural subgrade also contains A-5 material with M_R of 5000 psi. The resilient modulus (M_R) of the treated subgrade (TSG) is 8000 psi. The MEPDG does not include a special type 9 of material (for example: engineered materials) for treated subgrade, so this layer is treated as sandy soil (A-4) with an increased modulus of 8000 psi (MEPDG Interim Guide 2008).

Distress Criterion

The pavement performance criteria are shown in Table 5(b) (MEPDG Interim Guide 2008). Pavements are considered failed when the predicted distresses are equal to these target distress values. The MEPDG predicted results are analyzed based on surface-down cracking, fatigue cracking, AC rutting, total rutting, and International Roughness Index (IRI) over a period of 50 years. In this study however, priority is given to fatigue (bottom-up) cracking and asphalt concrete (AC) rutting. Indeed, the definition of a perpetual pavement is that a pavement having no bottom-up fatigue failure. Fatigue cracking is a major contributor to pavement failure and requires costly reconstruction. IRI is not considered in

selecting perpetual pavement designs, because periodic resurfacing of optimal perpetual pavement is planned with 3/4 in. open graded friction course (OGFC), which is assumed to take care of the IRI requirement. In this study, the predicted distress at the end of 50 years is directly compared to the target distress values shown in Table 5(b). These target distress values are recommended by the MEPDG for primary highway routes. Ideally, one should consider the reliability of distress model which is not considered in this study.

Analysis of Simulation Outputs Using Flow Charts

Using the inputs and performance criteria described above, MEPDG simulations are run for 50 years. From the outputs of 3213 simulations run, it is observed that none of the pavements experienced any thermal cracking over a period of 50 years. The use of modified binders and the location of the climate data (Albuquerque) might have reduced the impact of thermal cracking on the pavements analyzed. None of the 3213 pavements failed by surface-down cracking (> 700ft/mi). Thus, further investigation falls into the category of rutting and bottom-up (fatigue) cracking, which is done through flow charts in the next two sections.

Two options are sought for selecting perpetual pavement from 3213 simulation outputs. In option one, the pavements that pass the performance criteria at the end of 50 years do not need to be resurfaced. In option two, the assumption is it is most likely that the pavement top surface will deteriorate due to exposure, and

therefore, use 0.75 in. thick OGFC as a non-structural layer in every 10 year cycle.

Perpetual Pavements with No Resurfacing

In this section, perpetual pavements are identified that last 50 years without requiring resurfacing. A flow chart of 3213 perpetual pavements is created based on the performance criteria mentioned earlier and is illustrated in Figure 2(a). It can be seen that when fatigue cracking criteria of ≤ 20% at the end of 50 years is applied, only 8 pavements fail. Interestingly, thin pavements failed at relatively high annual average daily truck traffic (5000 AADTT). It can be noted that AADTT of 10000 is not applied to pavements with asphalt concrete (AC) thickness < 10″. Top-down and thermal cracking criterion (≤ 700ft/mi) is then applied to the remaining 3205 pavements and here it can be seen that none of the pavements failed by this performance criterion. However, when total rut criterion of ≤ 0.5″ is applied, none of the pavements pass. Figure 2(a) illustrates that using total rut criterion of ≤ 0.5″ and fatigue cracking ≤ 20%, no perpetual pavements can be found. The 8 eight pavements which failed by bottom-up cracking all have 8″ asphalt thickness and carry 5000 AADTT. None of these pavements contain a rich binder layer. As a next step, the rutting distress criterion is lifted from 0.5 to 0.75″. Once again, none of the pavements passed this criterion as Figure 2(b) illustrates.

Since none of the pavements passed the performance criterion for total rutting (AC + base + subgrade), priority is given to those pavements that pass by only AC rutting. Pavements that pass this criterion can have their subgrade material modified to prevent rutting in this layer. Hence, Figure 3(a) presents a flow chart which screens 3213 perpetual pavements based on AC rut criterion ≤ 0.25″ at the end of 50 years. It can be seen that about 405 perpetual pavements pass for AC rut ≤ 0.25″ and fatigue cracking ≤ 20%. However, all of these pavements have 15″ AC thickness for AADTT of 1750. In New Mexico, pavement thickness ranges from 4 to 10 inches. Therefore, a pavement with 15 inch AC layer thickness is not a viable option in New Mexico and therefore, thick pavements (AC greater than 10 inch) are not considered for further analysis. No perpetual pavements can be found using 5000 and 10000 AADTT.

As a next step, AC rut failure criterion is increased from 0.25 to 0.5″ at the end of 50 years. Based on a flow chart plotted in Figure 3(b), additional pavements are considered for further analysis. For AC rut ≤ 0.5″ and fatigue cracking ≤ 20%, perpetual pavements can be found for the following;

- For 1750 AADTT – 509 have 11″ and 648 have 13″ HMA thickness
- For 5000 AADTT – 5 have 14″ and 808 have 15″ HMA thickness
- For 10000 AADTT – 64 have 15″ HMA thickness

Findings

Table 6(a) presents perpetual pavements with 14″ HMA thickness and AADTT of 5000. All 5 pavements have a 3″ surface layer, 4″ intermediate layer, and 7″ RBL.

All of these pavements use PG 76-22 in their surface layers. All of these pavements have 8000 psi resilient modulus (M_R) in the treated subgrade layer.

Perpetual Pavements with Resurfacing

Figure 4(a) presents the same performance criteria (AC rut ≤ 0.25″) but resurfacing (using 0.75 inch non-structural OGFC) is considered every 10 years, if needed. Resurfacing is required if pavements show AC rutting of more than 0.25″ at the end of 50 years. Therefore, every 10 years pavements are allowed to have 0.05″ AC rutting. Thus at the end of 20 years, pavements are allowed to have 0.1″ AC rutting. Pavements failing this performance criterion need resurfacing (AC_1 rut → 0) and combined rutting in the intermediate and base layers are checked for having $AC_2 + AC_3 \leq 0.05″$ rutting every 10 years. At the end of 30 years, pavements are allowed to have 0.15″ rutting and so on. This criterion is checked against AC rut of intermediate and base AC layers but not for surface layers. This is logical as the surface layer is expected to have some OGFC treatment at 10 year intervals to maintain surface IRI and smoothness criteria. Therefore, in the analysis, rutting of the AC layer is set to zero after each maintenance cycle or 10 year.

For AC rut ≤ 0.25″ and fatigue cracking ≤ 20%, perpetual pavements can be as follows:

- For 1750 AADTT – 329 pavements have 11″, 621 pavements have 13″, and 293 pavements have 15″ HMA thickness

- For 5000 AADTT – 5 pavements have 14″ and 766 have 15″ HMA thickness
- For 10000 AADTT – 41 pavements have 15″ HMA thickness

Pavements with 14″ HMA thickness and 5000 AADTT are the same pavements mentioned earlier. Figure 4(b) presents a flow chart of pavements that are checked against AC rut criterion of 0.5″ at the end of 50 years. Resurfacing is also considered here if pavements show ≥ 0.1″ AC rutting after 10 years. Combined rutting in the intermediate and base layers is also monitored (AC_2 + AC_3 rut ≤ 0.1). For AC rut ≤ 0.5″ and fatigue cracking ≤ 20%, perpetual pavements can be found as follows;

- For 1750 AADTT – 37 pavements have 11″ HMA thickness
- For 5000 AADTT – 9 pavements have 10″, 17 pavements have 11″, 13 pavements have 12″, and 4 pavements have 15″ HMA thickness
- For 10000 AADTT – 357 pavements have 15″ HMA thickness

Findings

It can be seen that for 10000 AADTT, most of the perpetual pavements obtained are 15 inch thick. A pavement of 10 inch is considered very high and not feasible in New Mexico. Therefore, it is concluded that for very high traffic it is not possible to find a perpetual pavements thinner than 0 inch. Also, from the above discussion it can be seen that a number of perpetual pavements can be obtained for low traffic (AADTT 1750) roads. Ideally, perpetual pavements are not needed

for low traffic road. To this end, this continues to further analyze the perpetual pavement design alternatives obtained for 5000 AADTT. From the above discussion, itt is shown that 9 perpetual pavements have 10″ HMA thickness and 17 perpetual pavements have 11″ HMA thickness, each carrying 5000 AADTT, that pass the performance criteria for fatigue cracking and AC rutting.

Perpetual Pavements for 5000 AADTT

Table 6(b) presents perpetual pavements with 10″ AC thickness and 5000 AADTT. These pavements have shown to have the highest performance and the lowest thickness (10″). Material properties and pavement response data of these eight pavements are also shown. These perpetual pavements can carry up to 5000 annual average daily truck traffic (AADTT). This traffic is equivalent to 32 million ESALs at the end of 20 years, and 165 million ESALs at the end of 50 years.

- Run 2739 is not feasible due to lift thickness of the surface layer and the nominal size aggregate in this mix (SP-III).
- The remaining eight pavements have 3″ surface layer and use fine mixes (SP-III, SP-IV) and PG 76-22 in this layer.
- Six out the eight pavements have a 4″ intermediate layer.
- Two out of the eight pavements do not have a RBL, but they have thicker intermediate layers (7″).
- All of these pavements have 8000 psi resilient modulus (MR) in their treated subgrade.

- None of the pavements pass the total rut criterion of 0.75″. Resurfacing must be considered as total rutting will not be as high if the pavement is maintained every 10 years.

It can be noted that 10″ pavements carrying 5000 AADTT show very high rutting in the subgrade. Subgrade rutting is a major contributor to the failure of all pavements to pass the total rut criterion of 0.75″. However, by improving the material stiffness (MR) of the subgrade from 5000 psi to 15,500 psi (Default for A-5 material in MEPDG), subsequent rutting in this layer reduces, as Figure 5 illustrates. Figure 5 also shows the effect of this change to total rutting. Points to note from this analysis: Subgrade rutting reduces by 60% and total rutting reduces by 30% due to improved MR (from 5000 psi to 15500 psi) in the subgrade. However, AC rutting slightly increases in all of the pavements shown in Figure 5.

Table 7 ranks the perpetual pavements having 11″ HMA thickness (5000 AADTT) based on AC rut criterion ($AC_2+AC_3 \leq 0.1″$ after 10 years).

- Some of these pavements have AC1 = 0.09″. However, these pavements are not feasible due to lift thickness of the surface layer and the nominal size aggregate in this mix (SP-III). SP-III mix requires a minimum lift thickness of 2.5″.
- All of these pavements contain a RBL.
- All of these pavements have 8000 psi resilient modulus (MR) in their treated subgrade.

- Top-down cracking increases by 100% due to increased stiffness in the subgrade. However, all of the pavements pass the top-down cracking performance criterion (≤ 700ft/mi).
- Rutting in the combined AC2 and AC3 layers does not change due to increased stiffness in the subgrade.

Evaluate Design Alternatives Based on Life Cycle Cost Analysis

LCCA is performed to evaluate the feasibility of these design alternatives, in particular to identify the one that may be the most cost-effective to build and maintain. The candidate costs that are considered in a LCC analysis are: initial construction, maintenance, rehabilitation, salvage value, user delay (during future maintenance or resurfacing), and vehicle operating cost. The first four are agency costs that typically have the most impact on strategy selection. However, when considered, the last two user costs can have major effects on the selection of a strategy that is most cost-effective overall (Walls and Smith 1998). National lime association's LCCA program is used to determine the most economic design (National Lime Association 2003).

Based on the findings of this study, eight perpetual pavements can be implemented in the State of New Mexico based. Eight design alternatives are consolidated to these two groups: group one is a perpetual pavement without RBL and group two is a perpetual pavement with RBL. The LCAA parameters are shown in Table 8. The LCCA model input data for both pavements is identical

except for initial costs of construction. Traffic is about 5000 AADTT in one direction. All other traffic inputs are taken from MEPDG level 3 default values. User costs are those costs that are accrued by the user of the facility during the construction, maintenance and/or rehabilitation and everyday use of a roadway section. Work zone user costs are costs usually associated with construction, maintenance, and rehabilitation activities that restrict the normal traffic flow. Mean life cycle cost is compared between RBL versus no RBL pavements.

Analysis

Alternative 1: Perpetual Pavement (No RBL)

3″ Surface HMA = $100/cy

7″ Intermediate HMA = $110/cy

6″ Granular Base = $42/cy

12″ Treated Subgrade = $36/cy

Perpetual Pavement costs about $288/cy

Alternative 2: Perpetual Pavement (with RBL)

3″ Surface HMA = $100/cy

4″ Intermediate HMA = $110/cy

3″ Rich Binder HMA = $120/cy

6″ Granular Base = $42/cy

12″ Treated Subgrade = $36/cy

Perpetual Pavement costs about $408/cy

Estimated initial construction of the perpetual pavement with the rich binder layer is higher due to presence of three HMA different layers that require specific construction practices (lift compaction, density, etc.). Resurface rehabilitation is done every 10 years. It involves 0.75″ mill and fill with OGFC. User cost (lane rental fee) for a high-volume facility is considered to be $10,000 lane-mi/day. LCCA is performed over 50 years with a discount rate of 4%.

Results

Mean Life Cycle Cost ($) Per Lane Mile:

Perpetual Pavement (No RBL) = $2.3 million

Perpetual Pavement (RBL Incl.) = $3.3 million

It can be seen that Alternative 1 (no RBL) has a lower life cycle cost than Alternative 2 (RBL Included), which is expected.

Evaluate Impacts of Removing a Layer of a Perpetual Pavement

This study investigates whether the need for a rich binder layer (RBL) to minimize fatigue damage is justified. It is also debated whether selected perpetual pavement structures can be made less complex by removing the rich binder layers. As such, 50 perpetual pavements are selected from based on low AC rutting for carrying 5000 AADTT. Pavements analyzed in this section are further reduced from 50 to 21 due to removal of the RBL. By removing this layer, many of the 50 reference pavements become identical in design and material properties. Figure 6 highlights the effects of removing the rich binder layer from the

pavement structure. The X and Y axes on Figures 6(a) and (b) have the same scale and the 45° line indicates where rutting values for both cases (with and without a RBL) are the same. Figure 6(a) and 6(b) clearly shows that there is an increase in rutting in both the AC and subgrade layers due to removal of the RBL. Rich binder layers are generally used to minimize bottom-up fatigue cracking. An increase in rutting might be due to the reduced thickness of the pavement where stress intensity might have increased. As expected, Figure 7 shows a significant increase in fatigue cracking even though none of the pavements failed. Pavements that include RBLs show fatigue cracking ranging from 0–2%. However, pavements that do not have RBLs show fatigue cracking ranging from 3–35%. Minimizing fatigue cracking is important and the presence of a RBL ensures that the pavements shown in this study do not fail by fatigue cracking for 50 years or more.

Determine Effects of De-bonding on Perpetual Pavement Performance

In this study, the effects of HMA layer de-bonding on the performance of selected perpetual pavements are determined using MEPDG. The MEPDG program for flexible pavements accounts for bonding in terms of complete bonding or no bonding. Eight optimal perpetual pavements passing the design life criteria of 50 years or more, shown in Table 6(b), are analyzed for bonding and de-bonding. These eight optimal perpetual pavements have 10″ HMA thickness and carry 5000 AADTT. The results are then compared to the same pavements with full bonding between HMA layers.

Figure 8(a) presents MEPDG predicted top-down cracking in eight HMA perpetual pavements carrying 5000 AADTT at the end of 50 years for bonded and de-bonded cases. It can be seen here that all but one of the pavements fail (> 700 ft/mi) when there is complete de-bonding between all of the HMA layers with predicted top-down cracking in excess of 10,000 ft/mi for six of the eight pavements. These six pavements are predicted to fail within 2 years. The pavement that did not fail (Run 2751) showed an increase from 0.2 to 75 ft/mi. However, not all HMA layers are expected to experience de-bonding. Usually de-bonding occurs in the upper HMA layers due to the presence of moisture. Hence, analysis is done to determine the effect of de-bonding in upper HMA layers. Once again, the same eight pavements shown above are used in this analysis. Figure 8(b) presents predicted top-down cracking for these eight pavements with de-bonding occurring in the top two asphalt layers. None of the pavements fail but a significant increase in top-down cracking is predicted.

Predicted bottom-up cracking is presented in Figure 9(a) for the same 8 perpetual pavements shown earlier. Bottom-up cracking has increased significantly (150 – 700%) in all eight pavements with two of them failing (> 20%). The failed pavements do not contain a rich binder layer and are predicted to fail at the end of 20 years. Figure 9(b) presents predicted bottom-up cracking for eight perpetual pavements that have de-bonding in their upper asphalt layers. Bottom-up cracking increases in all of the pavements with two of them failing (> 20%). These two

pavements do not contain rich binder layers and they are predicted to fail after 30 years.

In terms of AC rutting, all of the pavements are predicted to have more than twice the amount of AC rutting than those with bonded HMA layers. This is illustrated in Figure 10(a) where AC rutting increases from 0.2 to 0.5″ at the end of 50 years. However, all eight pavements still pass the AC rut criterion (≤ 0.5″ after 50 years) even with de-bonded HMA layers. When there is de-bonding in only the upper asphalt layers, AC rutting is once again shown to be very high. Figure 10(b) shows that AC rutting increases from 0.2 to 0.46″ which is almost the same as the predicted AC rutting with de-bonding in all HMA layers. Thus, from this analysis, we can say that preventing de-bonding of upper asphalt layers will reduce potential AC rutting.

Summary of De-Bonding Study

- A total of 7 out of 8 perpetual pavements with de-bonded HMA layers fail by top-down cracking (< 700 ft/mi) at the end of 50 years.
- For bottom-up cracking ≤ 20%, 2 of the 8 pavements failed due to de-bonding of all asphalt layers. Bottom-up cracking also significantly increased in the remaining 6 pavements (150 – 700%).
- AC Rutting more than doubled (0.2 to 0.5″) in all of the pavements due to the de-bonding of all HMA layers. However, none of the pavements failed by AC rutting.

- De-bonding of upper asphalt layers still causes a significant increase in top-down cracking. However none of the pavements fail. A significant increase in bottom-up cracking is also noted, as well as AC rutting. AC rutting values are similar to those values predicted when all HMA layers are de-bonded. Hence, preventing de-bonding of upper asphalt layers will significantly reduce potential AC rutting.

Implementation Note

This study suggests two perpetual pavements: with and without RBL, which can be implemented in the State of New Mexico. These are presented below:

Option One: Implementable Perpetual Pavement (with RBL)

Choice one (pavement trial no. 2725), presented in Figure 11(a), has 3″ surface layer, 4″ intermediate layer, and 3″ rich binder layer. A fine mix (SP-IV) is used in both the surface and rich binder layers. A coarse mix (SP-II) is used in the intermediate layer. Stiffer PG binders are used in the surface and intermediate layers, and a softer binder, PG 64-22, is used in the rich binder layer. Both the surface and intermediate layers are compacted to traditional 6% air voids, while the rich binder layer has to contain a non-traditional 3% air voids. This pavement is shown to have very low fatigue cracking (< 2%) and top-down cracking (< 0.5 ft/mi), as well as little or no rutting in the intermediate and base layers at the end of 50 years.

Option Two: Optional Perpetual Pavement (without RBL)

Base on the life cycle cost analysis, it is evident that the use of rich binder layer is not an economic option. Pavement structure can be designed to meet perpetual pavement performance requirements without a RBL. Figure 11(b) presents an optimal perpetual pavement (pavement trial No. 2751) that does not contain a rich binder layer. This pavement has 3″ surface layer and 7″ intermediate layer. A fine mix (SP-IV) is used in the surface layer and a coarse mix (SP-II) is used in the intermediate layer. Both or these HMA layers contain modified binders and 6% air voids. Fatigue cracking, at the end of 50 years, is about 12% which is well below the failure value of 20%. It shows virtually no top-down or low-temperature (transverse) cracking. Very low rutting is predicted in the surface layer (< 0.2″) and intermediate layer (< 0.05″) at the end of 50 years.

A key factor of any implementation plan is to have a successful maintenance plan that fixes the rut in the top surface (if > 0.1″) every 10 years. This way, perpetual pavements can perform as expected and maintain a very high level of performance over the 50 year design life. Another major concern of perpetual pavement, as well as any pavement, is potential de-bonding of HMA layers. De-bonding of HMA layers due to moisture can cause significant top-down and bottom-up cracking, which can lead to failure of these pavements. The selected perpetual pavements are implementable but procedures must be enforced to prevent moisture from initiating de-bonded environments.

Conclusions

In this study, an optimal perpetual pavement is determined. This is done through a full analysis of design alternatives based on layer stiffness and thickness, as well as quantification of the impact of removing RBL layer and consideration of various degrees of de-bonding between layers of a perpetual pavement section. The findings of this study are summarized below:

- From a total of 3213 MEPDG simulations, it is shown that none of the pavements experienced any thermal cracking. The use of modified binders and the location of the climate data (Albuquerque) might have reduced the impact of thermal cracking on the pavements analyzed.
- None of the 3213 pavements failed by surface-down cracking. For criteria: bottom-up cracking ≤ 20% at the end of 50 years, only 8 pavements failed.
- For AC rut ≤ 0.25″ and fatigue cracking ≤ 20% at the end of 50 years (no rehab), 405 perpetual pavements are found to pass. However, all of these pavements have 15″ AC thickness for AADTT of 1750. No perpetual pavements can be found using 5000 and 10000 AADTT.
- For AC rut ≤ 0.5″ and fatigue cracking ≤ 20% at the end of 50 years (thin resurfacing every 10 years), 37 perpetual pavements are found to have 11″ thickness for carrying 1750 AADTT. Perpetual pavements carrying 1750 and 5000 AADTT are also found using 10″ (9 pavements), 11″ (17 pavements), and 12″ AC thickness (13

pavements). Perpetual pavements carrying 10000 AADTT all have 15″ AC thickness (293 pavements).

- By increasing the subgrade resilient modulus (M_R) from 5000 psi to 15,500 psi (Default for A-5 material in MEPDG), subsequent rutting in this layer reduces by 60% and total rutting reduces by 30%. Therefore, improved subgrade is an important factor for perpetual pavement design.
- Perpetual pavements are found both with and without rich binder layer (RBL). Life cycle cost analysis of these perpetual pavements shows that perpetual pavements that do not contain a RBL are the most economic design. Perpetual pavements of 10″ thickness (for 5000 AADTT) can be designed without RBL layers. Indeed, 2 perpetual pavements without RBL have shown to have performance similar to 7 perpetual pavements with RBL layer (10″ thickness, 5000 AADTT).
- When RBL layer is removed in certain perpetual pavements, predicted AC and base/subgrade rutting increases significantly, as well as bottom-up cracking increases. However, this is not the case in all simulations. Some perpetual pavements without an RBL did not fail by rutting or bottom-up cracking. A combination of appropriate mix design and sufficient layer thickness may be the reason for this.
- A total of 8 perpetual pavements are studied for de-bonding. MEPDG analysis shows that 7 out of 8 perpetual pavements with de-bonded HMA layers fail due to top-down cracking criterion (< 700 ft/mi) at

the end of 50 years. For bottom-up cracking ≤ 20%, 2 of the 8 pavements failed. Bottom-up cracking also significantly increased in the de-bonded pavements (150 – 700%). AC Rutting more than doubled (0.2 to 0.5″) in all of the pavements due to the de-bonding of all HMA layers. However, none of the pavements failed by AC rutting.

- For New Mexico's pavement conditions (using MEPDG), it is shown that fatigue cracking is not a major concern for designing perpetual pavements, rather rutting is more of a concern.

Acknowledgements

This project is funded by New Mexico Department of Transportation. The authors would like to thank the project sponsor: Larry Velasquez (District 3 Engineer, NMDOT), project advocate: Jeff Mann (Head of Pavement Design, NMDOT), project technical panel: Bob Meyers (Geotechnical Section Manager, NMDOT), Robert McCoy (Head of Pavement Exploration, NMDOT), and Parveez Anwar (State Asphalt Engineer, NMDOT), Steve Von Stein (FHWA representative and Pavement Engineer), and Scott McClure (Research Bureau Chief), and project manager: Virgil Valdez (Research Bureau, NMDOT) for valuable suggestions during quarterly meeting (every three month) throughout the entire duration (2-year) of the project. Special thanks to Pranav Shrestha for his computer-support to accomplish thousands of MEPDD simulation runs.

References

AASHTO T 166. "Standard Method of Test for Bulk Specific Gravity of Compacted Hot Mix Asphalt (HMA) Using Saturated Surface-Dry Specimens." *American Association of State Highway and Transportation Officials* (AASHTO), Washington D.C., (2007).

AASHTO T 269. "Standard Method of Test for Percent Air Voids in Compacted Dense and Open Asphalt Mixtures." *American Association of State Highway and Transportation Officials* (AASHTO), Washington D.C., (2007).

AASHTO T321-07. "Standard Test Method for Determining the Fatigue Life of Compacted Hot-Mix Asphalt (HMA) Subjected to Repeated Flexural Bending." *American Association of State Highway and Transportation Officials* (AASHTO), Washington D.C., (2007).

ASTM D7460-10. "Standard Test Method for Determining Fatigue Failure of Compacted Asphalt Concrete Subjected to Repeated Flexural Bending." ASTM International, West Conshohocken, PA, (2003).

Advanced Asphalt Technologies, LLC (2008). "Developing a Plan for Validating an Endurance Limit for HMA Pavements: HMA Endurance Limit Validation Study," National Cooperative Highway Research Program Project 9-44.

Bonnaure, F.P., Huibers, A.H.J.J., Boonders, A. (1982). "A Laboratory Investigation of the Influence of Rest Periods on the Fatigue Response of

Bituminous Mixes," *Proceedings, Association of Asphalt Paving Technologists*, Vol. 51, Kansas City, Missouri.

Brown, S. F., Hakim, B. and Thom, N. H., (2004). "Performance and Rehabilitation of Heavy-Duty Pavements in the UK: Some Case Studies." *Proceedings of the International Symposium on design & construction of long lasting asphalt pavement*. Auburn, Alabama. pp. 811-829.

Carpenter, S. H., Ghuzlan, K. A., and Shen, S. (2003). "Fatigue Endurance Limit for Highway and Airport Pavement." *Transportation Research Record*, No. 1832, pp. 131-138.

Carpenter, S. H., and Shen, S. (2005). "Application of the Dissipated Energy Concept in Fatigue Endurance Limit Testing." *Transportation Research Record*, No. 1929, pp. 165-173.

Carpenter, S. H., and Shen, S. (2006). "Dissipated Energy Approach to Study Hot-Mix Asphalt Healing in Fatigue." *Transportation Research Record*, No. 1970, pp. 178-185.

Carpenter, S. H. and Shen, S. (2009). "Effect of Mixture Variables on the Fatigue Endurance Limit for Perpetual Pavement Design." *Proceedings International Conference on Perpetual Pavements*. Columbus, Ohio 2009.

Chehab, G. R., Kim, Y. R., Schapery, R. A., Witczak, M. W., and Bonaquist, R. (2003). "Characterization of Asphalt Concrete in Uniaxial Tension Using a Viscoelastoplastic Continuum Damage Model." *Journal of the Association of Asphalt Paving Technologists*, Vol. 72: 315-355.

Clear, C. A. (1985). "The Effect of Autogenous Healing upon Leakage of Water Through Crack Initiation and Arresting in Epoxy." *International Journal of Fracture*, Vol. 55(3): 209-222.

Daniel J.S. and Kim, Y.R. (2002). "Development of a Simplified Fatigue Test and Analysis Procedure Using a Visco-Elastic Continuum Damage Model." *Journal of the Association of Asphalt Paving Technologists*, Vol. 71: 619-650.

Di Benedetto, H., Ashayer Soltani, M.A. and Chaverot, P., (1997). "Fatigue Damage for Bituminous Mixtures." *Proceedings of the 5th Int. RILEM Symposium MTBM*, Lyon 1997, pp. 263-270.

Edvardsen, C (1999). "Water Permeability and Autogenous Healing of Cracks in Concrete." *ACI Materials Journal*, Vol. 96(4): 448–454.

Epps, A. L., Harvey, J. T., and Monismith, C. L. (1999). "Performance Characteristics of Mixes Containing Asphalt Cements and Crumb Rubber Modified Binders." *Symposium on Asphalt, Number One Thermoplastic Polymer as part of the 217th American Chemical Society Meeting*, Anaheim, California, March 1999.

Freund, L. B., and Suresh, S. (2003). *Thin Film Materials: Stress, Defect Formation and Surface Evolution.* Cambridge University Press, Cambridge, United Kingdom.

Ghuzlan, K., and Carpenter, S. H. (2000). "Energy-Derived, Damage-Based Failure Criterion for Fatigue Testing." *Transportation Research Record*, No. 1723, pp. 141–149.

Ghuzlan, K (2001). "Fatigue damage analysis in asphalt concrete mixtures based upon dissipated energy concepts," thesis, presented to University of Illinois at Urbana-Champaign, IL, in partial fulfillment of the requirements for the degree of Doctor of Philosophy.

Harvey, J. T., Deacon, J.A., Taybali, A.A., and Leahy, R.B. (1997). "A Reliability-Based Mix Design and Analysis System for Mitigating Fatigues Distress." *Proceedings of the 8th International Conference on Asphalt Pavements*, Vol. 1. University of Washington, Seattle, WA, pp. 301-323.

Hibbeler, R.C. (2005). *Mechanics of Materials*. Prentice-Hall, Inc., Upper Saddle River, NJ.

Hopman, P.C., Kunst, P.A.J.C. and Pronk, A.C. (1989). "A Renewed Interpretation Method for Fatigue Measurements, Verification of Miner's Rule." *4th Eurobitumen Symposium*, Madrid, Spain, Vol. 1, pp. 557-561.

Jud, K., and Kausch, H. H. (1979). "Load Transfer Through Chain Molecules After Interpenetration at Interfaces." *Polymer Bulletin,* Vol. 1, pp. 697–707.

Kim, Y. R., Lee, H. J., and Little, D. N. (1997a). "Fatigue Characterization of Asphalt Concrete using Visco-Elasticity and Continuum Damage Theory." *Journal of the Association of Asphalt Paving Technologists*, Vol. 66, pp. 520-569.

Kim, Y. R., Lee, H. J, Kim, Y, and Little, D. N. (1997b). "Mechanistic evaluation of fatigue damage growth and healing of asphalt concrete: Laboratory and

field experiments." *Proceedings of the 8th International Conference on Asphalt Pavements,* ISAP, Seattle, Washington, August 10-14, 1089-1107.

Kim, Y., Allen, D. H., and Little, D. N. (2005). "Damage-induced Modeling of Asphalt Mixtures through Computational Micromechanics and Cohesive Zone Fracture." *Journal of Materials in Civil Engineering*, ASCE, 17(5), pp. 477-484.

Kim, Y.R. (2008). *Modeling of Asphalt Concrete*. McGraw-Hill Professional, New York.

Leahy, R.B., Hicks, R.G., Monismith, C.L., and Finn, F.N. (1995). "Framework for Performance-Based Approach to Mix Design and Analysis." *Proceedings of the Association of Asphalt Paving Technologists,* Vol. 64, pp 431-473.

Lee, H.J., Daniel, J.S., Kim, Y.R. (2000). "Continuum Damage Mechanics-Based Fatigue Model of Asphalt Concrete." *Journal of Materials in Civil Engineering*, Vol. 12(2), pp. 105-112.

Little, D. N., Lytton, R. L., Williams, D., and Kim, Y. R. (1999). "An Analysis of the Mechanism of Microdamage Healing Based on the Applications of Micromechanics First Principles of Fracture and Healing." *Journal of the Association of Asphalt Paving Technologists*, Vol. 68, pp. 501–542.

Lytton, R.L. (2000). "Characterizing Asphalt Pavements for Performance." *Transportation Research Record,* No. 1723, pp. 5–16.

Matthews, J., Monismith, C. L., and Craus, J. (1993). "Investigation of Laboratory Fatigue Testing Procedures for Asphalt Aggregate Mixtures." *Journal of Transportation Engineering*, Vol. 119, pp. 634-654.

Mechanistic-Empirical Pavement Design Guide – A Manual of Practice (Interim Edition). *American Association of State Highway and Transportation Officials* (AASHTO), Washington D.C., (2008).

Monismith, C. L., and Epps, J. A. (1970). "Asphalt Mixture Behavior in Repeated Flexure." *Report No. TE 70-5*, Institute of Transportation and Traffic Engineering, University of California, Berkley.

Mun, S., Guddati, M. N., and Kim, Y. R. (2004). "Fatigue Cracking Mechanisms in Asphalt Pavements with Viscoelastic Continuum Damage Finite-Element Program." *Transportation Research Record,* No. 1896, pp. 96-106.

Ott, R. L (2001). *An Introduction to Statistical Methods and Data Analysis*, 5th ed. Michael Longnecker, Texas A&M University, Tx.

Park, S.W., Kim, Y. R., and Schapery, R.A. (1996). ''A Viscoelastic Continuum Damage Model and its Application to Uniaxial Behavior of Asphalt Concrete.'' *Mechanics of Materials*, Vol. 24(4), pp. 241–255.

Petersen, J. C. (1984). "Chemical Composition of Asphalts Related to Asphalt Durability: State of the Art." *Transportation Research Record*, No. 999, pp. 13–30.

Pierce, L. M. and Mahoney, J.P. (1996). "Asphalt Concrete Overlay Design Case Studies." *Transportation Research Record*, No. 1543, pp 3-9.

Priest, A.L. (2006). "Methodology and Calibration of Fatigue Transfer Functions for Mechanistic-Empirical Flexible Pavement Design." *NCAT Report 06-03*, National Center for Asphalt Technology, Auburn University, Alabama.

Pronk, A.C. and Hopman, P.C. (1990). "Energy Dissipation: The Leading Factor of Fatigue. Highway Research: Sharing the Benefits." *Proceedings of the Conference, the United States Strategic Highway Research Program*, London, UK.

Pronk, A.C. (2008). "Analytical Investigation of the Correctness of Formulas Used in Bending Beam Tests." *Efficient Transportation and Pavement Systems: Characterization, Mechanisms, Simulation, and Modeling*. Taylor and Francis Group, London, UK.

Prowell, B., Brown, E. R., Daniel, J., Bhattacharjee, S., Von Quintus, H., Carpenter, S. H., Shen, S., Anderson, M., Swamy, A. K., and Maghsoodloo, S. (2008). "Endurance Limit of Hot Mix Asphalt Mixtures to Prevent Fatigue Cracking in Flexible Pavements." *Updated Draft Final Report, NCHRP 9-38*, National Cooperative Highway Research Program, Washington, D.C.

Romero, P., Stuart, K.D., and Mogawer, W. (2000). "Fatigue Response of Asphalt Mixtures Tested by the Federal Highway Administration's Accelerated Loading Facility." *Journal of the Association of Asphalt Paving Technologists*, Vol. 69, pp. 212-235.

Rowe, G.M. and Bouldin, M.G. (2000). "Improved Techniques to Evaluate the Fatigue Resistance of Asphaltic Mixtures." *Proceedings of 2nd Eurasphalt & Eurobitumen Congress*, Barcelona, Spain 2000.

Schapery, R. A. (1984). "Correspondence Principles and a Generalized J-integral for Large Deformation and Fracture Analysis of Viscoelastic Media." *International Journal of Fracture*, Vol. 25, pp. 195–223.

Schapery, R. A. (1990). "A Theory of Mechanical Behavior of Elastic Media with Growing Damage and Other Changes in Structure." *Journal of the Mechanics and Physics of Solids*, Vol. 38, pp. 215–253.

Shen, L. and Carpenter, S. H. (2005). "Application of Dissipated Energy Concept in Fatigue Endurance Limit Testing," *Transportation Research Record*, No. 1929, pp. 165-173.

Stavrinidis, B., and Holloway, D. G. (1983). "Crack Healing in Glass." *Physics and Chemistry of Glasses*, Vol. 24(1), pp. 19–25.

Sukhotskaya, S. S., Mazhorava, V. P., and Terekhin, Y. N. (1983). "Effect of Autogenous Healing of Concrete Subjected to Periodic Freeze–Thaw Cycles." *Journal of Hydrotechnical Construction*, Vol. 17(6), pp. 295–296.

Tangella, R., Craus, J., Deacon, J.A., and Monismith, C.L. (1990). "Summary Report of Fatigue Response of Asphalt Mixtures." *SHRP-A/IR-90-011*, Institute of Transportation Studies, University of California, Berkley.

Tayebali, A. A., Deacon, J. A., Coplantz, J. S., Harvey, J. T., and Monismith, C. L. (1992). "Fatigue Response of Asphalt-Aggregate Mixes." *Report No.*

SHRP A-404, Strategic Highway Research Program, National Research Council, Washington, D.C.

Thompson, M.R., ad Carpenter, S.H. (2004). "Design Principles for Long Lasting Pavement," *Proceedings, International Symposium of Design and Construction of Long Lasting Asphalt Pavements*, National Center for Asphalt Technology, Auburn, AL.

Thompson, M. and Carpenter, S.H. (2006). "Considering Hot-Mix-Asphalt Fatigue Endurance Limit in Full-Depth Mechanistic-Empirical Pavement Design." *Proceedings International Conference on Perpetual Pavement Design* (CD-ROM), Columbus, OH.

Thompson, M. and Carpenter, S.H. (2009). "Perpetual Pavement Design: An Overview." *Proceedings of the 2009 International Conference on Perpetual Pavement*, Columbus, OH, 2009.

Timm, D., H., and Young, J., B. (2004). "Effects of Load Spectra and Variability on Perpetual Pavement Design." *Proceedings, International Symposium of Design and Construction of Long Lasting Asphalt Pavements*, National Center for Asphalt Technology, Auburn, AL.

Tsai, B. W., Harvey, J. T., and Monismith, C. L. (2002). "High Temperature Fatigue and Fatigue Damage Process of Aggregate-Asphalt Mixes." *Journal of the Association of Asphalt Paving Technologists*, Vol. 71, pp. 345–385.

Tsai, B. W., Harvey, J. T., and Monismith, C. L. (2003). "Application of Weibull Theory in Prediction of Asphalt Concrete Fatigue Performance." *Transportation Research Record,* No. 1832, pp. 121-130.

Underwood, B.S. and Kim, Y.R. (2009). "Analytical Techniques for Determining the Endurance Limit of Hot Mix Asphalt Concrete," *Proceedings of the 2009 International Conference on Perpetual Pavement*, Columbus, OH 2009.

Walubita, L. (2006). "Comparison of Fatigue Analysis Approaches for Predicting Fatigue Lives of Hot-Mix Asphalt Concrete (HMAC) Mixtures." thesis, presented to University of Texas A&M, TX, in partial fulfillment of the requirements for the degree of Doctor of Philosophy.

Willis, J.R. and Timm, D.H. (2009). "A Comparison of Laboratory Fatigue Thresholds to Measured Strains in Full-Scale Pavements." *Proceedings, International Conference on Perpetual Pavements*, Columbus, Ohio 2009.

Zhou, F., Hu, S., Chen, D., and Scullion, T. (2007). "Overlay Tester: Simple Performance Test for Fatigue Cracking." *Transportation Research Record,* No. 2001, pp. 1-8.

Table 1 – Summary of Perpetual Pavement Data

State PP	Highway/ Interstate	Surface Life (yrs)	Design Life (yrs)	Traffic	Layer Thickness (in)								Layer Stiffness		PG Binder			
				AADTT	OGFC/ SMA	HMA_1	HMA_2	HMA_3	HMA_4	Total	GB	TSG	GB M_R (psi)	TSG M_R (psi)	HMA_1	HMA_2	HMA_3	HMA_4
California	I-710	19	40	10000	1 OGFC	3	6	3	-	13	6	-	-	-	-	64-40	64-16	-
Illinois	I-70	19	30	11760	2 SMA	5.5	10	-	-	17.5	8	-	-	28000	76-28	76-28	70-22	-
Iowa	US-60	15	40	8250	-	2	2	7.5	3	14.5	9	18	50000	20000	64-34	64-34	58-38	58-38
Kansas	US-75 (a)	-	10	450	-	1.5	2.5	9	-	13	-	6	-	5000	70-28	70-28	70-22	-
	US-75 (b)	-	10	5000	-	1.5	2.5	7	-	11	-	6	-	2500	70-28	70-28	64-22	-
	US-75 (c)	-	10	450	-	1.5	2.5	9	-	13	-	6	-	2500	70-28	70-28	64-22	-
	US-75 (d)	-	20	900	-	1.5	2.5	12	-	16	-	6	-	2500	70-28	70-28	64-22	-
Kentucky	I-64	20	40	10000	-	2	9	-	-	11	-	-	200,000	-	76-22	76-22	-	-
	I-65	20	40	-	-	-	-	-	-	-	-	-	200,000	-	76-22	70-20	-	-
Maryland	I-695	12.5	30	15750	2 SMA	1.5	12	-	-	15.5	6	12	30,000	8000	70-20	-	-	-
Michigan	US-24			-	-	2.5	3	4.5	-	10	12	14	30,000	5,000	70-28	70-22	70-22	-
	I-96	20	40	8900	-	1.5	2.5	10	-	14	16	12	30,000	12,000	76-22	76-22	70-22	-
	M-84			-	-	1.5	2	3	-	6.5	12	-	-	5000	70-28	70-28	58-22	-
Minnesota	TH-71			-	-	4.5	1.5	-	-	6	4.5	-	-	A-2-4	52-34	-	-	-
	TH-10			-	-	3.5	3	3	-	9.5	6	18	30,000	29,500	-	58-28	58-34	-
	TH-18			-	-	4	3	1.5	-	8.5	4.5	10	30,000	29,500	52-34	52-34	-	-
	TH-61			-	-	3	1	3	2	9	6	12	30,000	29,500	58-28	58-28	58-34	-
	I-35	16	30	864	-	4	4	4	-	16	3	9	100,000	22,000	58-28	58-28	64-28	-
New Jersey	I-287	12	20	12000	-	2	2	7	-	11	8	10	30,000	32,000	76-22	76-22	64-22	-
New Mexico	US-70	8	30	1338														
Ohio	I-77			-	-	1.5	1.75	10	4	17.25	6	-	30,000	-	76-22	76-22	58-28	58-28
	US-30	20	50	3747	1.5 SMA	1.75	9	4	-	14.75	6	-	30,000	-	76-22	76-22	64-22	64-22
Oklahoma	SH-152	20	50	2000	2 SMA	3	3	3	3	14	-	-	-	30,000	76-28	64-22	64-22	64-22
Oregon	I-5	15	30	12240	2 OGFC	2	8	-	-	12	12	-	30,000	-	64-22	64-22	-	-
Texas	IH-35 (a)			-	3 SMA	3	13	4	-	23	-	8	-	30,000	76-22	70-22	64-22	-
	IH-35 (b)			-	3 SMA	3	8	2	-	16	-	8	-	30,000	76-22	70-22	64-22	-
	IH-35 (c)			-	3 SMA	3	8	3	-	17	-	8	-	30,000	76-22	70-22	70-22	-
	IH-35 (d)			-	1.5 OGFC	2	2	12	4	21.5	-	6	-	30,000	76-22	64-22	64-22	-
	IH-35 (e)			-	1.5 OGFC	2	3	10	4	20.5	-	6	-	30,000	76-22	70-22	64-22	-
	IH-35 (f)			-	1.5 OGFC	2	3	12	4	20.5	-	6	-	30,000	76-22	70-22	64-22	-
	SH-114	20	30	18000	2 HDAMA	3	13	4	-	22	-	8	-	30,000	76-22	70-22	64-22	-
Virginia	I-95	-	-	2950	1.5 SMA	2	17	-	-	20.5	3	6	30,000	30,000	70-22	64-22	-	-
Washington	I-90	18.5	50	5400	2 SMA	14	-	-	-	16	12	-	29,500	-	64-22	-	-	-
Wisconsin	STH-50 (a)	-	20	770	-	2	3.5	3.5	-	9	4	8	29,500	30,000	58-28	64-22	64-22	-
	STH-50 (b)	-	20	770	-	2	3.5	3.5	-	9	4	8	29,500	30,000	64-28	58-28	58-28	-
	STH-50 (c)	-	20	770	-	2	3.5	3.5	-	9	4	8	29,500	30,000	58-28	70-22	70-22	-
	I-94 (a)	-	20	9476	-	2	4.5	4.5	-	11	4	17	29,500	30,000	76-28	70-22	64-22	-
	I-94 (b)	-	20	9476	-	2	4.5	4.5	-	11	4	17	29,500	30,000	70-28	70-22	64-22	-
STATISTICAL ANALYSIS	Average =	17	29	7498	2	3	5	6	3	14	7	9	15,000	12,563	-	-	-	
	Std. Dev.=	3.77	12.48	5370	-	2	4	3	1	5	4	4	86603	12,266	-	-	-	
	Mode =	20	20	770	-	2	3	3	4	11	6	6	200,000	2500	76-22	70-22	64-22	64-22

Note: AADTT=Annual average daily truck traffic, OGFC=open graded friction coarse, SMA=stone matrix asphalt, HMA=hot mix asphalt, GB=granular base, M_R=resilient modulus, TSG=treated subgrade, and PG=performance grade.

Table 2 – Perpetual Pavement Structural Design Information

No.	State Pavement	Perpetual Pavement Concept		Design Method Or Software
		Limiting Strain in Base Layer	Rich Binder Layer (RBL)	
1	California (I-710)	70 με	Yes	CIRCLY, CA-4PRS
2	Illinois (I-70)	60 με	No	ILLIPAVE
3	Iowa (US-60)	70 με	No	-
4	Kansas (US-75)	70 με	Yes	1993 AASHTO, EVERSTRESS
5	Kentucky (I-695)	70 με	No	Mechanistic Design
6	Maryland (I-695)	No	Yes	AASHTO 1993
7	Michigan (US-24)	65 με	Yes	-
8	Minnesota (I-35)	No	No	ELSYM 5, Von Quintus Cat. 2001
9	New Jersey (I-287)	No	No	-
10	New Mexico (US-70)	No	Yes	Asphalt Institute
11	Ohio (US-30)	70 με	Yes	Kenlayer
12	Oklahoma (SH-152)	70 με	Yes	PerRoad
13	Oregon (I-5)	70 με	Yes	AASHTO 1993, WESLEA
14	Texas (SH-114)	70 με	Yes	FPS 19W, PerRoad
15	Virginia (I-95)	No	No	-
16	Washington (I-90)	No	No	AASHTO 1993, EVERSERIES
17	Wisconsin (STH-50)	-	Yes	AASHTO 1972, WisPave

Note: No = no limiting strain or rich-binder used in base layer,
YES = there is a limiting strain or rich binder used in base layer, and
"–" means data is not available.

Table 3 – Parameters Used for MEPDG Test Matrix

Layer Type	Layer Thickness (in)	Mix Design	PG Binder
Surface, T_1	1.5 2 - 2.5 3	SP-III SP-IV	76-22 70-22
Intermediate	15-T_1-T_3 15-T_1-T_3-2 15-T_1-T_3-4	SP-II SP-III SP-IV	76-22 70-22
Rich Binder Layer (RBL), T_3	3 5 7	SP-II SP-III SP-IV	64-22
Granular Base	6 10	A-5	NA
Treated Subgrade	12	A-5	NA

Note: NA = Not Applicable, SP = SuperPave

Table 4 – HMA Mix Gradations (NMDOT specifications)

Mix Design	Percent Passing Sieve Size						% Asphalt Content (Volumetric)	% Air Voids	Lift Thickness Range (in)
	1″	3/4″	1/2″	3/8″	#4	#200			
SP-II	95	85	-	55	33	4	9.0	6	3 - 3.5
SP-III	100	97	90	65	41	5	10.5	6	2.5 - 3.5
SP-IV	-	100	95	75	45	5.5	11.5	6	1.5 - 3
Granular Base	Stiffness, E = 20,000 psi						NA	7	6. - 12
Treated Subgrade	Stiffness, E = 8,000 psi						NA	5	10. - 12

Note: SP = SuperPave, NA = Not Applicable

Table 5(a) – AADTT and Cumulative ESALs

AADTT	Cum. ESALs
1750	57,829,092
5000	165,226,044
10000	330,451,948

Table 5(b) – Performance Criteria of Perpetual Pavements

Performance Criteria	Max. Value
Alligator Cracking (% of Lane Area)	20
Total Rutting (in)	0.50
10 Year AC Rutting (in)	0.25
Thermal Cracking (ft/mi)	700
Surface-Down Cracking (ft/mi)	700
International Roughness Index - IRI (in/mi)	200

Table 6(a) – Design Criteria of 14″ Perpetual Pavements Carrying 5000 AADTT

		Layer Thickness (in)					Mix Design			PG Binder			50 Yr. MEPDG Predicted Distress			10 Yr. Predicted Distress		
Run	Traffic (AADTT)	Surf	Itmd.	RBL	Total	GB	Surf. Mix	Itmd. Mix	RBL Mix	Surf. PG	Itmd. PG	Treated SG M_R (psi)	Top-Down Cracking (ft/mi)	Bottom-Up Cracking (%)	Thermal Cracking (ft/mi)	IRI (in/mi)	AC_1 Rut (in)	AC_2 + AC_3 Rut (in)
2730	5000	3	4	7	14	6	SP-IV	SP-II	SP-IV	76-22	76-22	8000	0	0.208	0	96.7	0.09	0.02
2731	5000	3	4	7	14	6	SP-IV	SP-III	SP-III	76-22	76-22	8000	0	0.362	0	97.9	0.09	0.02
2732	5000	3	4	7	14	6	SP-IV	SP-III	SP-IV	76-22	76-22	8000	0	0.308	0	98.0	0.09	0.02
2716	5000	3	4	7	14	6	SP-III	SP-IV	SP-II	76-22	70-22	8000	0	0.458	0	97.5	0.08	0.03
2717	5000	3	4	7	14	6	SP-III	SP-IV	SP-III	76-22	70-22	8000	0	0.358	0	97.7	0.08	0.03

Table 6 (b) – Design Criteria of 10″ Perpetual Pavements Carrying 5000 AADTT

		Layer Thickness (in)					Mix Design			PG Binder			50 Yr. MEPDG Predicted Distress			10 Yr. Predicted Distress		
Run	Traffic (AADTT)	Surf	Itmd.	RBL	Total	GB	Surf. Mix	Itmd. Mix	RBL Mix	Surf. PG	Itmd. PG	Treated SG M_R (psi)	Top-Down Cracking (ft/mi)	Bottom-Up Cracking (%)	Thermal Cracking (ft/mi)	IRI (in/mi)	AC_1 Rut (in)	AC_2 + AC_3 Rut (in)
2712	5000	3	4	3	10	6	SP-III	SP-IV	SP-IV	76-22	70-22	8000	0.48	1.8	0	107.6	0.14	0.05
2711	5000	3	4	3	10	6	SP-III	SP-IV	SP-III	76-22	70-22	8000	0.41	2.1	0	107.5	0.14	0.05
2710	5000	3	4	3	10	6	SP-III	SP-IV	SP-II	76-22	70-22	8000	0.31	2.8	0	107.3	0.14	0.05
2744	5000	3	7	-	10	6	SP-III	SP-IV	-	76-22	70-22	8000	0.45	8.1	0	107.7	0.14	0.05
2726	5000	3	4	3	10	6	SP-IV	SP-III	SP-IV	76-22	76-22	8000	0.42	1.7	0	107.7	0.16	0.04
2725	5000	3	4	3	10	6	SP-IV	SP-II	SP-IV	76-22	76-22	8000	0.42	1.6	0	107.4	0.16	0.04
2724	5000	3	4	3	10	6	SP-IV	SP-II	SP-II	76-22	76-22	8000	0.27	2.5	0	107.2	0.16	0.04
2751	5000	3	7	-	10	6	SP-IV	SP-II	-	76-22	76-22	8000	0.14	11.8	0	107.1	0.16	0.03

Table 7 – Ranking of 11″ Perpetual Pavements Based on Rutting in $AC_2 + AC_3$

Run	Traffic (AADTT)	Layer Thickness (in)					Mix Design			PG Binder		TSG M_R (psi)	50 Yr. MEPDG Predicted Distress			10 Yr. Predicted Distress		
		Surf	Itmd	RBL	Total	GB	Surf. Mix	Itmd. Mix	RBL Mix	Surf. PG	Itmd. PG		Top-Down Crack (ft/mi)	Bottom-Up Crack (%)	Thermal Crack (ft/mi)	IRI (in/mi)	AC_1 Rut (in)	$AC_2 + AC_3$ Rut (in)
2686	5000	2	6	3	11	6	SP-III	SP-II	SP-II	70-22	76-22	8000	0.03	1.42	0	105	0.11	0.07
2688	5000	2	6	3	11	6	SP-III	SP-II	SP-III	70-22	76-22	8000	0.04	1.06	0	105	0.11	0.07
2690	5000	2	6	3	11	6	SP-III	SP-II	SP-IV	70-22	76-22	8000	0.05	0.90	0	105	0.11	0.07
2695	5000	2	4	5	11	6	SP-III	SP-II	SP-II	70-22	76-22	8000	0.03	1.50	0	105	0.11	0.08
2697	5000	2	4	5	11	6	SP-III	SP-II	SP-III	70-22	76-22	8000	0.04	1.16	0	105	0.11	0.08
2699	5000	2	4	5	11	6	SP-III	SP-II	SP-IV	70-22	76-22	8000	0.05	1.01	0	105	0.11	0.08
2692	5000	2	6	3	11	6	SP-III	SP-III	SP-II	76-22	76-22	8000	0.02	1.51	0	105	0.09	0.09
2693	5000	2	6	3	11	6	SP-III	SP-III	SP-III	76-22	76-22	8000	0.03	1.13	0	105	0.09	0.09
2694	5000	2	6	3	11	6	SP-III	SP-III	SP-IV	76-22	76-22	8000	0.04	0.96	0	105	0.09	0.09
2687	5000	2	6	3	11	6	SP-III	SP-II	SP-II	76-22	70-22	8000	0.03	1.50	0	105	0.09	0.09
2701	5000	2	4	5	11	6	SP-III	SP-III	SP-II	76-22	76-22	8000	0.02	1.52	0	105	0.09	0.09
2689	5000	2	6	3	11	6	SP-III	SP-II	SP-III	76-22	70-22	8000	0.03	1.12	0	105	0.09	0.09
2691	5000	2	6	3	11	6	SP-III	SP-II	SP-IV	76-22	70-22	8000	0.04	0.95	0	105	0.09	0.09
2702	5000	2	4	5	11	6	SP-III	SP-III	SP-III	76-22	76-22	8000	0.03	1.18	0	105	0.09	0.09
2696	5000	2	4	5	11	6	SP-III	SP-II	SP-II	76-22	70-22	8000	0.02	1.52	0	105	0.09	0.09
2698	5000	2	4	5	11	6	SP-III	SP-II	SP-III	76-22	70-22	8000	0.03	1.18	0	105	0.09	0.09
2700	5000	2	4	5	11	6	SP-III	SP-II	SP-IV	76-22	70-22	8000	0.04	1.02	0	105	0.09	0.10

Table 8 – Input Values for LCCA of Two Perpetual Pavement Types

Alternative 1	Perpetual Pavement (Run 2744) - No RBL			*Alternative 2*	Perpetual Pavement (Run 2710) – RBL Included		
Initial Pavement Design	Initial Construction			Initial Pavement Design	Initial Construction		
	Mean	Std. Dev	COV		Mean	Std. Dev	COV
AADTT = Average Daily Traffic (one way)	5000	100	10%	AADTT = Average Daily Traffic (one way)	5000	100	10%
% T = Percent Trucks	25%	0.025	10%	% T = Percent Trucks	25%	0.025	10%
TF = Truck Factor	0.38	0.038	10%	TF = Truck Factor	0.38	0.038	10%
G = Growth Rate	4	0.004	10%	G = Growth Rate	4	0.004	10%
N = Analysis Period	50			N = Analysis Period	50		
PSIi = Initial PSI	4.2	0.2814	6.7	*PSIi* = Initial PSI	4.2	0.2814	6.7
PSIt = Terminal PSI	2			*PSIt* = Terminal PSI	2		
Mr = Effective Mr	5000	500	10%	*Mr* = Effective Mr	5000	500	10%
a1 = Surf Layer Coeff.	0.44	0.044	10%	a1 = Surf Layer Coeff.	0.44	0.044	10%
a2 = Base Layer Coeff.	0.14	0.014	10%	a2 = Base Layer Coeff.	0.14	0.014	10%
m2 = Base Drainage Coeff.	1	0.1	10%	m2 = Base Drainage Coeff.	1	0.1	10%
a3 = Subbase Layer Coeff.	0.11	0.011	10%	a3 = Subbase Layer Coeff.	0.11	0.011	10%
m3 = Subbase Drainage Coeff.	1	0.1	10%	m3 = Subbase Drainage Coeff.	1	0.1	10%
Mill and Fill (in)	0.75 OGFC			Mill and Fill (in)	0.75 OGFC		
1=US/State, 2=County	1			1=US/State, 2=County	1		
Discount Rate, %	4			Discount Rate, %	4		
Surf HMA ($/cy)	100	10	10%	Surf HMA ($/cy)	100	10	10%
Intermediate HMA ($/cy)	100	11	10%	Intermediate HMA ($/cy)	100	11	10%
Granular Base ($/cy)	42	4.2	10%	Granular Base ($/cy)	42	4.2	10%
Treated Subgrade ($/cy)	36	3.6	10%	Treated Subgrade ($/cy)	36	3.6	10%
Surface Treatment ($/lane-mi)	10000	1000	10%	Surface Treatment ($/lane-mi)	10000	1000	10%
				Rich Binder HMA ($/cy)	120	12	10%

Table 9 - Initial Construction and Overlay Costs of Pavements

Pavement Layer Type	AC Pavement		PP_1 (No RBL)		PP_2 (Incl. RBL)	
	Thickness (in)	Cost ($) /cyd	Thickness (in)	Cost ($) /cyd	Thickness (in)	Cost ($) /cyd
AC	9	100	3	100	3	100
Int. AC	-	-	7	100	4	100
RBL	-	-	-	-	3	120
GB	4	42	6	42	6	42
TSG	12	36	12	36	12	36
Total	25	178	28	278	28	398

Surf. AC = Surface AC, Int. AC = Intermediate AC, RBL = Rich Binder Layer, GB = Granular Base, TSG = Treated Subgrade, PP = Perpetual Pavement

Table 10. New Mexico DOT Treatment Costs (1997)

Flexible Pavement Treatment	Mean Cost/ Lane Mile ($)
Fog Sealing	1,156
Crack Sealing	14,600
Chip Sealing	7,893
Open Graded Friction Course Overlay	32,160
Plant Mix Wearing Course Overlay	43,400
2" Hot Mix Overlay	80,960
In Plant Recycle (Brazer)	49,000
Heater Scarification & Overlay (Cutler)	64,125
Microsurfacing	58,560
Cold Mill/Inlay	350,000
Cold In-Situ Recycle Overlay	350,000
Rehabilitation	750,000
Reconstruction	1,835,000

Table 11. Construction, Maintenance, and User Costs Comparison

Rehabilitation Year	AC Pavement		PP_1(No RBL)		PP_2(Incl. RBL)	
	MC($)	UC($)	MC($)	UC($)	MC($)	UC($)
0	$1,835,000	$10,000	$2,100,000	$10,000	$3,000,000	$10,000
7	$350,000	$10,000	-	-	-	-
10	-	-	$350,000	$10,000	$350,000	$10,000
14	$350,000	$10,000	-	-	-	-
20	-	-	$350,000	$10,000	$350,000	$10,000
21	$1,835,000	$10,000	-	-	-	-
28	$350,000	$10,000	-	-	-	-
30	-	-	$350,000	$10,000	$350,000	$10,000
35	$350,000	$10,000	-	-	-	-
40	-	-	$350,000	$10,000	$350,000	$10,000
42	$1,835,000	$10,000	-	-	-	-
49	-	-	-	-	-	-
50	-	-	-	-	-	-
Undiscounted Total	$6,817,500	$70,000	$3,500,000	$50,000	$4,400,000	$50,000
Present Value	$3,654,823	$35,557	$2,676,996	$26,486	$3,576,996	$26,486

0: Initial Construction Cost, MC: Maintenance Cost, UC: User Cost.

Table 12. Analysis of Variance

	Bottom-Up Cracking			*AC Rutting*			*IRI*		
Groups	*P-Values*	*F*	*F crit*	*P-Values*	*F*	*F crit*	*P-Values*	*F*	*F crit*
Traffic	0.08	5.41	7.71	0.08	5.41	7.71	0.08	5.22	7.71
GB Thickness	0.03	30.22	18.51	0.02	46.29	18.51	0.00	9440.02	18.51
Treated SG M_R	0.10	9.00	18.51	0.10	9.00	18.51	0.10	8.84	18.51
Surface AC Mix	0.20	3.60	18.51	0.04	21.38	18.51	0.00	29344.17	18.51
Intmd AC Mix	0.61	0.31	7.71	0.04	9.74	7.71	0.00	31501.25	7.71
RBL AC Mix	0.95	0.00	7.71	0.04	9.78	7.71	0.00	32934.92	7.71

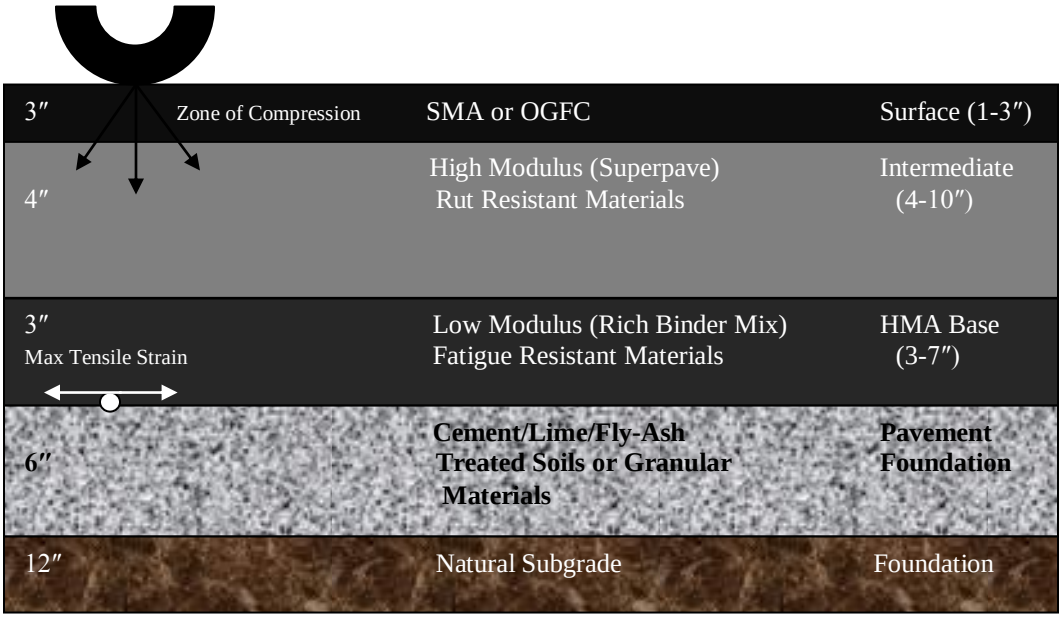
3″
Zone of Compression
SMA or OGFC
Surface (1-3″)
4″
High Modulus (Superpave)
Rut Resistant Materials
Intermediate
(4-10″)
3″
Max Tensile Strain
Low Modulus (Rich Binder Mix)
Fatigue Resistant Materials
HMA Base
(3-7″)
6″
Cement/Lime/Fly-Ash
Treated Soils or Granular
Materials
Pavement
Foundation
12″
Natural Subgrade
Foundation

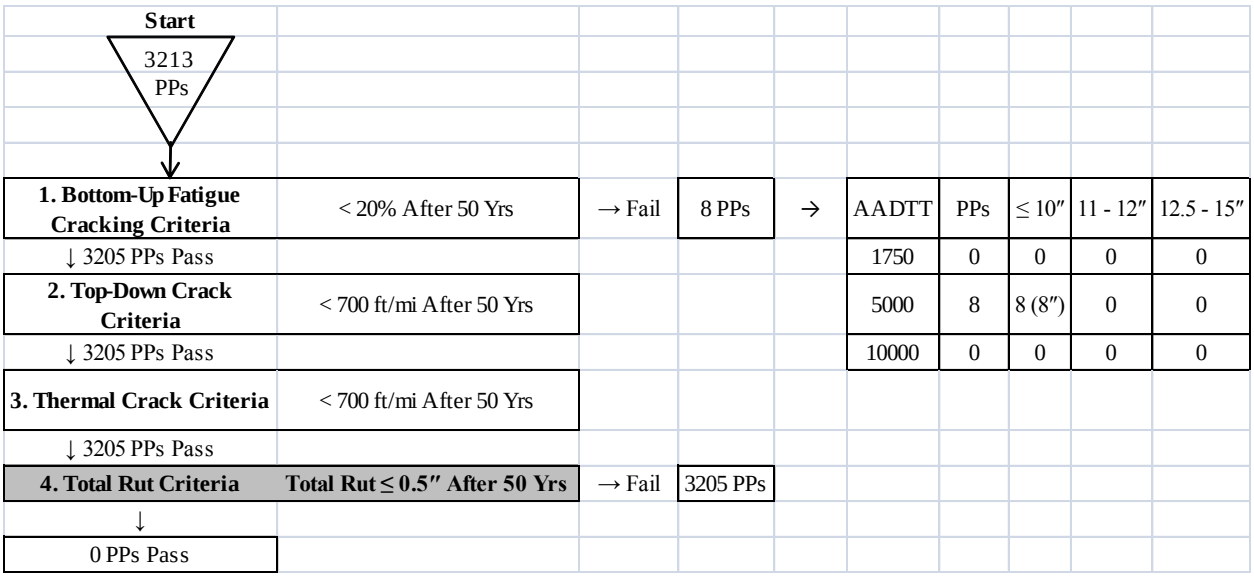

(a) Total Rut ≤ 0.5″ after 50 Years

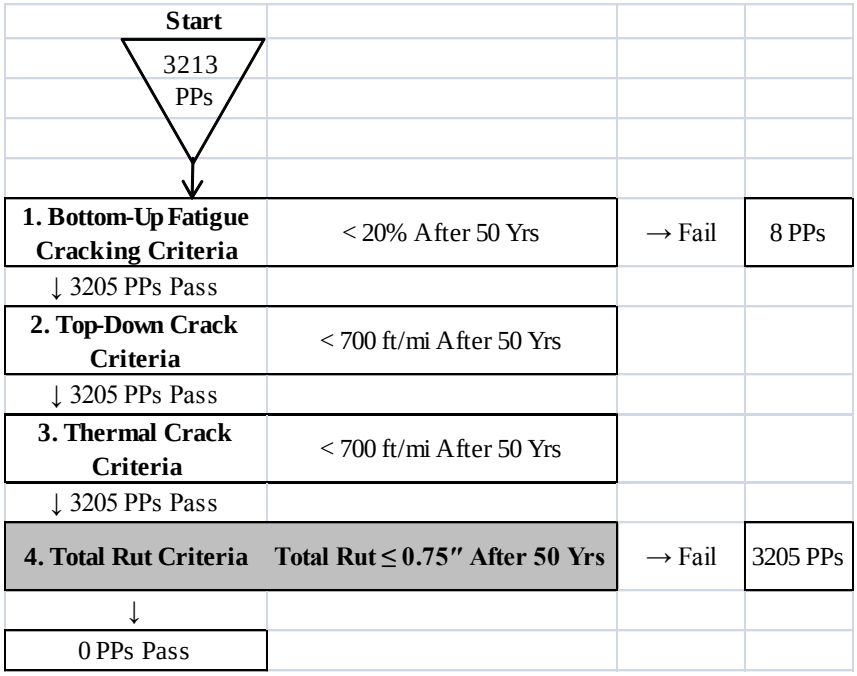

(b) Total Rut ≤ 0.75″ after 50 Years

Figure 2. Pavement Performance Flow Charts Based on Total Rut Criteria (No Resurfacing)

Start				
3213 PPs				
1. Bottom-Up Fatigue Cracking Criteria	< 20% After 50 Yrs	→ Fail	8 PPs	
↓ 3205 PPs Pass				
2. Top-Down Crack Criteria	< 700 ft/mi After 50 Yrs			
↓ 3205 PPs Pass				
3. Thermal Crack Criteria	< 700 ft/mi After 50 Yrs			
↓ 3205 PPs Pass				
4. AC Rut Criteria	**AC Rut ≤ 0.25″ After 50 Yrs**	→ Fail	2327 PPs	
405 PPs Pass	↓			

AADTT	PPs	≤ 10″	11 - 12″	12.5 - 15″
1750	405	0	0	405
5000	0	0	0	0
10000	0	0	0	0

(a) AC Rut ≤ 0.25″ after 50 Years

Start				
3213 PPs				
1. Bottom-Up Fatigue Cracking Criteria	< 20% After 50 Yrs	→ Fail	8 PPs	
↓ 3205 PPs Pass				
2. Top-Down Crack Criteria	< 700 ft/mi After 50 Yrs			
↓ 3205 PPs Pass				
3. Thermal Crack Criteria	< 700 ft/mi After 50 Yrs			
↓ 3205 PPs Pass				
4. AC Rut Criteria	**AC Rut ≤ 0.5″ After 50 Yrs**	→ Fail	473 PPs	
↓ 2732 PPs Pass				

AADTT	PPs	≤ 10″	11 - 12″	12.5 - 15″
1750	1855	0	509 (11″)	648 (13″) + 698 (15″) = 1346
5000	813	0	0	5 (14″) + 808 (15″) = 813
10000	64	0	0	64

(b) AC Rut ≤ 0.5″ after 50 Years

Figure 3. Pavement Performance Flow Charts Based on AC Rut Criteria (No Rehab)

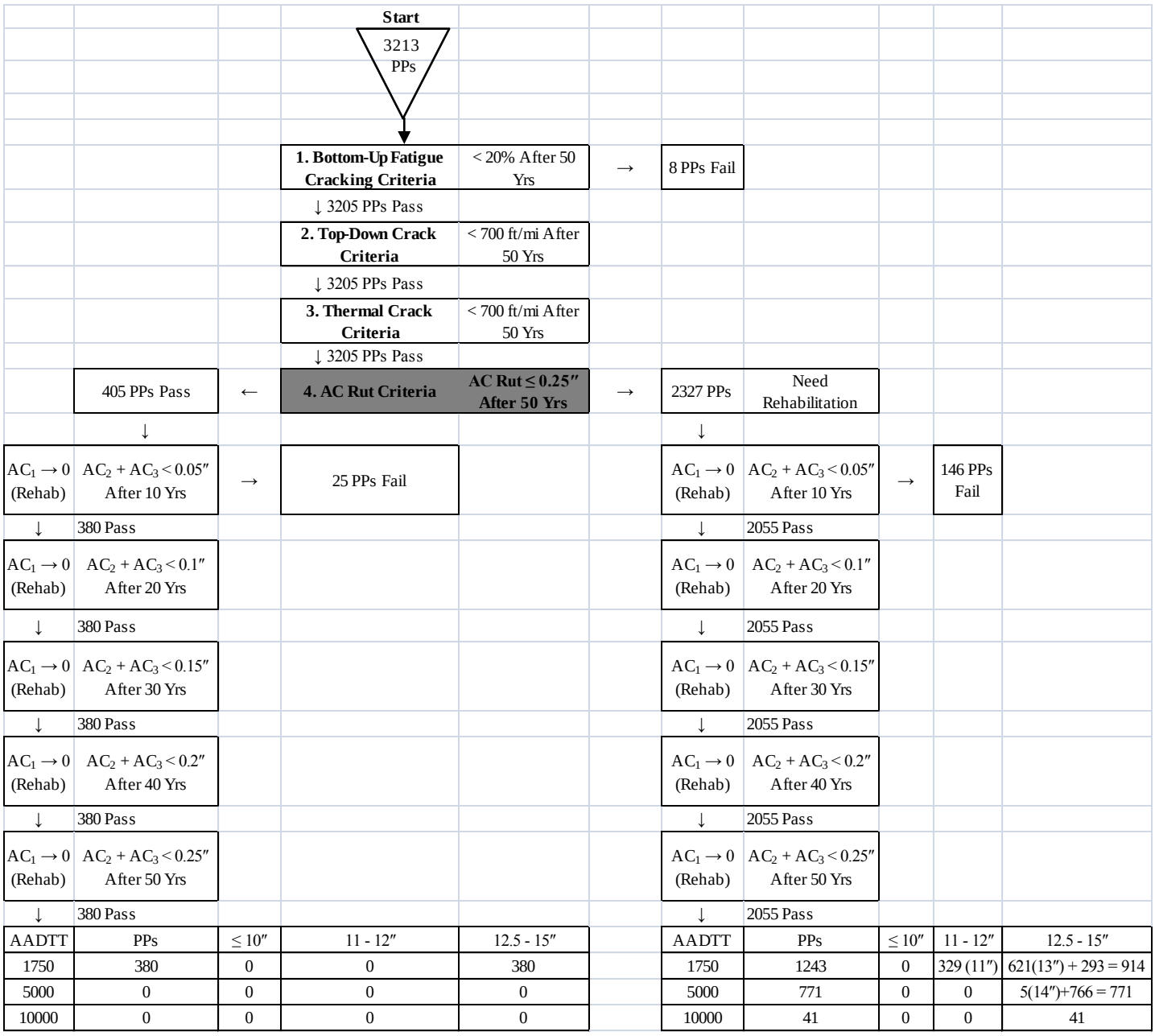

AADTT	PPs	≤ 10″	11 - 12″	12.5 - 15″	AADTT	PPs	≤ 10″	11 - 12″	12.5 - 15″
1750	380	0	0	380	1750	1243	0	329 (11″)	621(13″) + 293 = 914
5000	0	0	0	0	5000	771	0	0	5(14″)+766 = 771
10000	0	0	0	0	10000	41	0	0	41

(a) AC Rut ≤ 0.25″ after 50 Years (Rehab = AC_1 rut → 0, $AC_2 + AC_3$ rut ≤ 0.05)

Figure 4. Pavement Performance Flow Charts Based on AC Rut Criteria (Resurfacing Included)

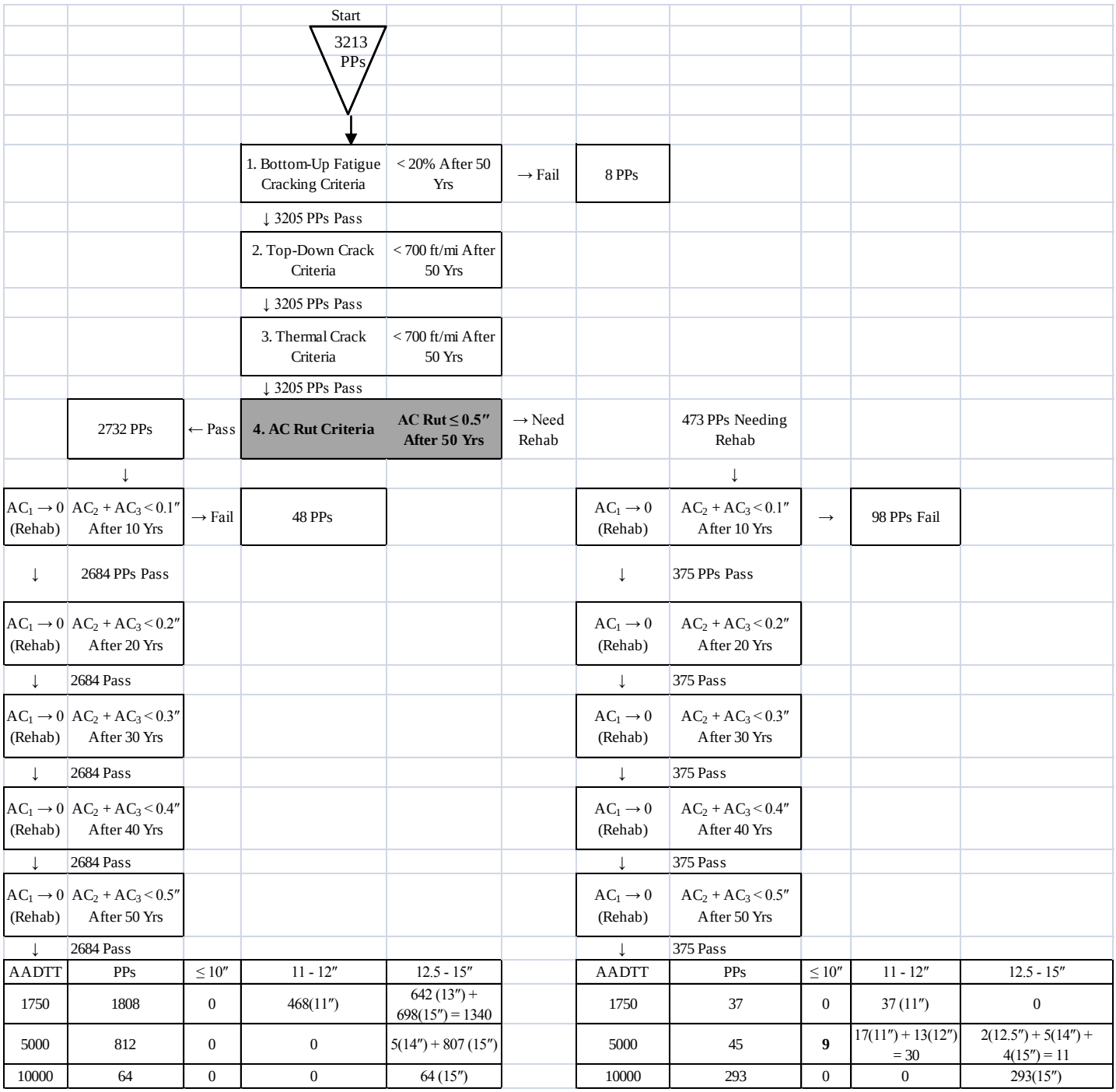

AADTT	PPs	≤ 10″	11 - 12″	12.5 - 15″	AADTT	PPs	≤ 10″	11 - 12″	12.5 - 15″
1750	1808	0	468(11″)	642 (13″) + 698(15″) = 1340	1750	37	0	37 (11″)	0
5000	812	0	0	5(14″) + 807 (15″)	5000	45	**9**	17(11″) + 13(12″) = 30	2(12.5″) + 5(14″) + 4(15″) = 11
10000	64	0	0	64 (15″)	10000	293	0	0	293(15″)

(b) AC Rut ≤ 0.5″ after 50 Years (Rehab = AC_1 rut → 0, AC_2 + AC_3 rut ≤ 0.1)

Figure 4. Pavement Performance Flow Charts Based on AC Rut Criteria (Resurfacing Included)

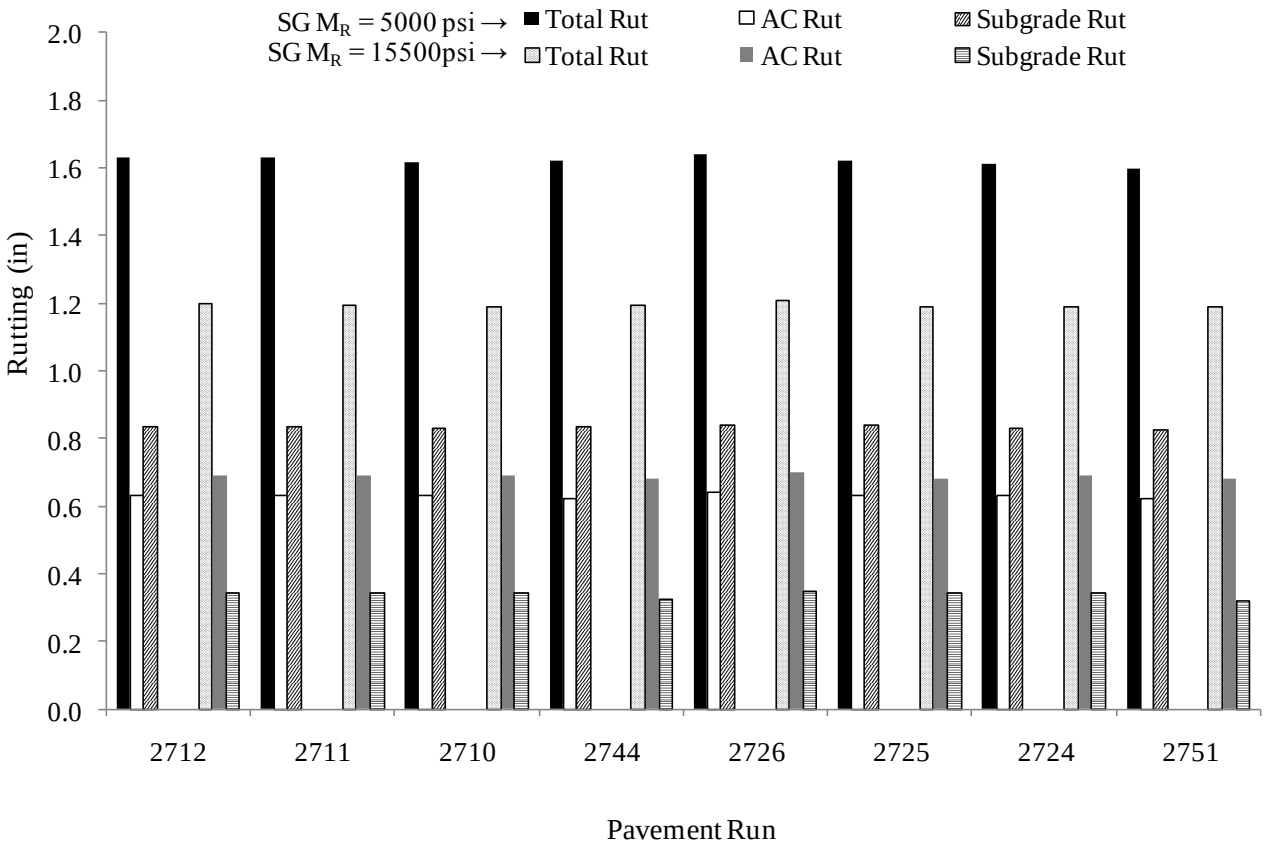

Figure 5. Effects of Improving Subgrade modulus on Total, AC, and Subgrade Rutting of Perpetual Pavements

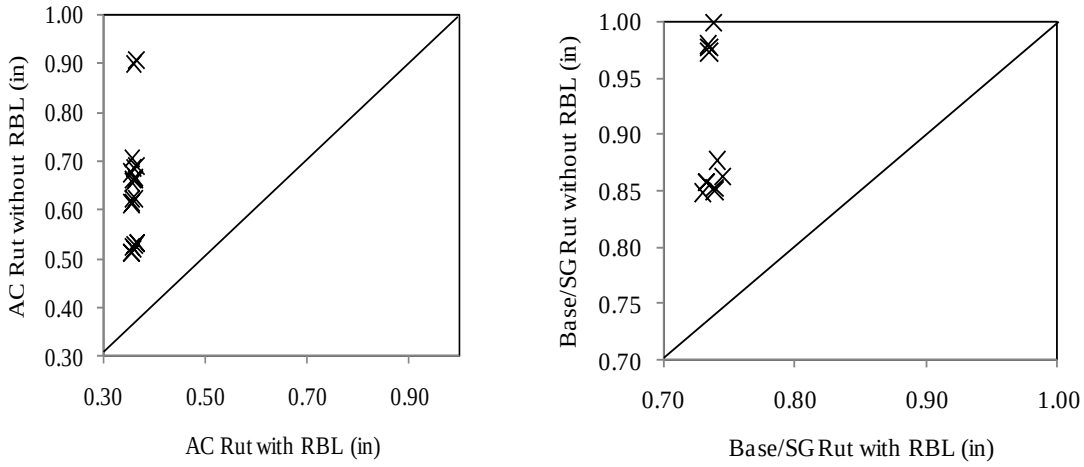

(a) AC-Rutting (b) Base/Subgrade Rutting

Figure 6. MEPDG Predicted Rutting With and Without Using a Rich Binder Layer

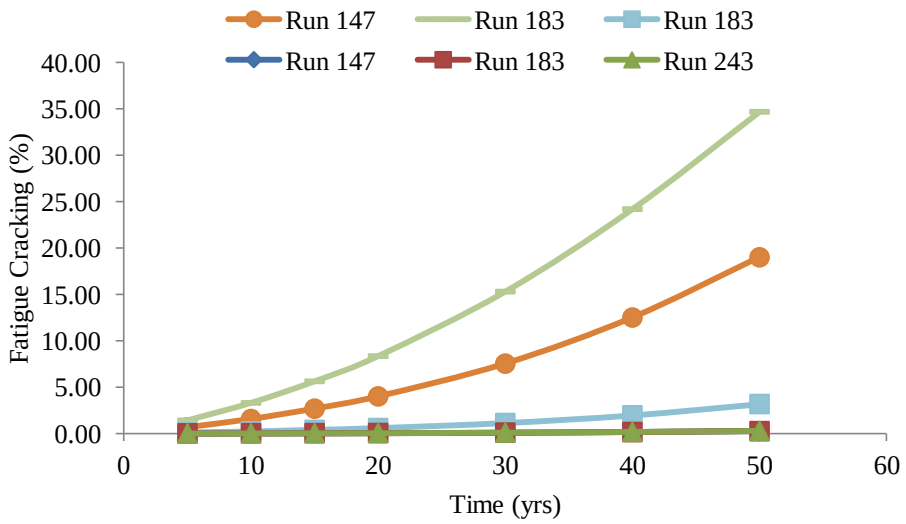

Figure 7. Fatigue Cracking for Pavements without Rich Binder Layer

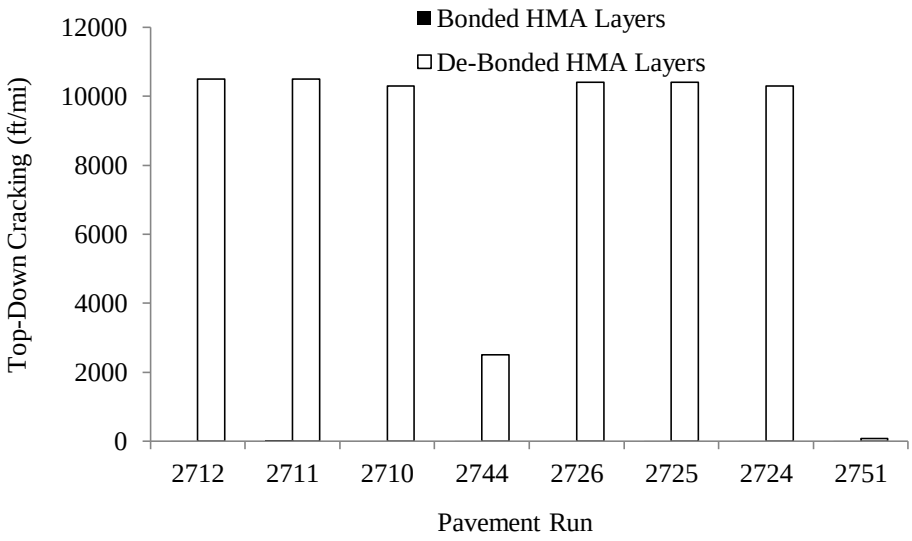

(a) Bonded/De-Bonded State in All HMA Layers

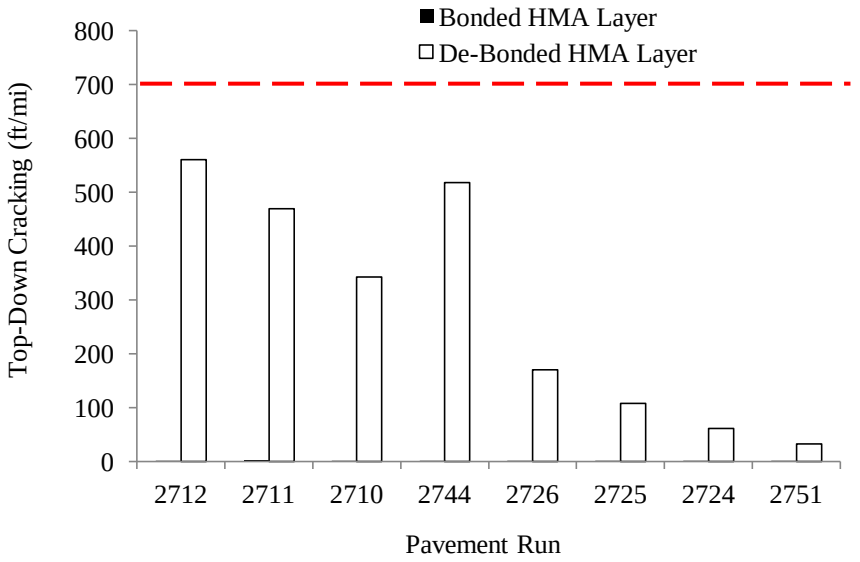

(b) Bonded/De-Bonded State in Upper HMA Layers

Figure 8. Top-Down Cracking in Bonded/De-Bonded HMA Pavements

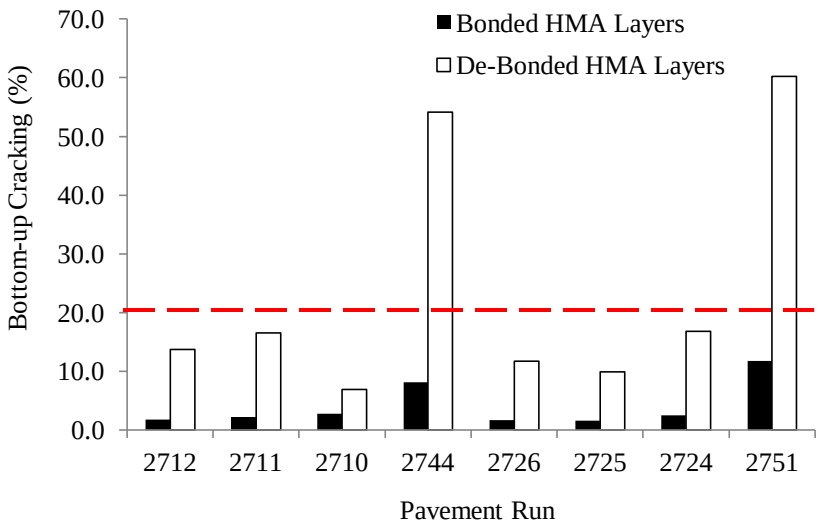

(a) Bonded/De-Bonded State in All HMA Layers

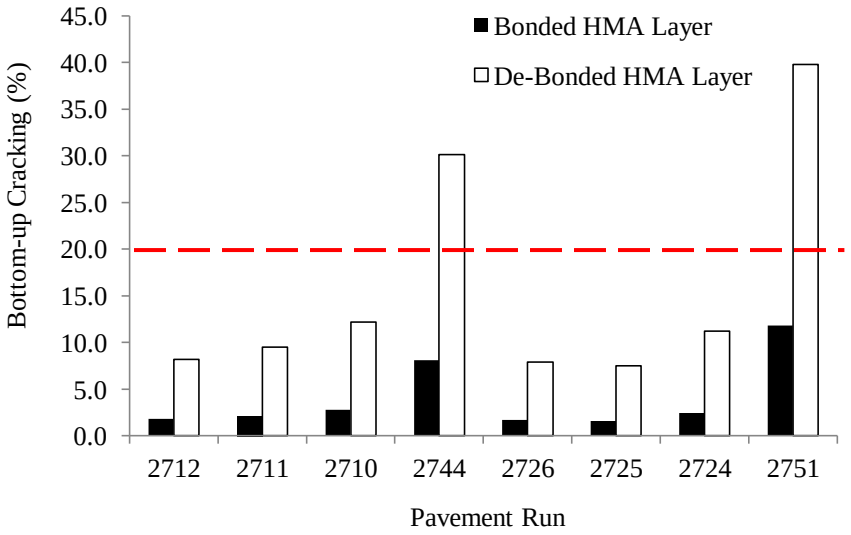

(b) Bonded/De-Bonded State in Upper HMA Layers

Figure 9. Bottom-Up Cracking in Bonded/De-Bonded HMA Pavements

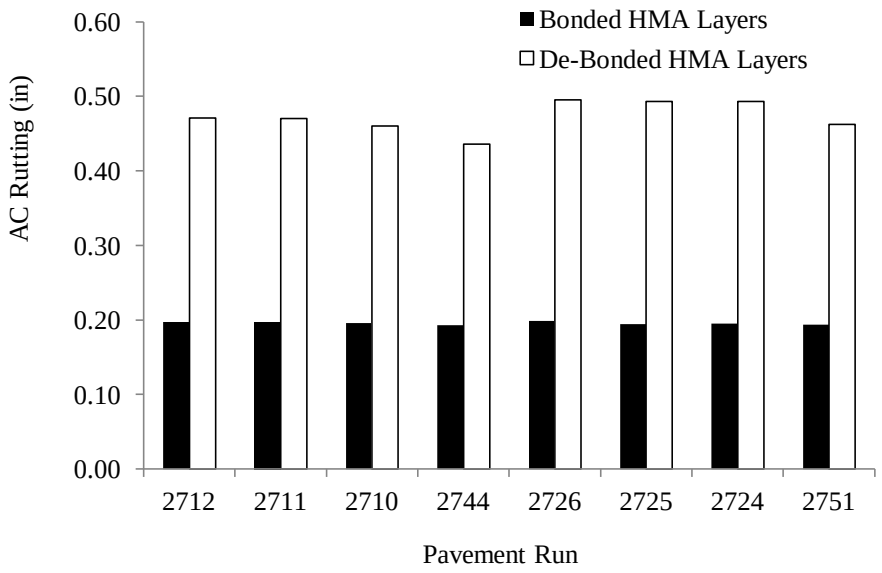

(a) Bonded/De-Bonded State in All HMA Layers

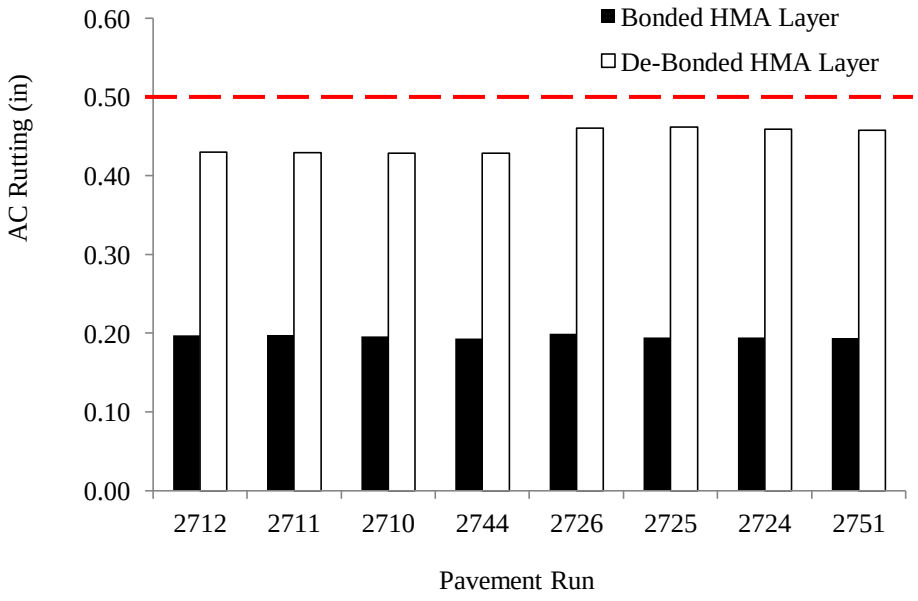

(b) Bonded/De-Bonded State in Upper HMA Layers

Figure 10. AC Rutting in Bonded/De-Bonded HMA Pavements

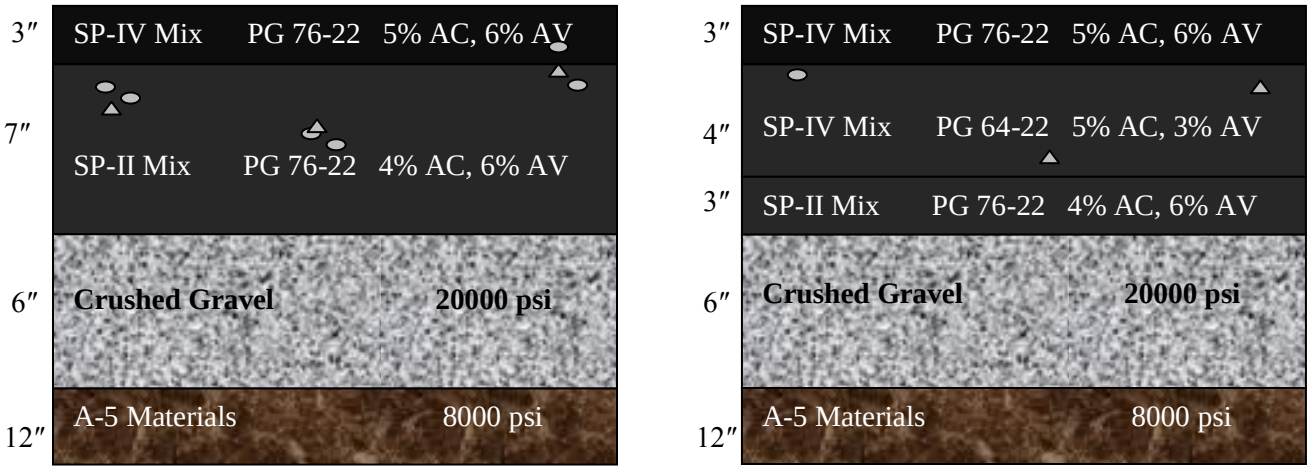

(a) Pavement Trial No. 2751 (no RBL)

(b) Pavement Trial No. 2725 (with RBL)

Figure 11. Implementable Perpetual Pavements

APPENDIX B

DYNAMIC MODULUS TEST DATA

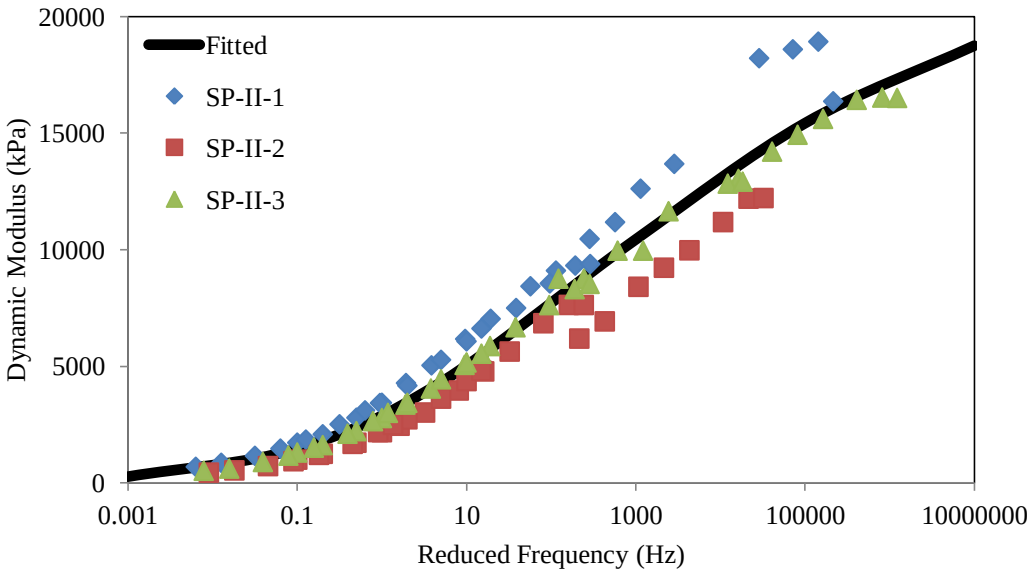

Figure B1 Dynamic Modulus Mastercurve of SP-II Mixture

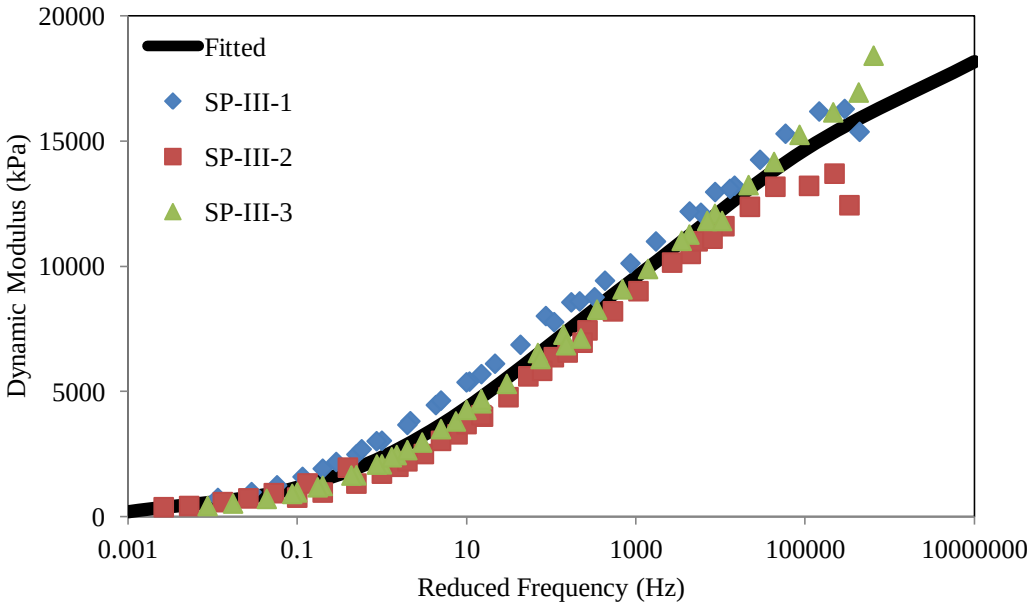

Figure B2 Dynamic Modulus Mastercurve of SP-III Mixture

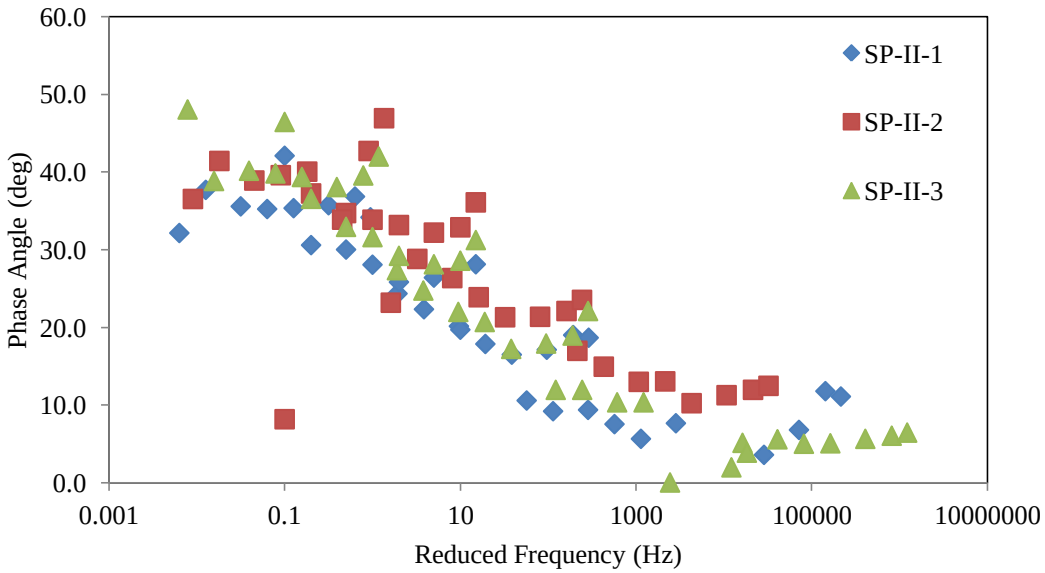

Figure B3 Phase Angle Mastercurve of SP-II Mixture

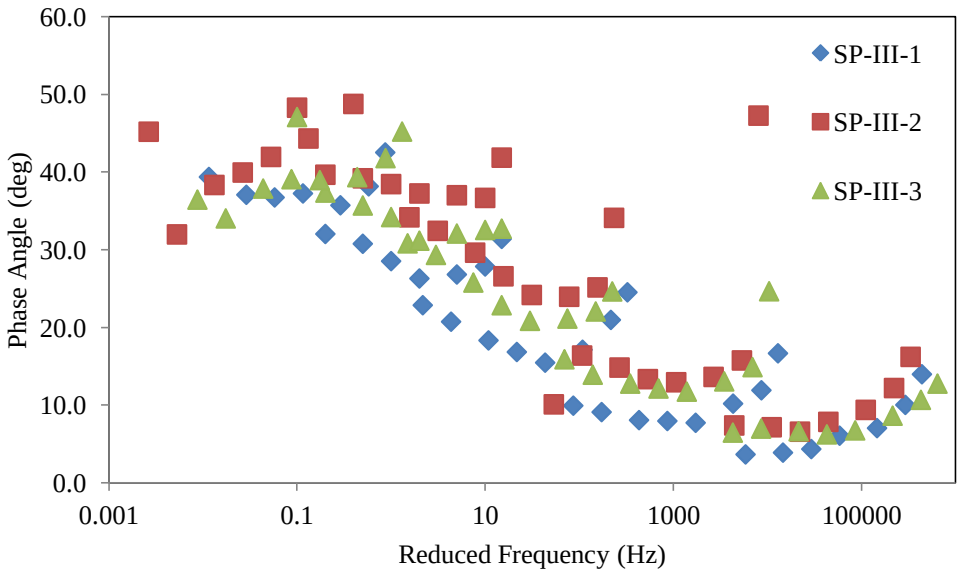

Figure B4 Phase Angle Mastercurve of SP-III Mixture

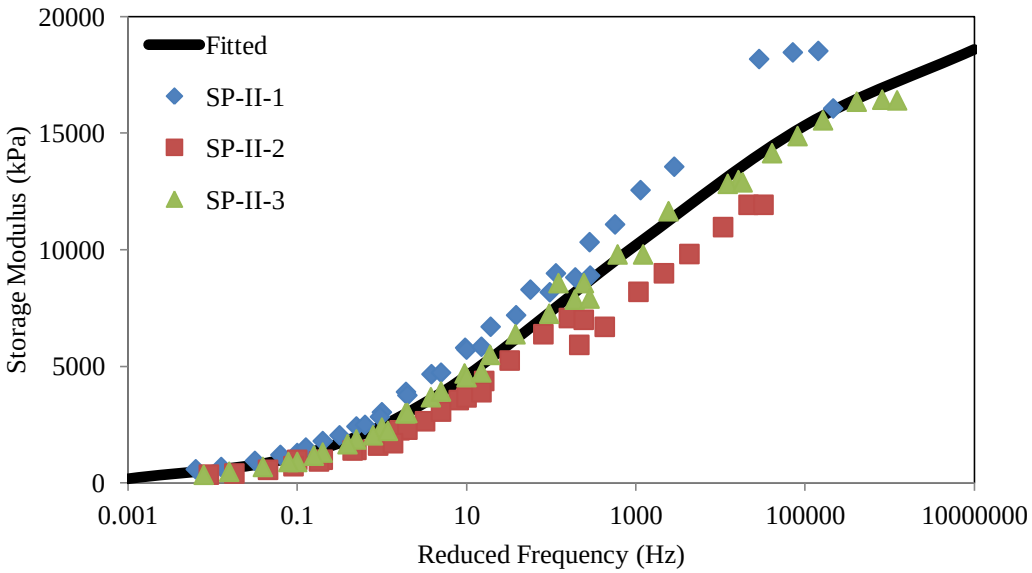

Figure B5 Storage Modulus Mastercurve of SP-II Mixture

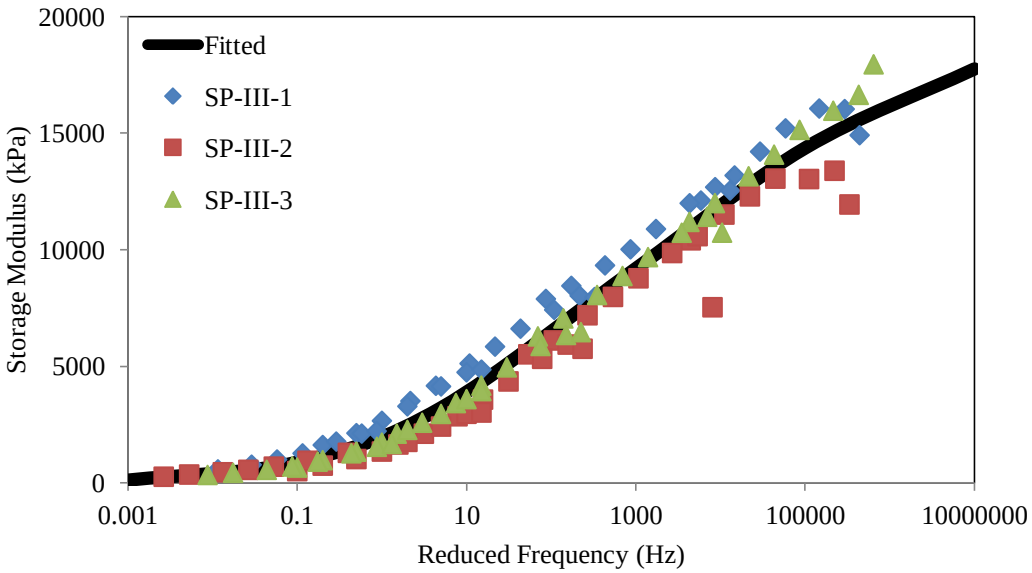

Figure B6 Storage Modulus Mastercurve of SP-III Mixture

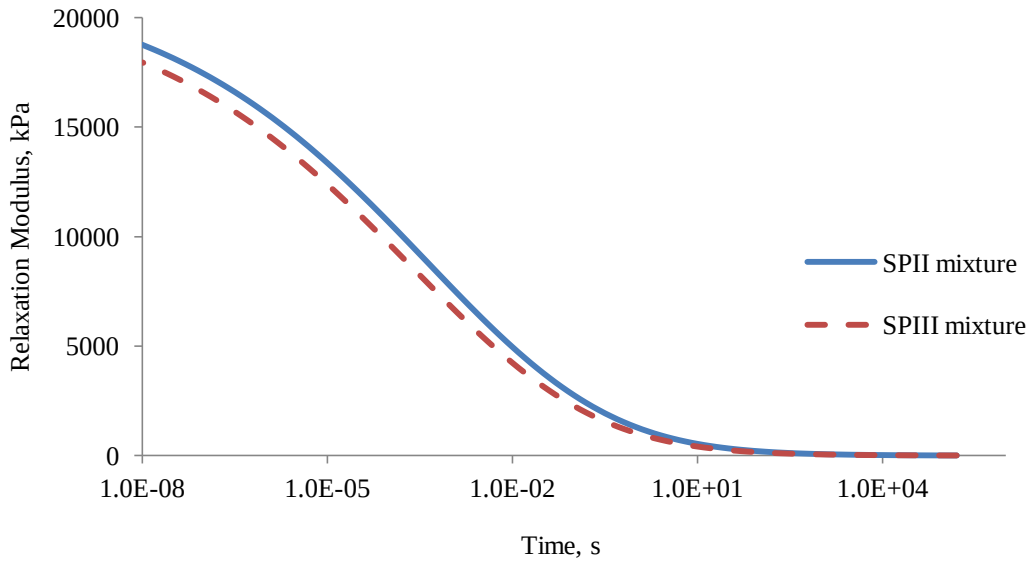

Figure B7 Relaxation Modulus of SP-II and SP-III Mixtures